

NACA RM L55I23a

FOR REFERENCE

NACA

NOT TO BE TAKEN FROM THIS ROOM

# RESEARCH MEMORANDUM

INVESTIGATION AT HIGH SUBSONIC SPEEDS OF THE STATIC  
LONGITUDINAL STABILITY CHARACTERISTICS OF A MODEL  
HAVING CROPPED-DELTA AND UNSWEPT WING PLAN  
FORMS AND SEVERAL TAIL CONFIGURATIONS

By Albert G. Few, Jr.

Langley Aeronautical Laboratory  
Langley Field, Va.

UNCLASSIFIED

LIBRARY COPY

To: \_\_\_\_\_

By authority of *NACA Res abs*  
*RM-123* Date *effective*  
*Dec. 13, 1957*  
*AMT 2-7-58*

NOV 1 1956  
LANGLEY AERONAUTICAL LABORATORY  
LANGLEY, NACA  
LANGLEY FIELD, VIRGINIA

This material contains information affecting the National Defense of the United States within the meaning of the espionage laws, Title 18, U.S.C., Secs. 793 and 794, the transmission or revelation of which in any manner to an unauthorized person is prohibited by law.

## NATIONAL ADVISORY COMMITTEE FOR AERONAUTICS

WASHINGTON  
November 30, 1955

## NATIONAL ADVISORY COMMITTEE FOR AERONAUTICS

## RESEARCH MEMORANDUM

INVESTIGATION AT HIGH SUBSONIC SPEEDS OF THE STATIC  
LONGITUDINAL STABILITY CHARACTERISTICS OF A MODEL  
HAVING CROPPED-DELTA AND UNSWEPT WING PLAN  
FORMS AND SEVERAL TAIL CONFIGURATIONS

By Albert G. Few, Jr.

## SUMMARY

An investigation has been made in the Langley high-speed 7- by 10-foot tunnel of various tail configurations used in conjunction with a model having either an unswept wing or a wing of moderate sweep (cropped-delta wing). The tail configurations included a horizontal tail at the top of the vertical tail for two tail lengths, a horizontal tail in the plane of the wing at a rather long tail length, and some combinations of high and low horizontal tails (called bitails). The cropped-delta and unswept wings were of aspect ratio 3, had taper ratios of 0.14 and 0.20, respectively, and had streamwise section thicknesses of 6 percent and 4 percent of the chord. Test Mach numbers ranged from 0.80 to 0.92, with corresponding Reynolds numbers ranging from about  $4.0 \times 10^6$  to  $4.2 \times 10^6$ .

None of the tail arrangements used with the unswept wing was capable of producing essentially linear pitching-moment curves for the complete model. In general, the large increase in stability at the higher lift coefficients, which was contributed by the unswept-wing-body combination, still was reflected to some degree in the complete-model characteristics.

Reasonably linear pitching-moment characteristics were obtained with several tail arrangements in conjunction with the cropped-delta-wing model for which the tail-off characteristics were quite linear. A slight tendency toward pitch-up near maximum lift at a Mach number of 0.80 with the high tail and long tail length was alleviated by moving the tail forward, although with some associated loss in stabilizer effectiveness. The bitail arrangements provided the most nearly linear pitching-moment curves, but at some expense in drag.

## INTRODUCTION

The tendency of airplanes with sweptback wings to exhibit longitudinal instability (or pitch-up) at high lift coefficients has in many instances been alleviated by the use of such devices as wing fences, chord extensions, or leading-edge flaps, or by placing the horizontal tail in a low position. (See refs. 1 to 5.) The stability characteristics resulting from these approaches are not always satisfactory, however, and it therefore is desirable to investigate other design approaches.

Recent tests at high subsonic speeds (ref. 6) have shown that certain wing plan forms in conjunction with a T-tail arrangement exhibit fairly linear pitching-moment characteristics through most of the lift-coefficient range except at the high angles of attack as the tail enters and passes through the wing wake where large variations in downwash and dynamic pressure may exist. For high tails, however, the angle of attack at which the tail enters the wing wake increases considerably with decreases in tail length and therefore a reduction in tail length may improve the characteristics at high angles of attack.

The main purpose of the present investigation therefore is to determine the effect of horizontal-tail length on the static longitudinal stability characteristics of a complete model having a T-tail. The model was tested with both a cropped-delta and an unswept wing. In addition to the T-tail, tests were also made with a low tail (on wing chord plane) and a bitail arrangement with both the T-tail and the low tail. The bitail was tested to determine the degree to which the nonlinear pitching-moment characteristics of high and low tails can be combined to create essentially linear characteristics. The cropped-delta and unswept wings had aspect ratios of 3 and taper ratios of 0.14 and 0.20, respectively. The section thickness of the cropped-delta wing was 6 percent of the streamwise chord; whereas, the section thickness of the unswept wing was 4 percent of the streamwise chord. Test Mach numbers ranged from 0.80 to 0.92 with corresponding Reynolds numbers ranging from about  $4.0 \times 10^6$  to  $4.2 \times 10^6$  based on the mean aerodynamic chord of the wings.

## COEFFICIENTS AND SYMBOLS

All data are presented with respect to the stability system of axes as shown in figure 1. The pitching-moment coefficients are referred to the quarter-chord point of the wing mean aerodynamic chord. Symbols are defined as follows:

$C_L$  lift coefficient,  $\frac{\text{Lift}}{qS}$

|                 |   |
|-----------------|---|
| $C_D$           | drag coefficient, $\frac{\text{Drag}}{qS}$                              |
| $C_m$           | pitching-moment coefficient, $\frac{\text{Pitching moment}}{qS\bar{c}}$ |
| $q$             | dynamic pressure, $\frac{\rho V^2}{2}$ , lb/sq ft                       |
| $\rho$          | mass density of air, slugs/cu ft  |
| $V$             | free-stream velocity, ft/sec  |
| $M$             | Mach number   |
| $S$             | wing area, sq ft  |
| $c$             | local chord parallel to plane of symmetry, ft                           |
| $c_r$           | root chord, ft  |
| $c_t$           | tip chord, ft   |
| $\lambda$       | taper ratio   |
| $\bar{c}$       | wing mean aerodynamic chord, $\frac{2}{S} \int_0^{b/2} c^2 dy$ , ft     |
| $\bar{c}_v$     | vertical-tail mean aerodynamic chord, ft                                |
| $b$             | wing span, ft   |
| $y$             | spanwise distance from plane of symmetry, ft                            |
| $\alpha$        | angle of attack, deg  |
| $i_t$           | horizontal-tail incidence angle, deg                                    |
| $A$             | aspect ratio  |
| $\Lambda_{c/2}$ | sweep of half-chord line, deg   |

|               |  |
|---------------|--|
| $\Lambda_c/4$ | sweep of quarter-chord line, deg   |
| $l_t$         | horizontal-tail length, distance from quarter chord of wing mean aerodynamic chord to quarter chord of horizontal-tail mean aerodynamic chord, in. |
| $l_{t,v}$     | vertical-tail length, distance from quarter chord of wing mean aerodynamic chord to quarter chord of vertical-tail mean aerodynamic chord, in.     |
| W             | wing   |
| F             | fuselage   |
| $V_1$         | vertical tail, $l_{t,v} = 6.89$ in.  |
| $H_1$         | high horizontal tail, $l_t = 10.28$ in.  |
| $V_2$         | vertical tail, $l_{t,v} = 15.29$ in.   |
| $H_2$         | high horizontal tail, $l_t = 18.68$ in.  |
| $H_3$         | low horizontal tail, $l_t = 20.01$ in.   |

#### MODEL AND APPARATUS

Details of the test model are given in figure 2 and a photograph of the model mounted on the sting-type support system is shown as figure 3. With this sting-support system, the model can be remotely operated through an angle-of-attack range of about  $-2^\circ$  through  $24^\circ$ . Both the cropped-delta and unswept wing ( $\Lambda_c/2 = 0^\circ$ ) were made of aluminum and had an aspect ratio of 3. The taper ratios were 0.14 and 0.20 for the cropped-delta and unswept wings, respectively. The cropped-delta wing had NACA 65A006 airfoil sections parallel to free stream, while the unswept wing had NACA 65A004 airfoil sections in a streamwise direction. The vertical and horizontal tails were made of steel covered with fiber glass and plastic and had NACA 65A006 airfoil sections in a streamwise direction. The model could be tested with two vertical-tail lengths and the high horizontal tail (mounted on the vertical tail as a T-tail configuration) set at either  $0^\circ$  or  $-3^\circ$  incidence, while the low tail (on wing chord plane extended) was fixed at one tail length and  $0^\circ$  incidence. The low tail, in combination with the high tail at either tail length, could be tested as bitail configurations. The fuselage was of fineness ratio 10.94 and

was constructed of aluminum. The fuselage geometry, including afterbody ordinates, is given in figure 4. A six-component electrical strain-gage balance was mounted internally in the fuselage to measure the forces and moments presented herein.

### TESTS

The sting-supported model was tested in the Langley high-speed 7-by 10-foot tunnel through a Mach number range of 0.80 to 0.92, which corresponds to a Reynolds number range from about  $4.0 \times 10^6$  to  $4.2 \times 10^6$ , based on the wing mean aerodynamic chord. The angle-of-attack range varied with loading conditions (the maximum range being from about  $-2^\circ$  to  $24^\circ$ ). Lift, drag, and pitching moment were measured by means of an electrical strain-gage balance mounted internally in the fuselage.

### CORRECTIONS

Jet-boundary corrections to the angle of attack and drag were applied in accordance with reference 7. Blockage corrections were applied to the data by the method of reference 8, and corrections for the effects of longitudinal pressure gradient over the model length have been applied to the drag.

Model support tares have not been applied, except for a fuselage base-pressure adjustment to the drag. The adjusted drag data represent a condition of free-stream static pressure at the fuselage base. From past experience, it is felt that the influence of the sting support system on the model lift and pitching moment is very small.

The angle of attack has been corrected for deflection of the sting support and balance system under load. No attempt has been made, however, to correct the data for aeroelastic distortion of the model.

### RESULTS AND DISCUSSION

#### Presentation of Results

An outline giving figure numbers where the basic-aerodynamic data can be found is given as table I for the various configurations tested, and figures related to analyses of the results are presented as follows:

|  | <u>Figure</u> |
|--|---------------|
| Effect of tail length on the tail contribution to pitching moment; $i_t = 0^\circ$ . . . . .   | 27            |
| Effect of various tail arrangements on the tail contribution to pitching-moment coefficient for the model with a cropped-delta wing; $i_t = 0^\circ$ . . . . . | 28            |
| Effect of Mach number on the rate of change of pitching-moment coefficient with lift coefficient at zero-lift coefficient; $i_t = 0^\circ$ . . . . .           | 29            |
| Effect of tail length on the stabilizer effectiveness . . . . .  | 30            |
| Effect of tail location on the drag at zero-lift coefficient; $i_t = 0^\circ$ . . . . .  | 31            |

All wing-off data, lift, drag, and pitching-moment coefficients presented herein are based on the cropped-delta wing geometry.

#### Pitching-Moment Characteristics

General discussion.- Figures 5 and 6 present the effect of horizontal-tail length on the pitching-moment characteristics of the model with a cropped-delta wing and high (atop vertical tail) horizontal-tail positions. For the range of Mach number investigated, a reduction in horizontal-tail length resulted in somewhat more linear pitching-moment

curves; although, as was expected, both the low-lift stability  $\left(\frac{\partial C_m}{\partial C_L}\right)_{C_L=0}$

and the stabilizer effectiveness were reduced. (See figs. 29 and 30.) A more desirable high-tail configuration from considerations of both stability and controllability, probably could be obtained with a tail length between the two lengths investigated. The addition of a low horizontal tail (on the wing chord plane extended) in conjunction with the high horizontal tail to form a bitail arrangement provided further improvement in the pitching-moment curve linearity through the lift-coefficient range (figs. 7 and 8). For the most part, the bitail configurations show some increase in stability with increased angle of attack, especially when the tail length of the high horizontal tail is reduced. This characteristic (increase in stability with increased angle of attack) is similar to, but more moderate than, that noted for the cropped-delta wing with a low horizontal tail as shown in figure 9(a).

It is interesting to note that figure 9(a) indicates the horizontal-tail-off pitching-moment characteristics for the cropped-delta wing to be somewhat influenced by the longitudinal position of the vertical tail on the fuselage. With the vertical tail in the forward position, significant reductions in pitching-moment coefficient for a given angle of attack over that realized for the vertical tail in the rearward position is noted at moderate to high angles of attack through the Mach number range investigated. Similar trends are noted for the horizontal-tail-off pitching-moment characteristics for the unswept wing in figures 10 and 12. Results obtained with both the horizontal and the vertical tails removed, although not presented herein, were found to be in almost exact agreement with the results presented for the aft vertical-tail location. The reason for the rather large effect indicated for the forward vertical tail is not established by these tests. It is noted, however, that the forward vertical tail overlaps the wing trailing edge by an appreciable distance. It is possible, therefore, that for this location, the vertical tail induces positive increments of pressure on the upper surface of the rear portion of the wing, thus reducing the nose-down tendency. Another possibility is that the vertical tail may alter the pressure distribution on the rear part of the fuselage.

Some effects of horizontal-tail length on the pitching-moment characteristics of the model with an unswept wing ( $\Lambda_c/2 = 0^\circ$ ) and high horizontal tail are presented in figures 10 and 11. The stable breaks in the pitching-moment curves for this wing, which generally occur at about the lift coefficient where a reduction in lift-curve slope takes place, are characteristic of both horizontal-tail lengths investigated through the Mach number range. In general, this large increase in stability which was contributed by the wing-body combination still was reflected to some degree for all horizontal-tail arrangements (figs. 10 to 13). However, the unstable breaks noted at a Mach number of 0.80 (fig. 10) and at high angles of attack, well above the lift-curve breaks noted in figure 18(a), are somewhat alleviated by the reduction in horizontal-tail length. Additional improvements in the pitching-moment characteristics above the lift-curve break are realized with the bitail configurations as indicated in figures 12 and 13.

Horizontal-tail contribution to pitching moment.- To further illustrate the effects of tail length on the pitching-moment characteristics, especially at high angles of attack, the contribution to the pitching moment by the horizontal tail ( $C_{m_t}$ ) is presented in figures 27 and 28.

In general, the contribution of the high horizontal tail to pitching moment (fig. 27) for the model with reduced tail length had a less pronounced decrease at the high angles of attack and a Mach number of 0.80 than that for the model with a greater tail length. For the high tail, then, it would appear that the angle of attack of the model at which the horizontal tail enters the region of increased downwash can increase considerably with decreases in tail length. Figure 28 presents the contribution to the pitching moment by the low, high, and bitail configurations

in conjunction with a cropped-delta wing at Mach numbers of 0.80 and 0.92. In addition, the bitail contribution estimated by adding the contribution of the high tail to that of the low tail alone is compared with the measured bitail contribution. Figure 28 indicates that less interference between the two tails may exist for the short tail length, particularly at a Mach number of 0.92. It should be pointed out that the bitail was formed simply by combining the high and low tails used for the single-tail configurations. If an actual design of a bitail should be considered, it is likely that the total tail area would be reduced, and probably the relative sizes of the high and low tails would be altered.

Pitching moment at zero lift.- There existed a positive pitching-moment increment at zero lift for the high horizontal tail and bitail arrangements at  $i_t = 0^\circ$  through the Mach number range investigated for both wing plan forms as shown in figures 5 to 13. A reduction in tail length reduced this positive value of pitching-moment coefficient at zero lift for the high tail, but for the bitail arrangement a reduction in the high tail length increased the positive value of pitching moment at zero lift. The low horizontal tail which was mounted on the wing chord line extended of the cropped-delta wing plan form provided no significant pitching-moment coefficient at zero lift (fig. 9(b)). Wing-off tests with the high horizontal tail indicated out-of-trim moments of the same order of magnitude as that with the wing on, as indicated in figure 14. The vertical-tail profile inducing negative pressures on the lower surface of the high horizontal tail (atop the vertical tail) could be an explanation for this phenomenon as has been pointed out in reference 1.

Aerodynamic center.- Some effects of horizontal-tail length on the aerodynamic center through the Mach number range investigated for various configurations are shown in figure 29. For the tail-off and low-tail configurations only the vertical tail was moved fore and aft, and this change in vertical-tail location on the fuselage produces some small changes in aerodynamic center with Mach number. For the high horizontal tail and bitail arrangements, the change in aerodynamic center with Mach number is about the same as that with tail off for the cropped-delta wing plan form. The change in aerodynamic center with Mach number of the unswept wing plan form for the high-tail and bitail configurations was not as great as that with tail off. The reduction in stability due to decreased horizontal-tail length is about constant through the Mach number range for all configurations investigated and the change in tail contribution is about proportional to tail length.

Stabilizer effectiveness.- Figure 30 presents, for a Mach number of 0.80 and 0.92, some effects of tail length on the stabilizer effectiveness in conjunction with the cropped-delta and unswept wing plan forms. A reduction in tail length produces the expected decrease in stabilizer effectiveness at a constant lift coefficient for both a Mach number of 0.80 and 0.92. Generally speaking, the reductions in stabilizer

effectiveness due to decreased tail length were larger at high lift coefficients than at low lift coefficients.

### Lift and Drag Characteristics

Lift and drag characteristics for the various model configurations are presented in figures 15 to 20 and figures 21 to 26, respectively. Lift-curve slopes and drag due to lift of the wing-fuselage vertical-tail configurations for the wings tested herein have been reported in reference 6 and consequently need no further discussion in this paper.

It should be pointed out that the two stabilizer incidences tested did not provide sufficient data for an evaluation of the effects of horizontal-tail length on the trim-drag characteristics of the model tested in the investigation; however, a decrease in tail length would be expected to result in increases in the trim-drag as was indicated in reference 5.

In order to illustrate some effects of tail length on the drag at zero-lift coefficient, comparisons of various configurations have been made for the Mach number range investigated and are presented in figure 31. In general, a reduction in tail length provides some increases in drag at zero-lift coefficient as the Mach number increases from about 0.85 to 0.92 for both wings tested. The drag-rise Mach number is somewhat lower for the bitail arrangements than for the single-tail arrangements, although, within the speed range investigated the difference is small when the bitail includes the long tail length of the upper surface.

### CONCLUDING REMARKS

An investigation at high subsonic speeds of the static longitudinal stability characteristics of a model having both cropped-delta and unswept wing plan forms and several horizontal-tail locations indicates the following results.

None of the tail arrangements with the unswept wing was capable of producing essentially linear pitching-moment curves for the complete model. In general, the large increase in stability at the higher lift coefficients, which was contributed by the unswept wing-body combination, still was reflected to some degree in the complete-model characteristics.

Reasonably linear pitching-moment characteristics were obtained with several tail arrangements in conjunction with the cropped-delta wing for which the tail-off characteristics were quite linear. A slight tendency

toward pitch-up near maximum lift with the high tail and long tail length was alleviated by moving the tail forward, although with some associated loss in stabilizer effectiveness. The bitail arrangements provided the most nearly linear pitching-moment curves, but at some penalties in drag.

Langley Aeronautical Laboratory,  
National Advisory Committee for Aeronautics,  
Langley Field, Va., September 16, 1955.

## REFERENCES

1. Smith, Willard G.: Wind-Tunnel Investigation at Subsonic and Supersonic Speeds of a Fighter Model Employing a Low-Aspect-Ratio Unswept Wing and a Horizontal Tail Mounted Well Above Wing Plane - Longitudinal Stability and Control. NACA RM A54D05, 1954.
2. Few, Albert G., Jr. and Fournier, Paul G.: Effects of Sweep and Thickness on the Static Longitudinal Aerodynamic Characteristics of a Series of Thin, Low-Aspect-Ratio, Highly Tapered Wings at Transonic Speeds - Transonic-Bump Method. NACA RM L54B25, 1954.
3. Alford, William J., Jr., and Pasteur, Thomas B., Jr.: The Effects of Changes in Aspect Ratio and Tail Height on the Longitudinal Stability Characteristics at High Subsonic Speeds of a Model With a Wing Having 32.6° Sweepback. NACA RM L53L09, 1954.
4. Goodson, Kenneth W., and Becht, Robert E.: Wind-Tunnel Investigation at High Subsonic Speeds of the Stability Characteristics of a Complete Model Having Sweptback-, M-, W-, and Cranked-Wing Plan Forms and Several Horizontal-Tail Locations. NACA RM L54C29, 1954.
5. Tinling, Bruce E., and Lopez, Armando E.: The Effects of Horizontal-Tail Location and Size on the Subsonic Longitudinal Aerodynamic Characteristics of an Airplane Model Having a Triangular Wing of Aspect Ratio 3. NACA RM A53L15, 1953.
6. Goodson, Kenneth W., and Becht, Robert E.: Wind-Tunnel Investigation at High Subsonic Speeds of the Static Longitudinal Stability Characteristics of a Complete Model Having Cropped-Delta, Swept, and Unswept Wings and Several Horizontal-Tail Heights. NACA RM L54H12, 1954.
7. Gillis, Clarence L., Polhamus, Edward C., and Gray, Joseph L., Jr.: Charts for Determining Jet-Boundary Corrections for Complete Models in 7- by 10-Foot Closed Rectangular Wind Tunnels. NACA WR L-123, 1945. (Formerly NACA ARR L5G31.)
8. Herriot, John G.: Blockage Corrections for Three-Dimensional-Flow Closed-Throat Wind Tunnels, With Consideration of the Effect of Compressibility. NACA Rep. 995, 1950. (Supersedes NACA RM A7B28.)

TABLE I. TAIL CONFIGURATIONS INVESTIGATED AND FIGURES IN WHICH BASIC DATA ARE PRESENTED.

| Cropped-Delta Wing  |                |                |                |                |                |                | Unswept Wing  |                |                |                |                |                |                | Wing Off  |                |                |                |                |                |                |
|---|----------------|----------------|----------------|----------------|----------------|----------------|---|----------------|----------------|----------------|----------------|----------------|----------------|---|----------------|----------------|----------------|----------------|----------------|----------------|
| Tail Configuration  | Tail Incidence |                |                | Data Figure    |                |                | Tail Configuration  | Tail Incidence |                |                | Data Figure    |                |                | Tail Configuration  | Tail Incidence |                |                | Data Figure    |                |                |
|   | H <sub>1</sub> | H <sub>2</sub> | H <sub>3</sub> | C <sub>m</sub> | C <sub>L</sub> | C <sub>D</sub> |   | H <sub>1</sub> | H <sub>2</sub> | H <sub>3</sub> | C <sub>m</sub> | C <sub>L</sub> | C <sub>D</sub> |   | H <sub>1</sub> | H <sub>2</sub> | H <sub>3</sub> | C <sub>m</sub> | C <sub>L</sub> | C <sub>D</sub> |
|    | -              | -              | -              | 5-15-21        |                |                |    | -              | -              | -              | 10-18-24       |                |                |    | -              | -              | -              | 14-20-26       |                |                |
|    | 0°             | -              | -              | 5-15-21        |                |                |    | 0°             | -              | -              | 10-18-24       |                |                |    | 0°             | -              | -              | 14-20-26       |                |                |
|    | 3°             | -              | -              | 6-15-21        |                |                |    | 3°             | -              | -              | 11-18-24       |                |                |    | 3°             | -              | -              | 14-20-26       |                |                |
|    | -              | -              | 0°             | 9-17-23        |                |                |    | -              | -              | 0°             | 12-19-25       |                |                |    | -              | -              | 0°             | 14-20-26       |                |                |
|    | 0°             | -              | 0°             | 7-16-22        |                |                |    | 0°             | -              | 0°             | 13-19-25       |                |                |    | 0°             | -              | 0°             | 14-20-26       |                |                |
|   | 3°             | -              | 0°             | 8-16-22        |                |                |   | 3°             | -              | 0°             | 10-18-24       |                |                |   | 3°             | -              | 0°             | 14-20-26       |                |                |
|  | -              | -              | -              | 5-15-21        |                |                |  | -              | -              | -              | 10-18-24       |                |                |  | -              | -              | -              | 14-20-26       |                |                |
|  | -              | 0°             | -              | 5-15-21        |                |                |  | -              | 0°             | -              | 10-18-24       |                |                |  | -              | 0°             | -              | 14-20-26       |                |                |
|  | -              | 3°             | -              | 6-15-21        |                |                |  | -              | 3°             | -              | 11-18-24       |                |                |  | -              | 3°             | -              | 14-20-26       |                |                |
|  | -              | -              | 0°             | 9-17-23        |                |                |  | -              | -              | 0°             | 12-19-25       |                |                |  | -              | -              | 0°             | 14-20-26       |                |                |
|  | -              | 0°             | 0°             | 7-16-22        |                |                |  | -              | 0°             | 0°             | 12-19-25       |                |                |  | -              | 0°             | 0°             | 14-20-26       |                |                |
|  | -              | 3°             | 0°             | 8-16-22        |                |                |  | -              | 3°             | 0°             | 13-19-25       |                |                |  | -              | 3°             | 0°             | 14-20-26       |                |                |

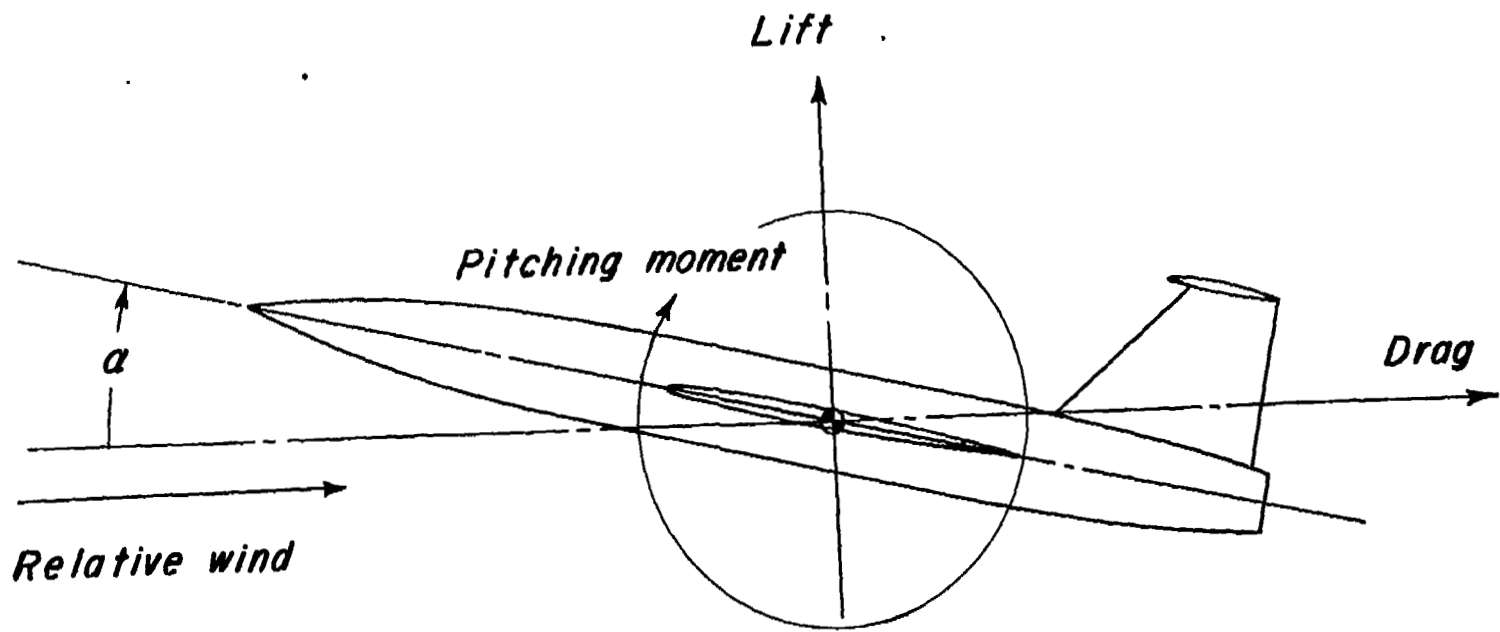
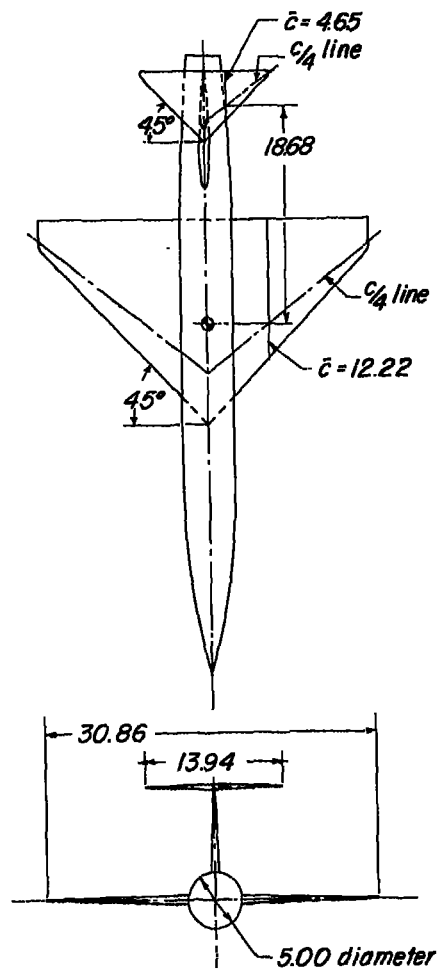
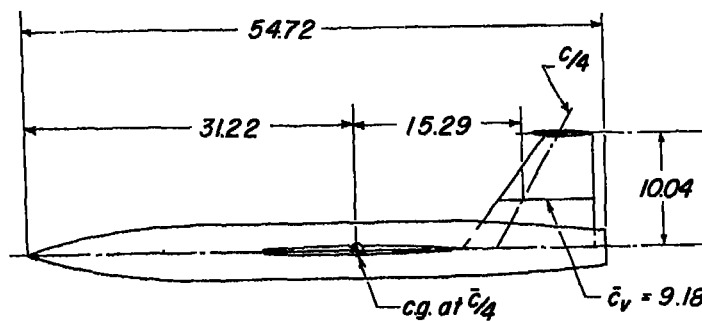


Figure 1.- System of axes. (Positive values of forces, moments, and angles are indicated by arrows.)



### Geometric Characteristics of Test Model

|                        | Cropped delta wing | Horizontal tail | Vertical tail |
|------------------------|--------------------|-----------------|---------------|
| Area, sqft             | 2.20               | 0.337           | 0.603         |
| $A$                    | 300                | 4               | 1.16          |
| $\lambda$              | 0.143              | 0               | 0.411         |
| $c_t$ , in.            | 2.57               | 0               | 5.04          |
| $c_r$ , in.            | 18.00              | 6.97            | 12.27         |
| $\Delta c_{1/4}$ , deg | 36.85              | 36.85           | 28.0          |
| Airfoil section        | NACA 65A006        | NACA 65A006     | NACA 65A006   |



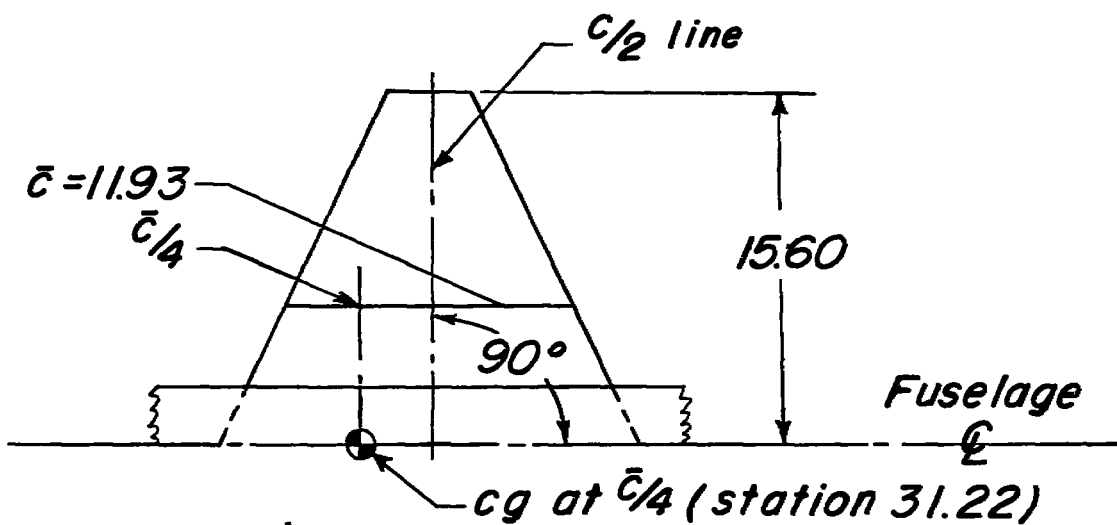
(a) Three-view drawing of model with a cropped-delta wing.

Figure 2.- Geometric characteristics of the test model. (All dimensions are in inches.)

**Geometric Characteristics - Con't.**

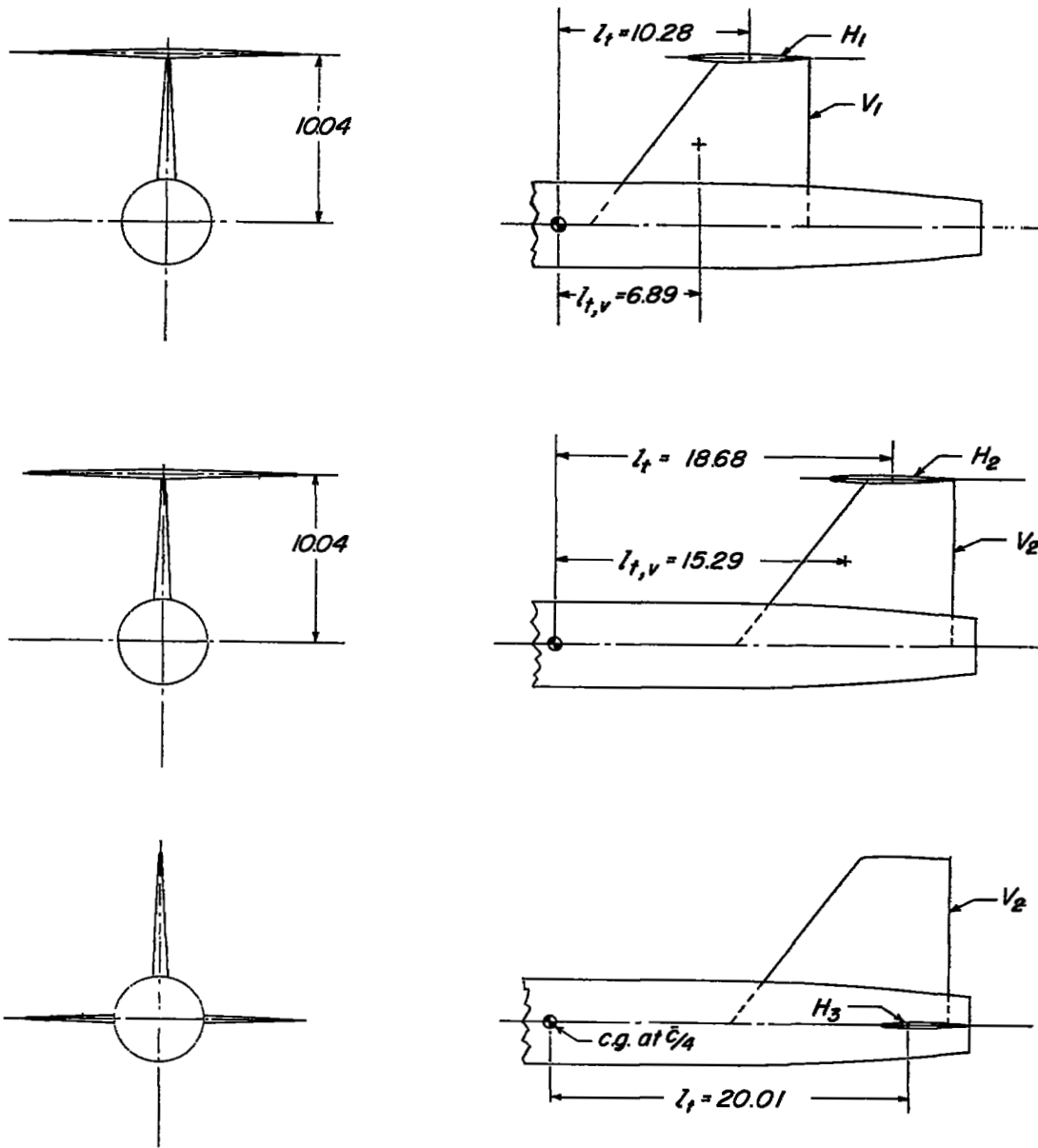
**Unswep wing**

|                                |                        |
|--------------------------------|------------------------|
| <b>Area , sq ft</b>            | <b>2.25</b>            |
| <b>A</b>                       | <b>3.00</b>            |
| <b><math>\lambda</math></b>    | <b>0.20</b>            |
| <b><math>c_t</math>, in.</b>   | <b>3.46</b>            |
| <b><math>c_r</math>, in.</b>   | <b>17.32</b>           |
| <b><math>\Delta c/4</math></b> | <b>12.53°</b>          |
| <b>Airfoil section</b>         | <b>NACA<br/>65A004</b> |



(b) Unswep wing.

Figure 2.- Continued.



(c) Horizontal- and vertical-tail locations.

Figure 2.- Concluded.

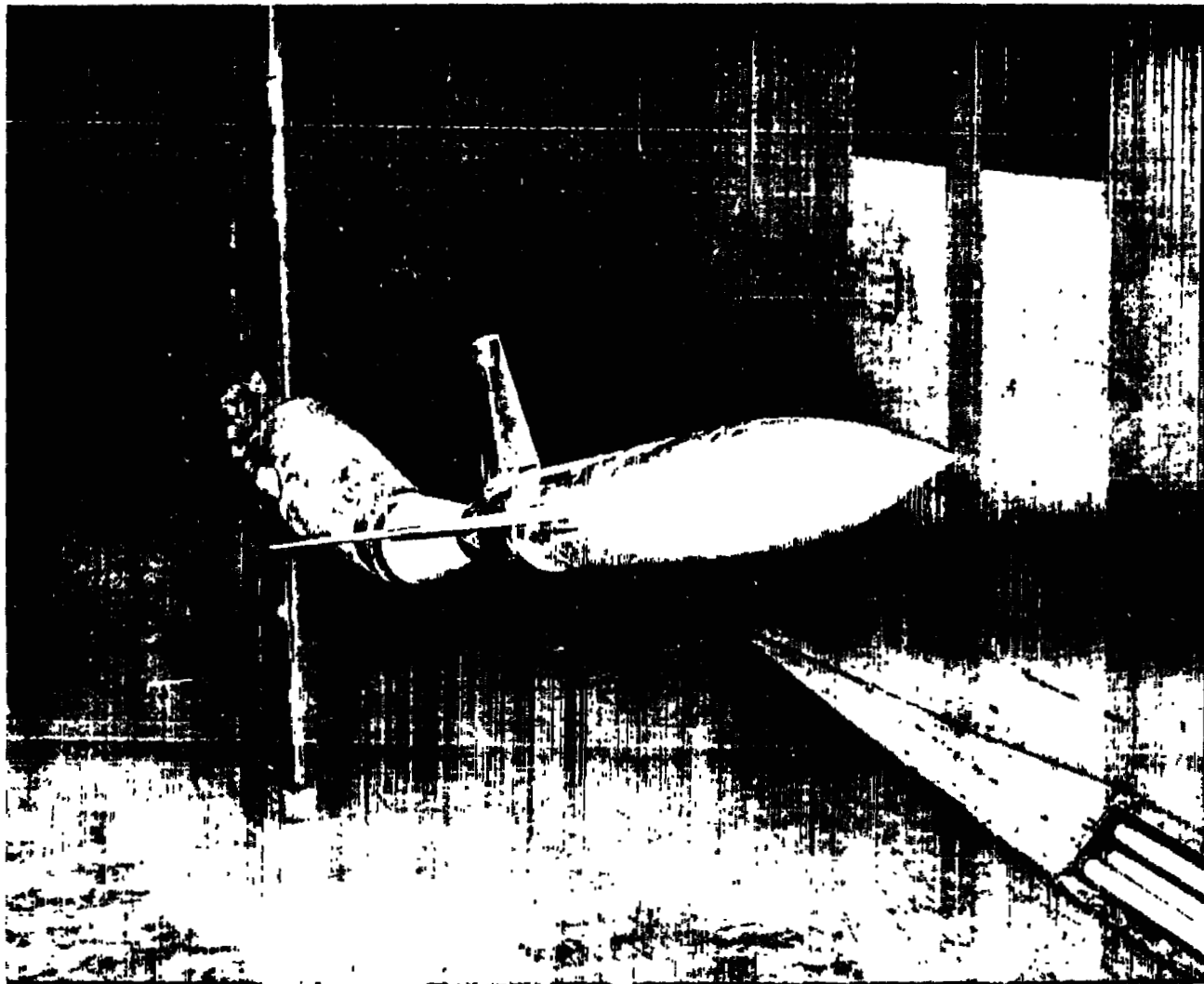
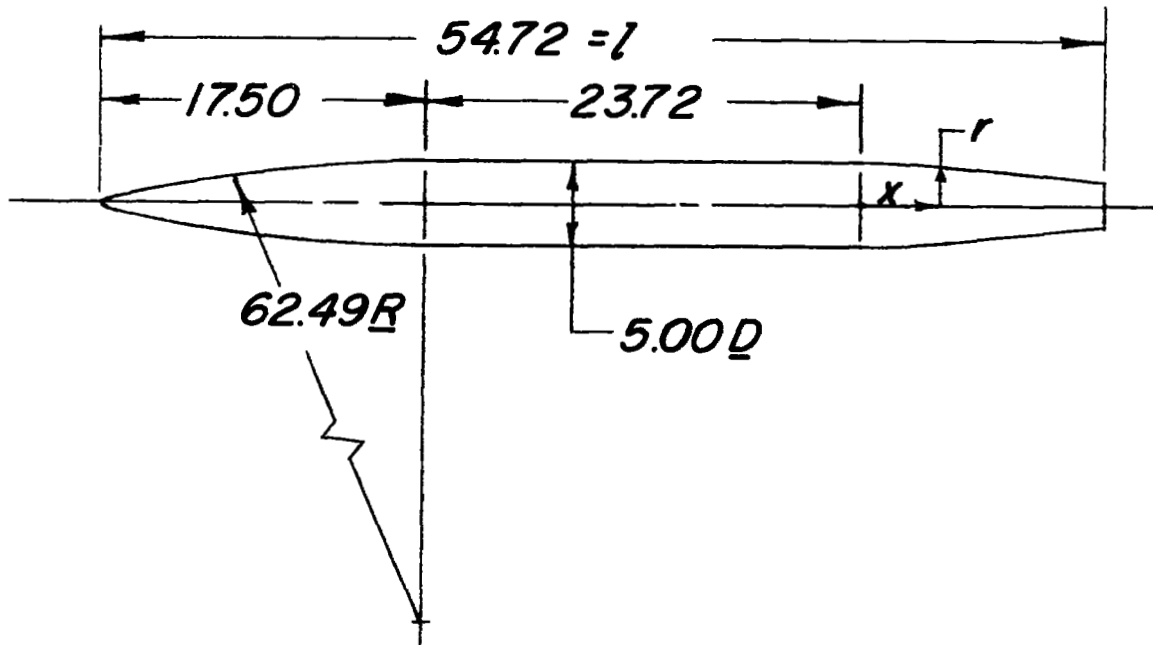


Figure 3.- Model mounted on the sting-support system.

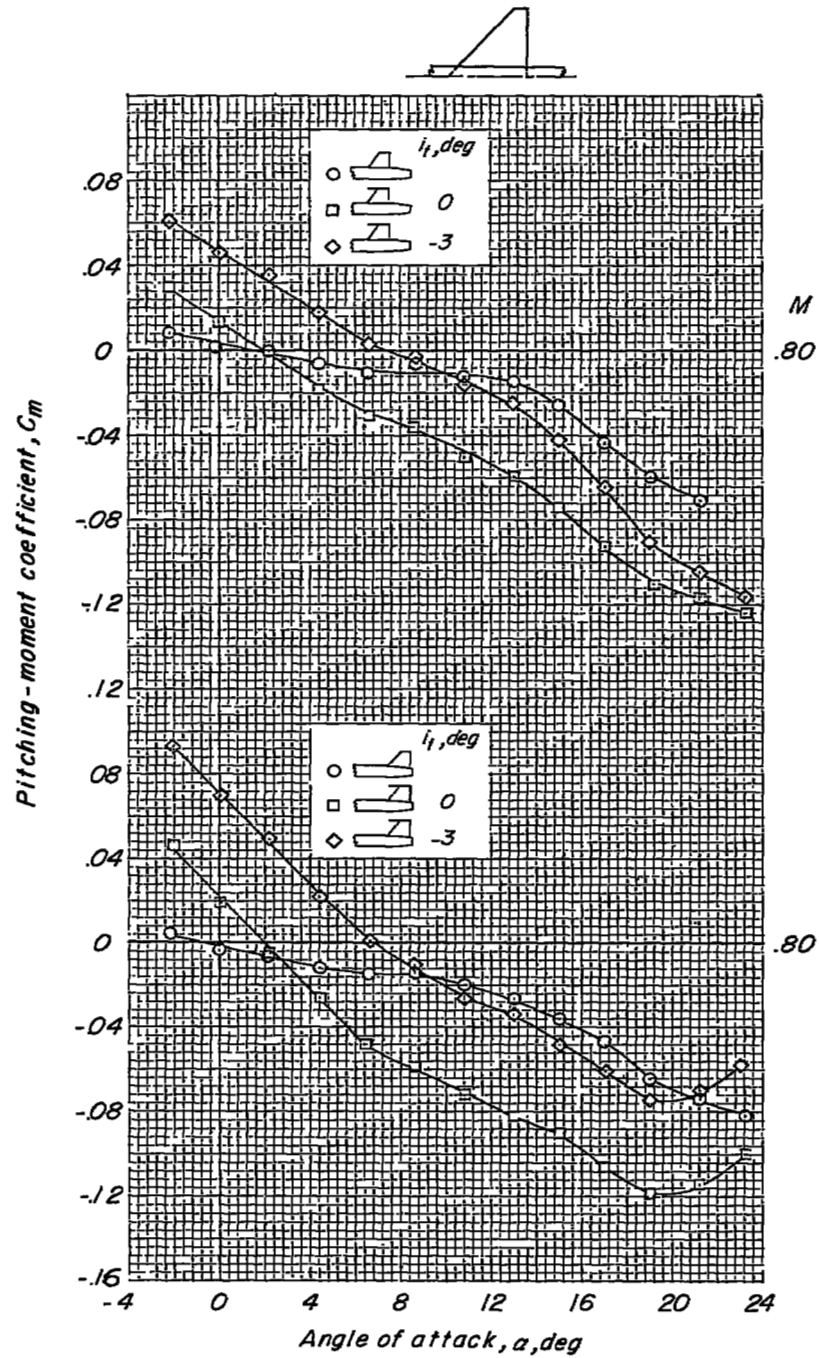
L-83149



### Afterbody Coordinates

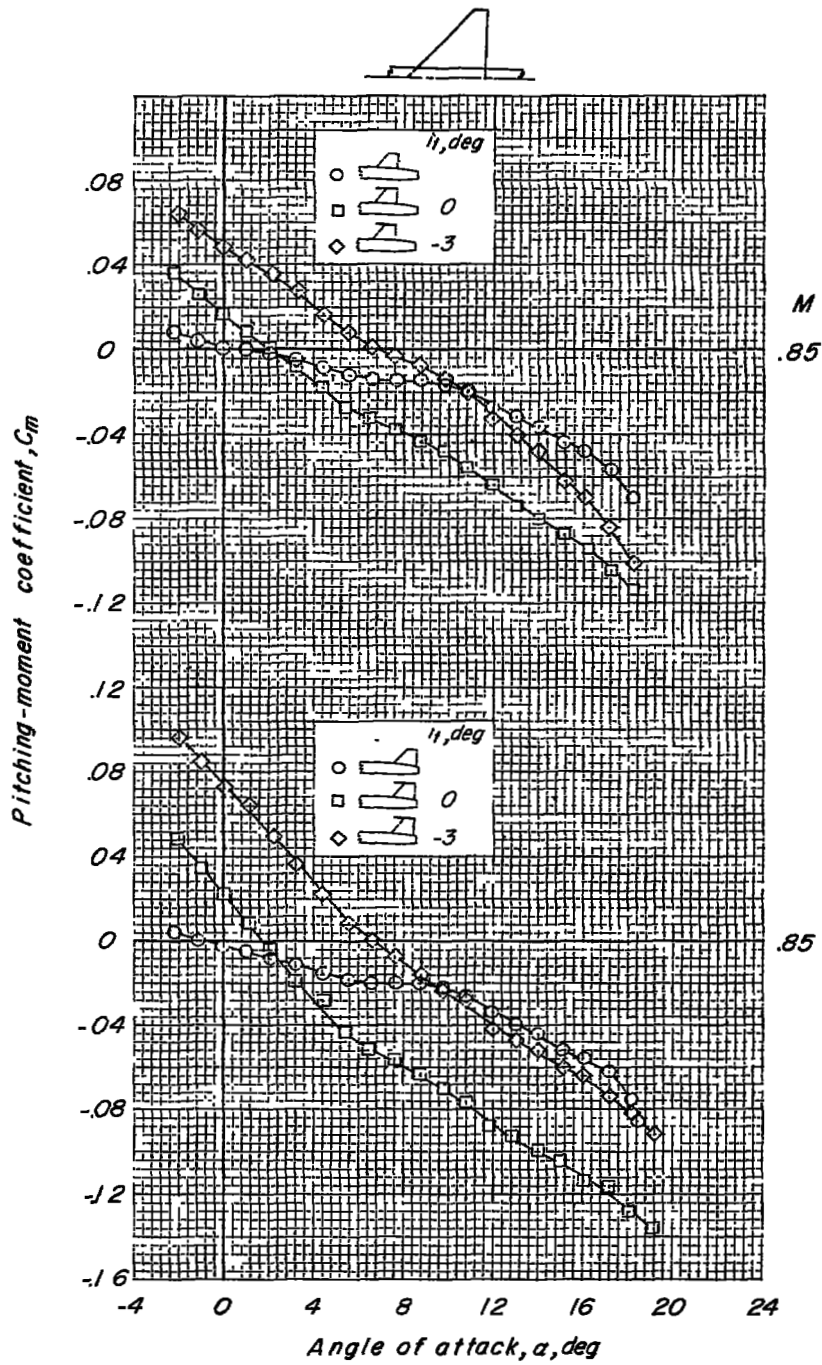
| $x/2$                  | $r/2$ |
|------------------------|-------|
| 0                      | .0456 |
| .0320                  | .0445 |
| .0639                  | .0427 |
| .1187                  | .0390 |
| Straight line<br>taper |       |
| .2460                  | .0301 |

Figure 4.- Fuselage dimensions in inches; fineness ratio, 10.94.



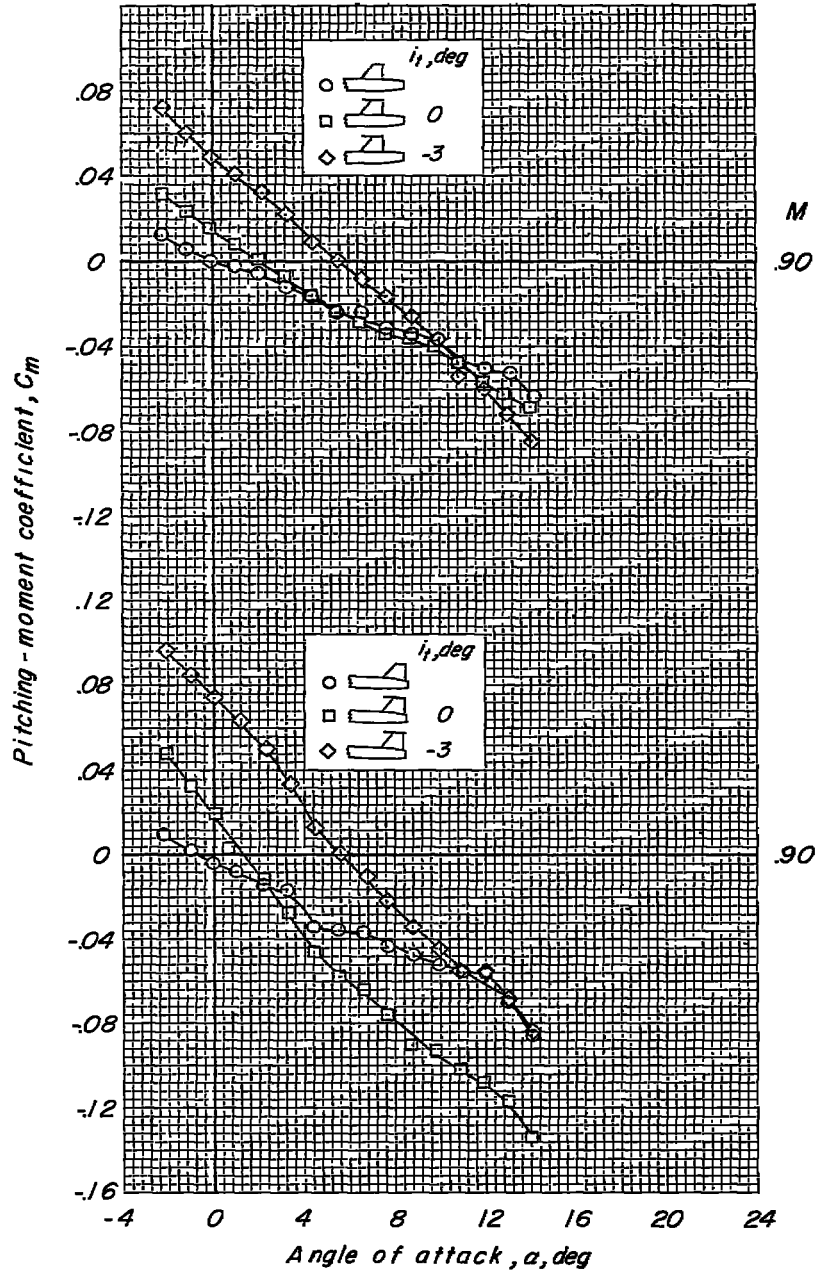
(a)  $M = 0.80$ .

Figure 5.- Variation of pitching-moment coefficient with angle of attack for the model having a high tail and cropped-delta wing.



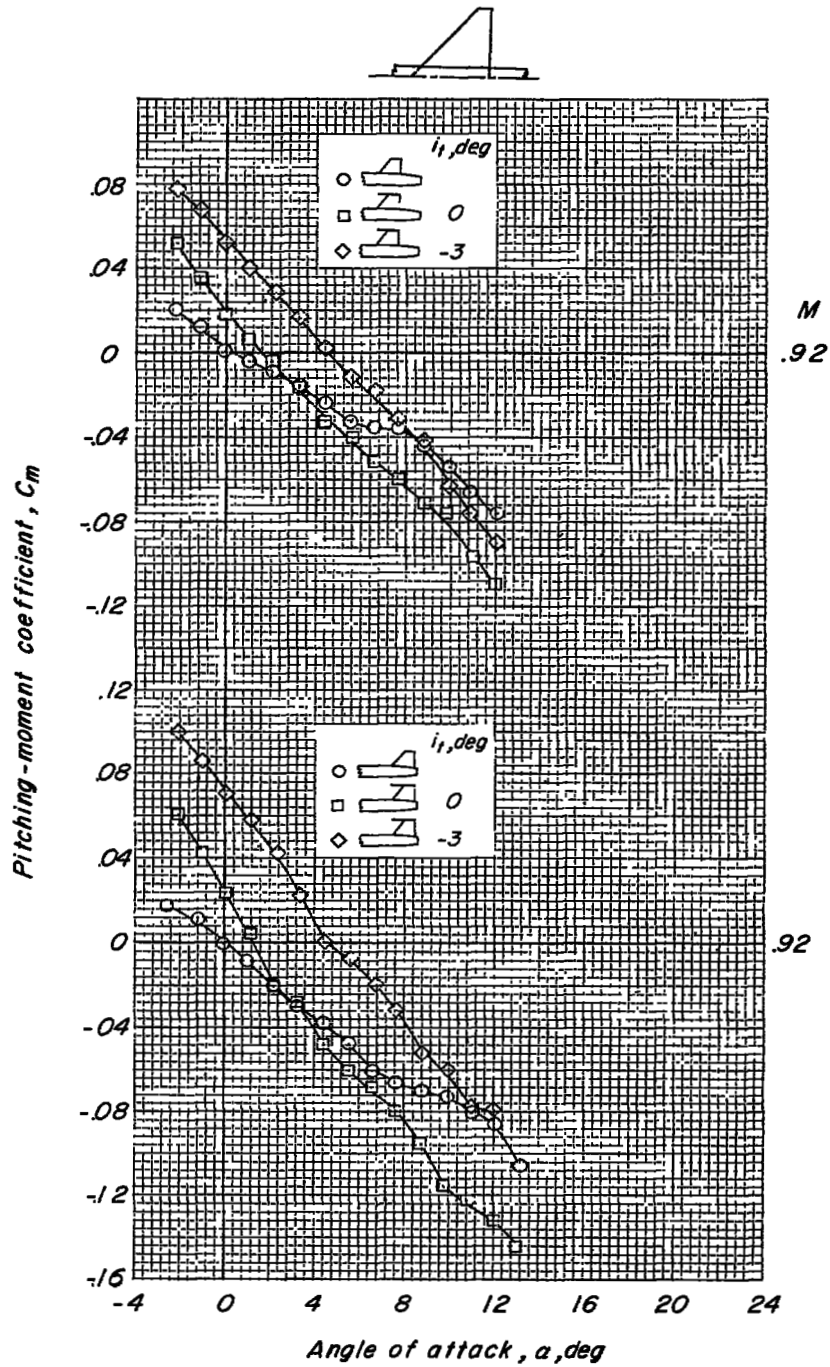
(b)  $M = 0.85$ .

Figure 5.- Continued.



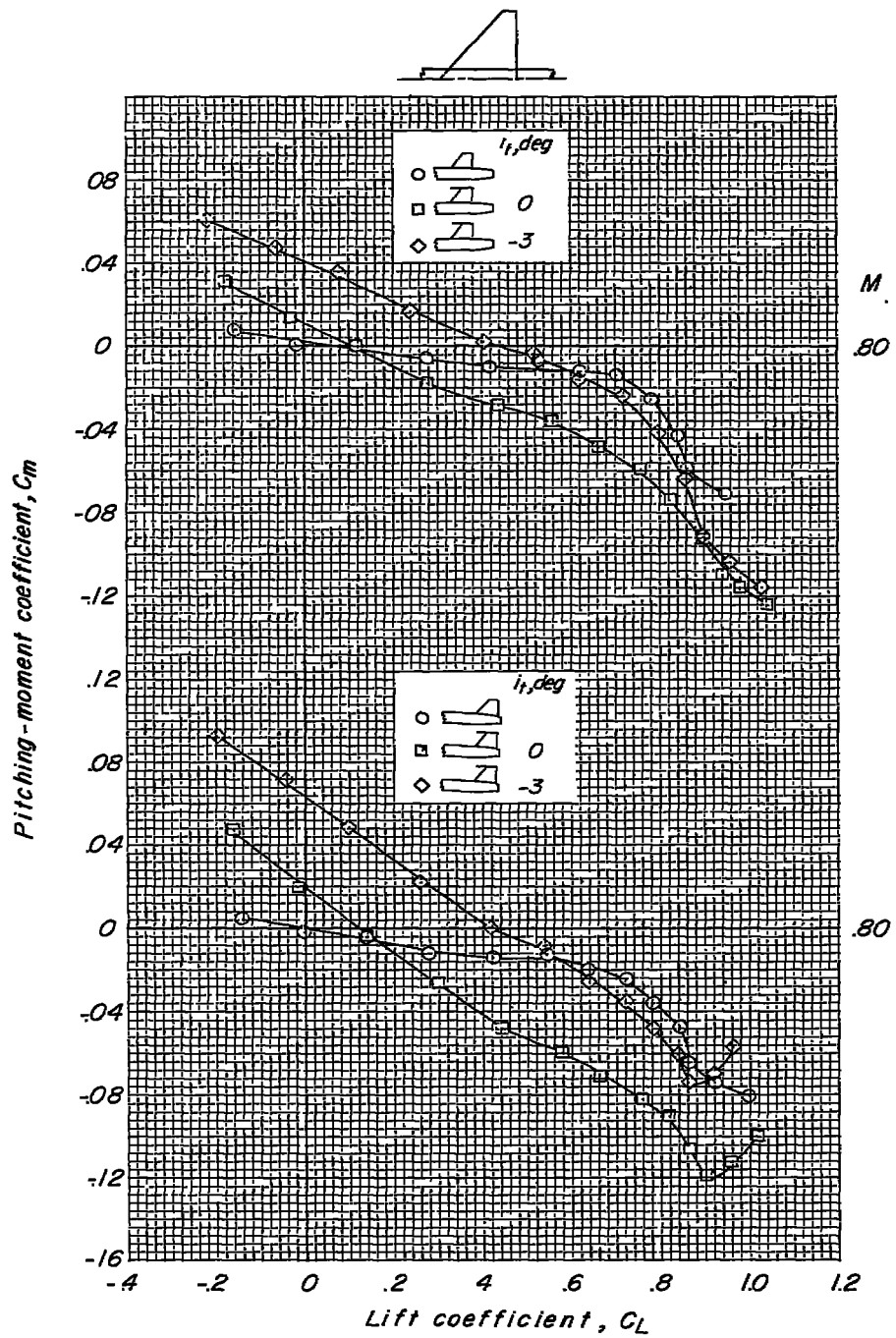
(c)  $M = 0.90$ .

Figure 5.- Continued.



(d)  $M = 0.92$ .

Figure 5.- Concluded.



(a)  $M = 0.80$ .

Figure 6.- Variation of pitching-moment coefficient with lift coefficient for the model having a high tail and cropped-delta wing.

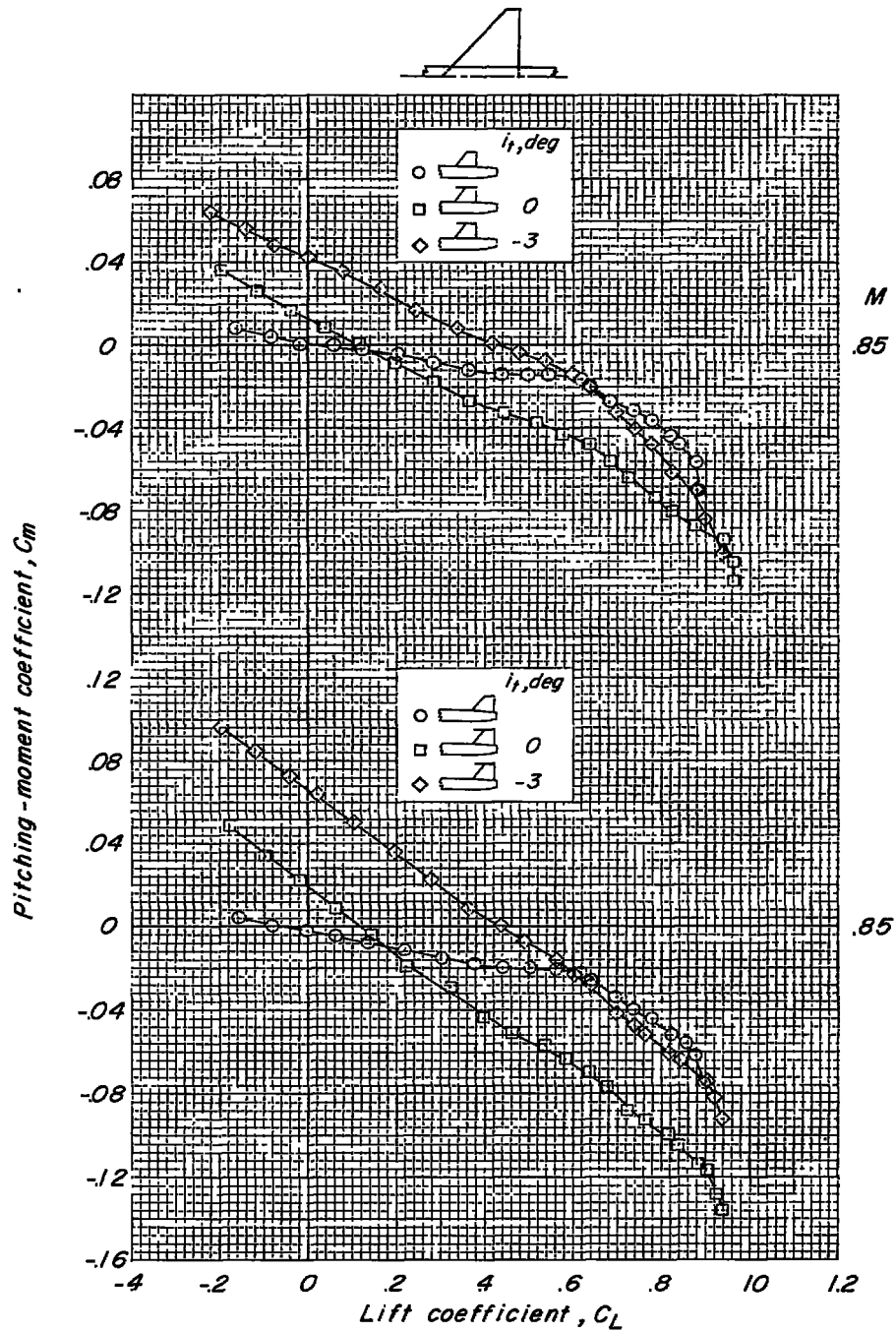
(b)  $M = 0.85$ .

Figure 6.- Continued.

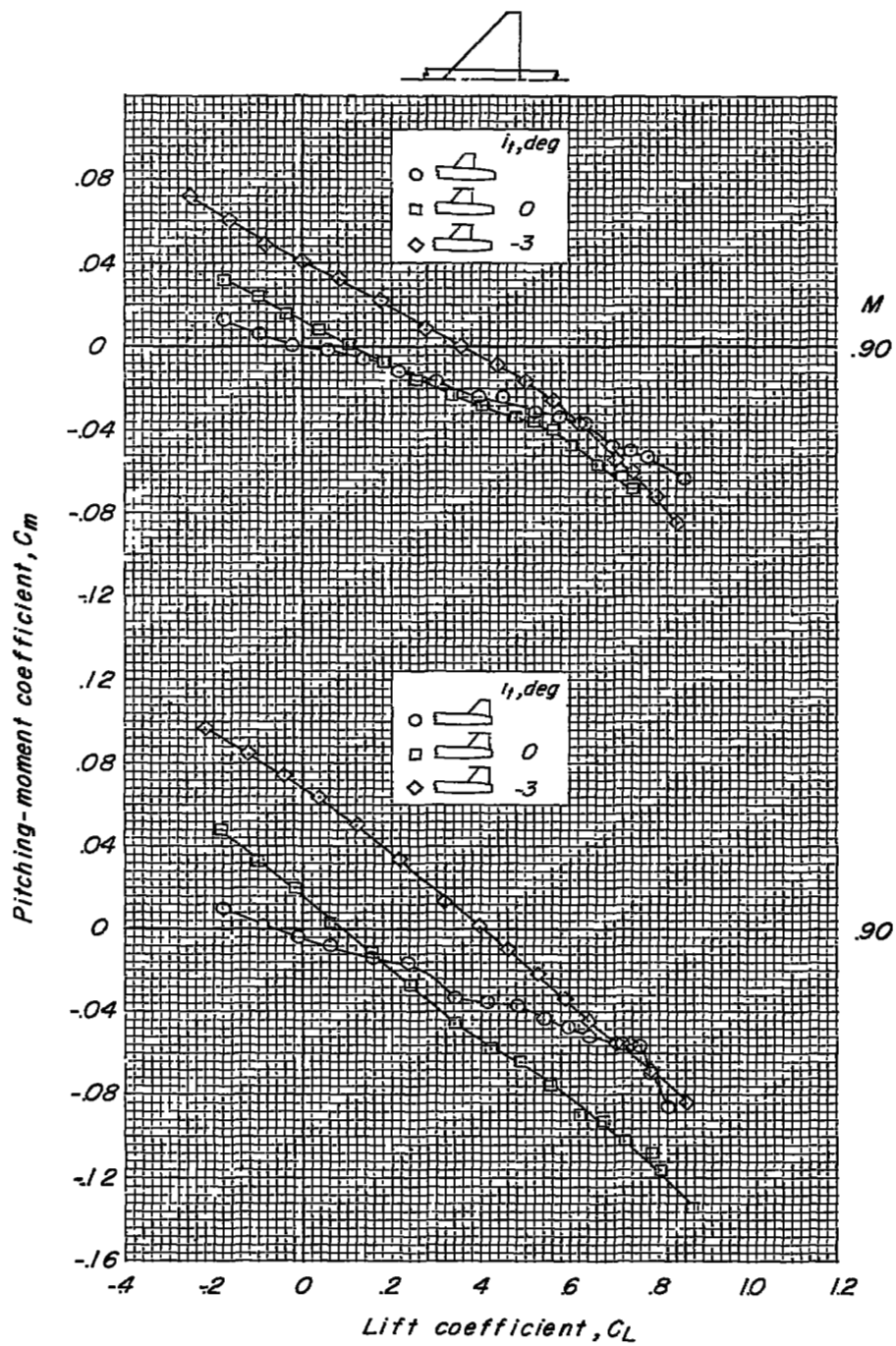
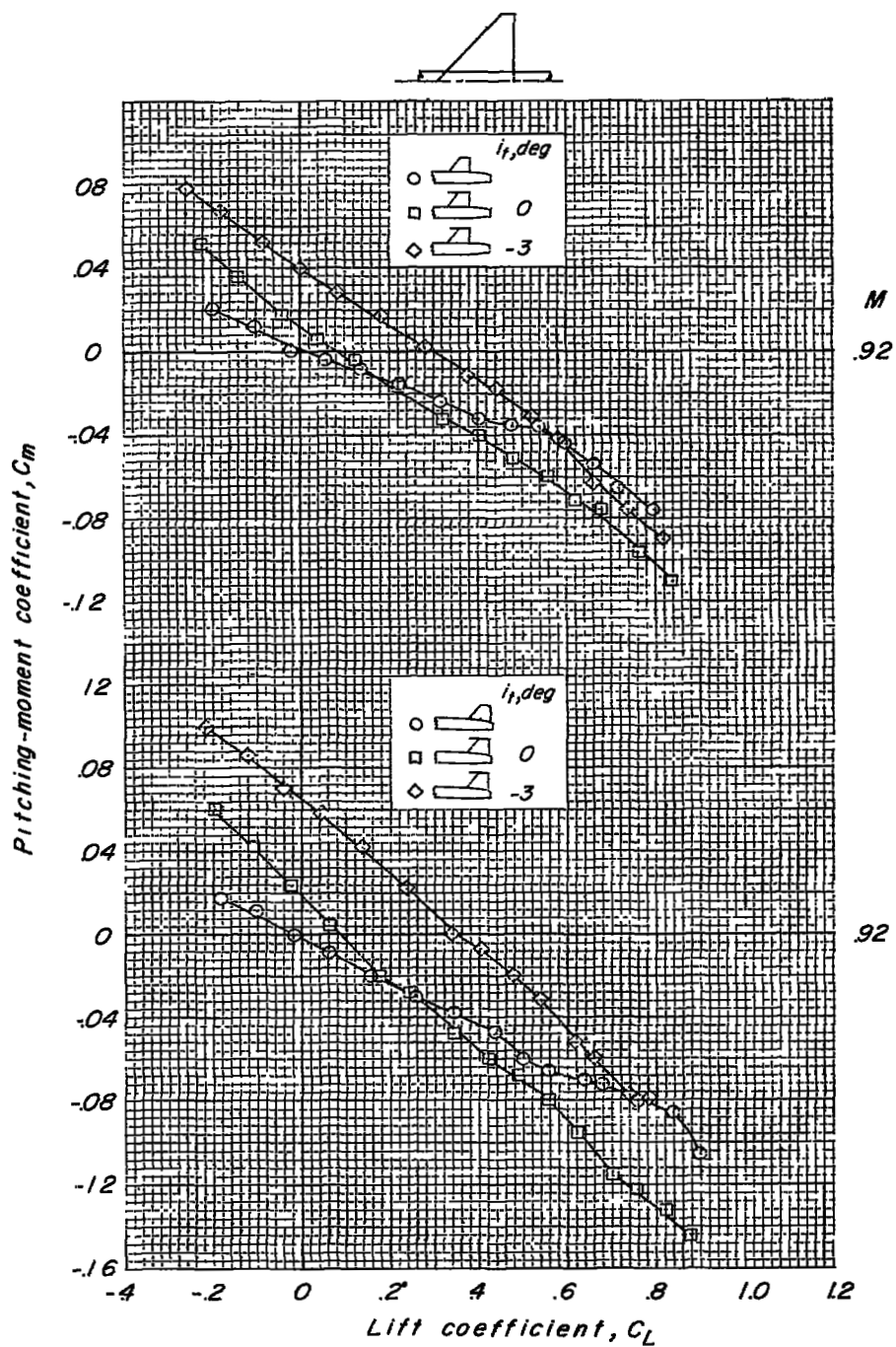
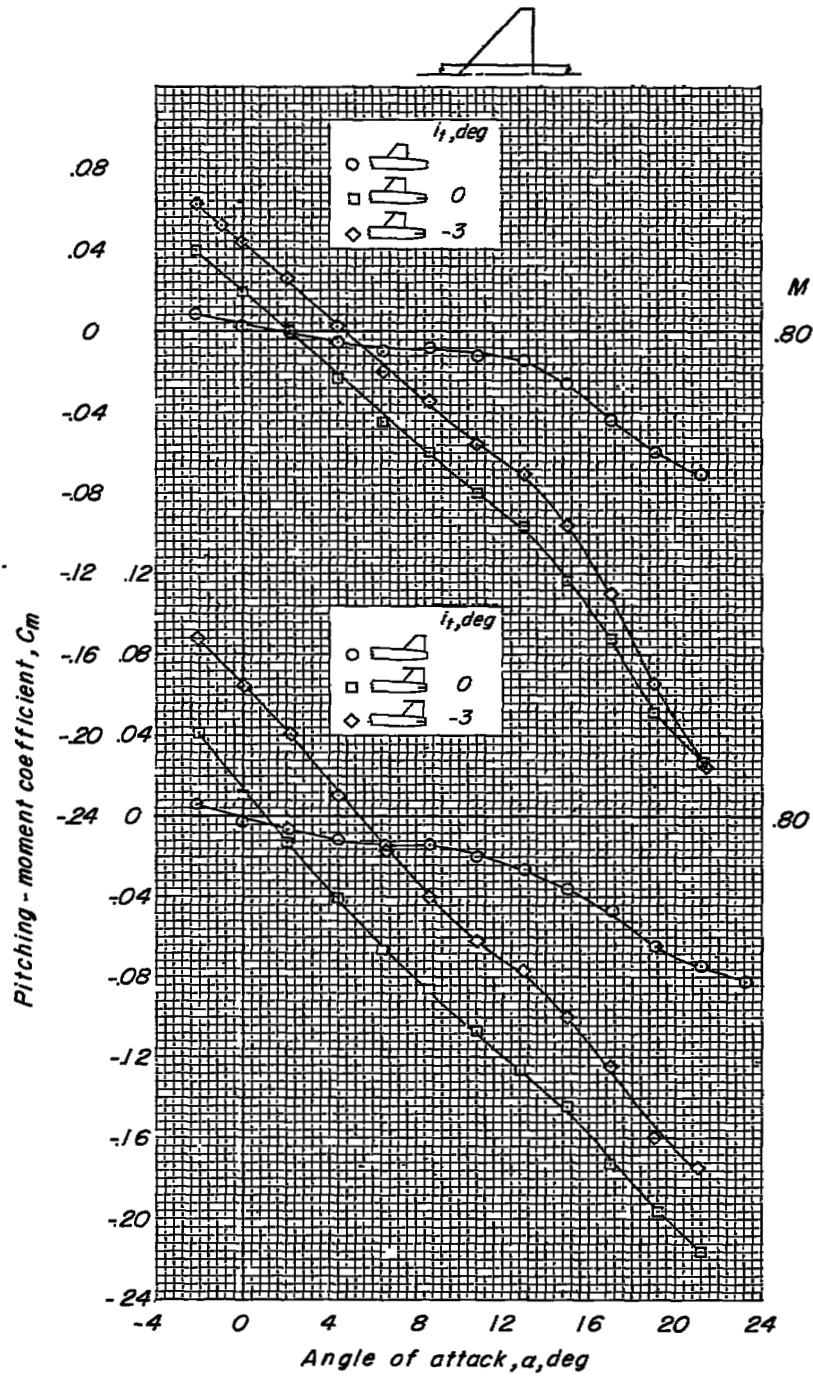
(c)  $M = 0.90$ .

Figure 6.- Continued.



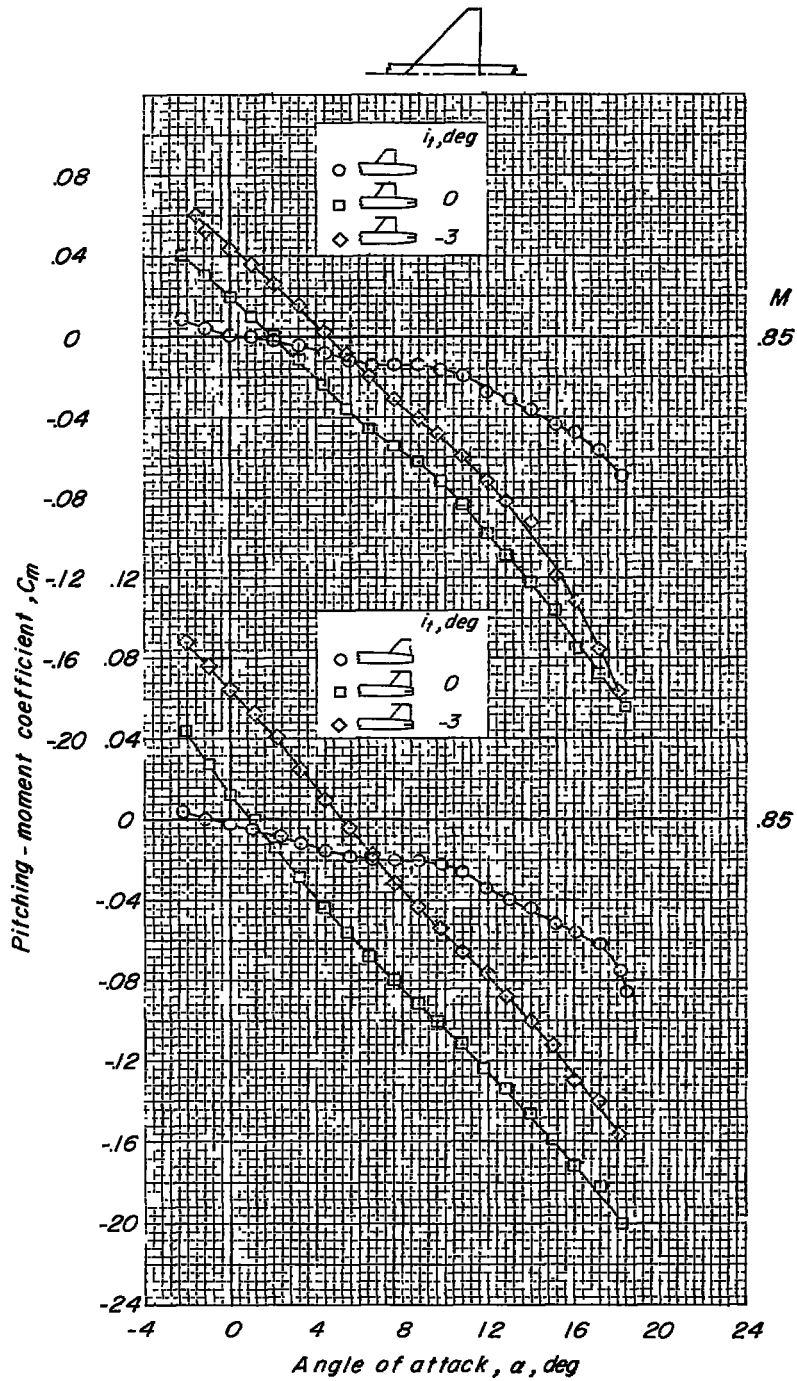
(d)  $M = 0.92$ .

Figure 6.- Concluded.



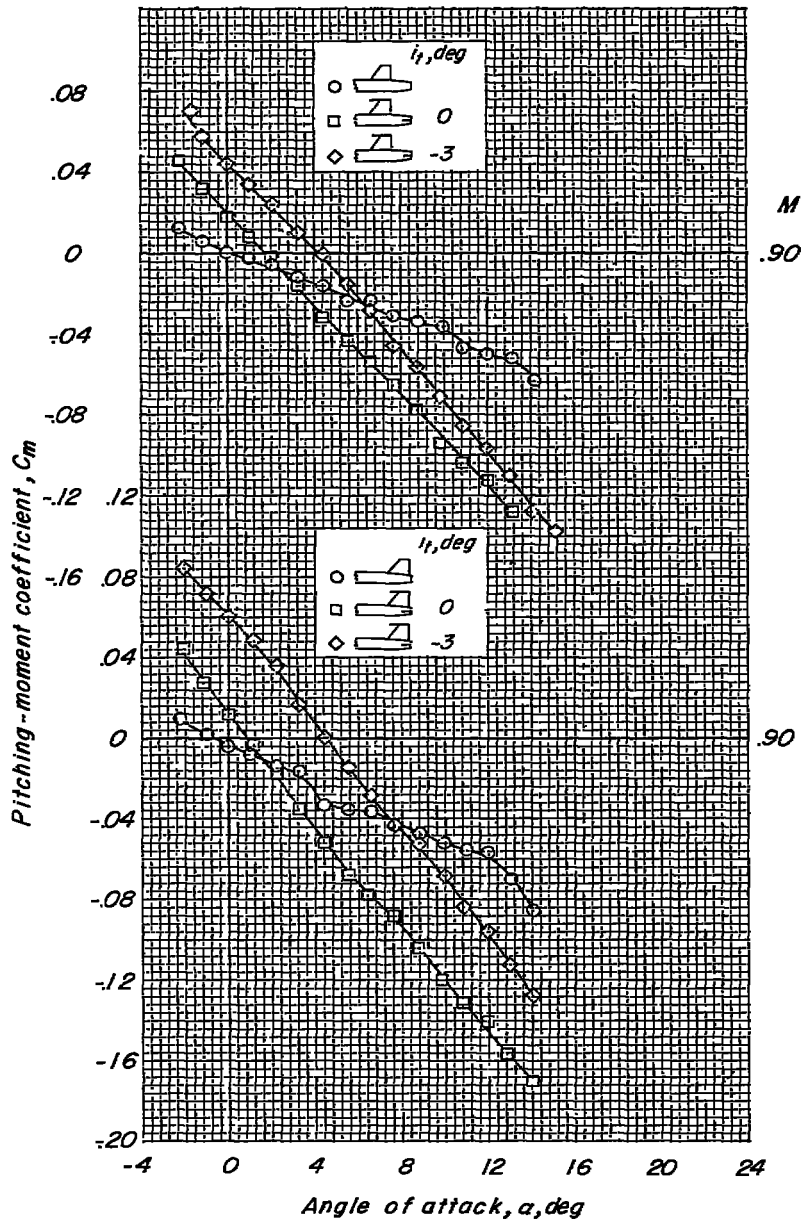
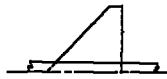
(a) M = 0.80.

Figure 7.- Variation of pitching-moment coefficient with angle of attack for the model with a bitail and cropped-delta wing.



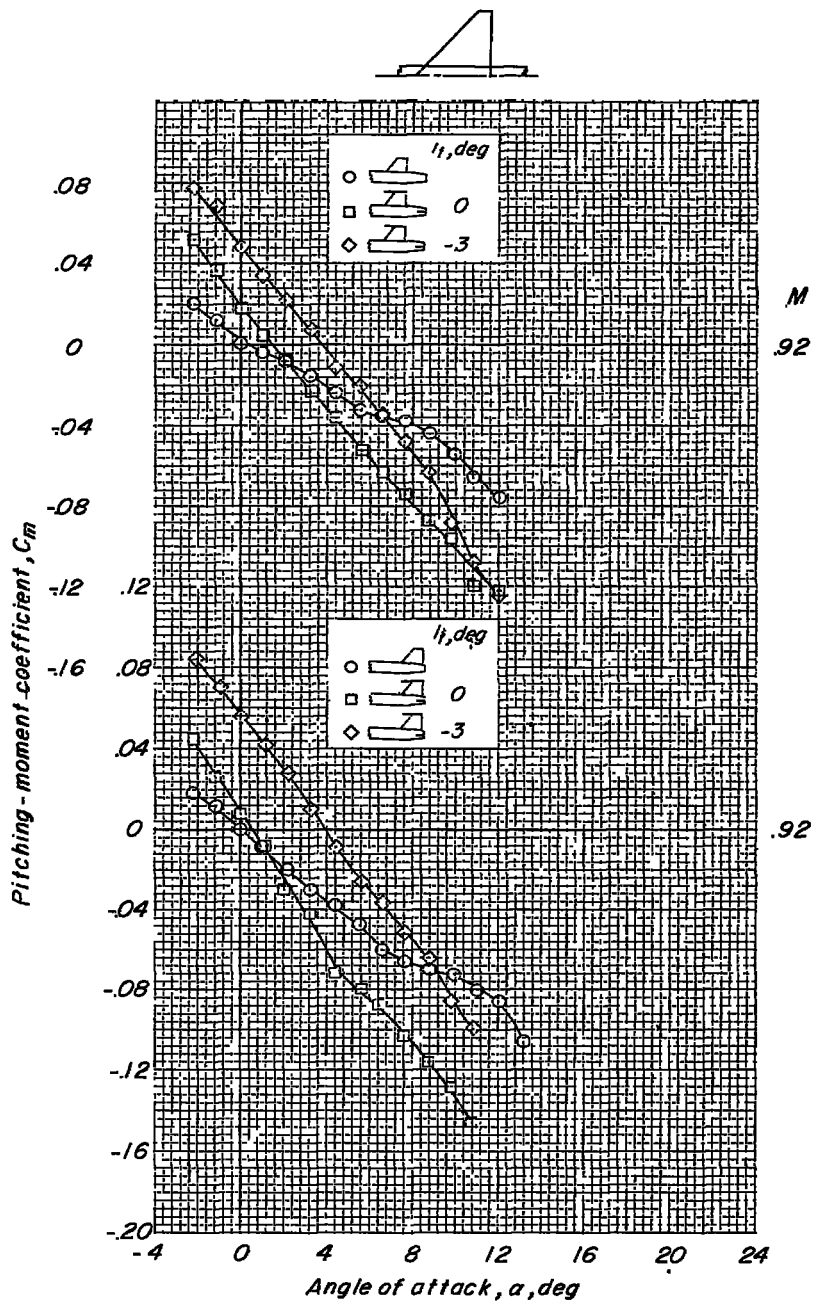
(b)  $M = 0.85$ .

Figure 7.- Continued.



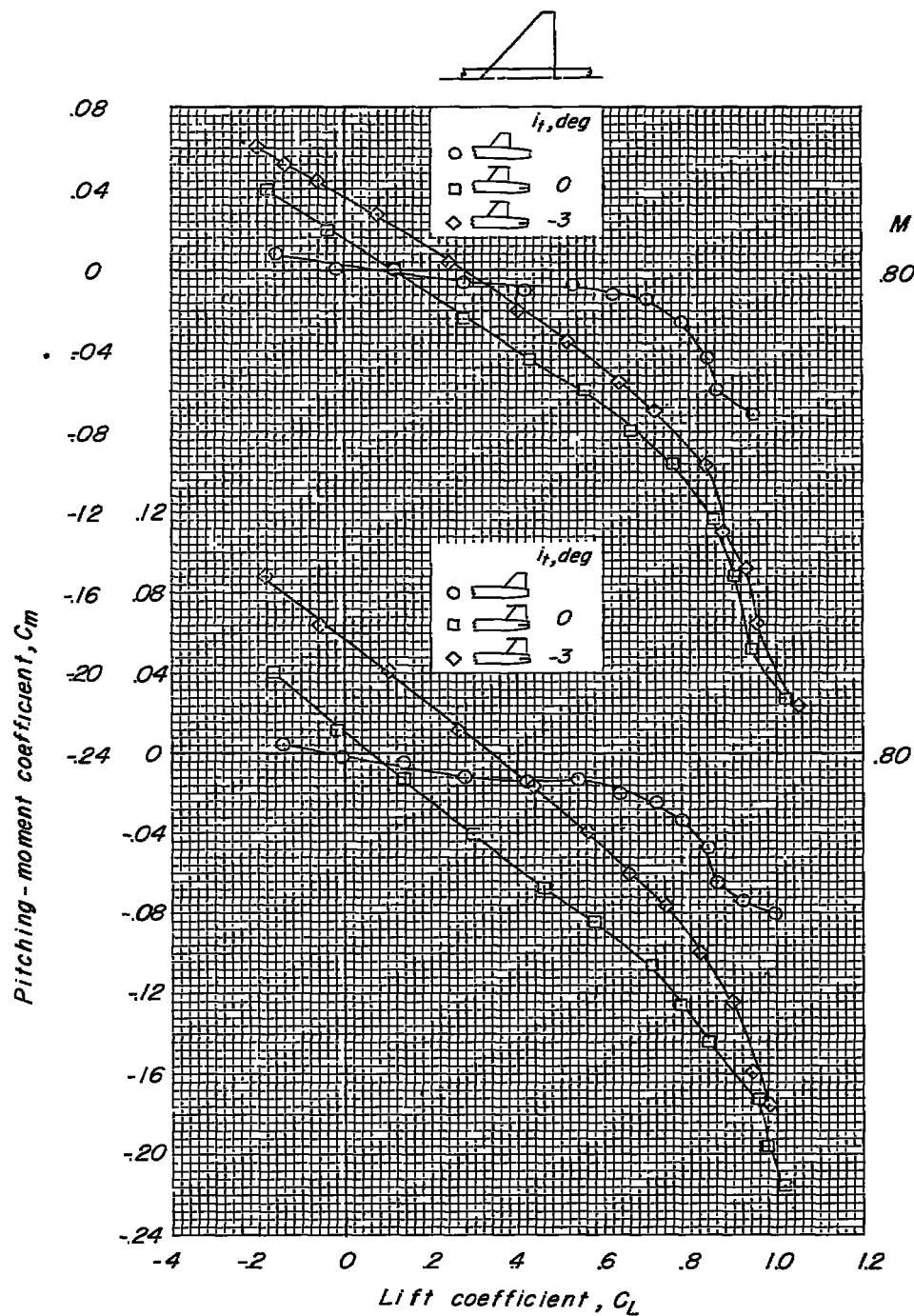
(c)  $M = 0.90$ .

Figure 7.- Continued.



(d)  $M = 0.92$ .

Figure 7.- Concluded.



(a)  $M = 0.80$ .

Figure 8.- Variation of pitching-moment coefficient with lift coefficient for the model with a bitail and cropped-delta wing.

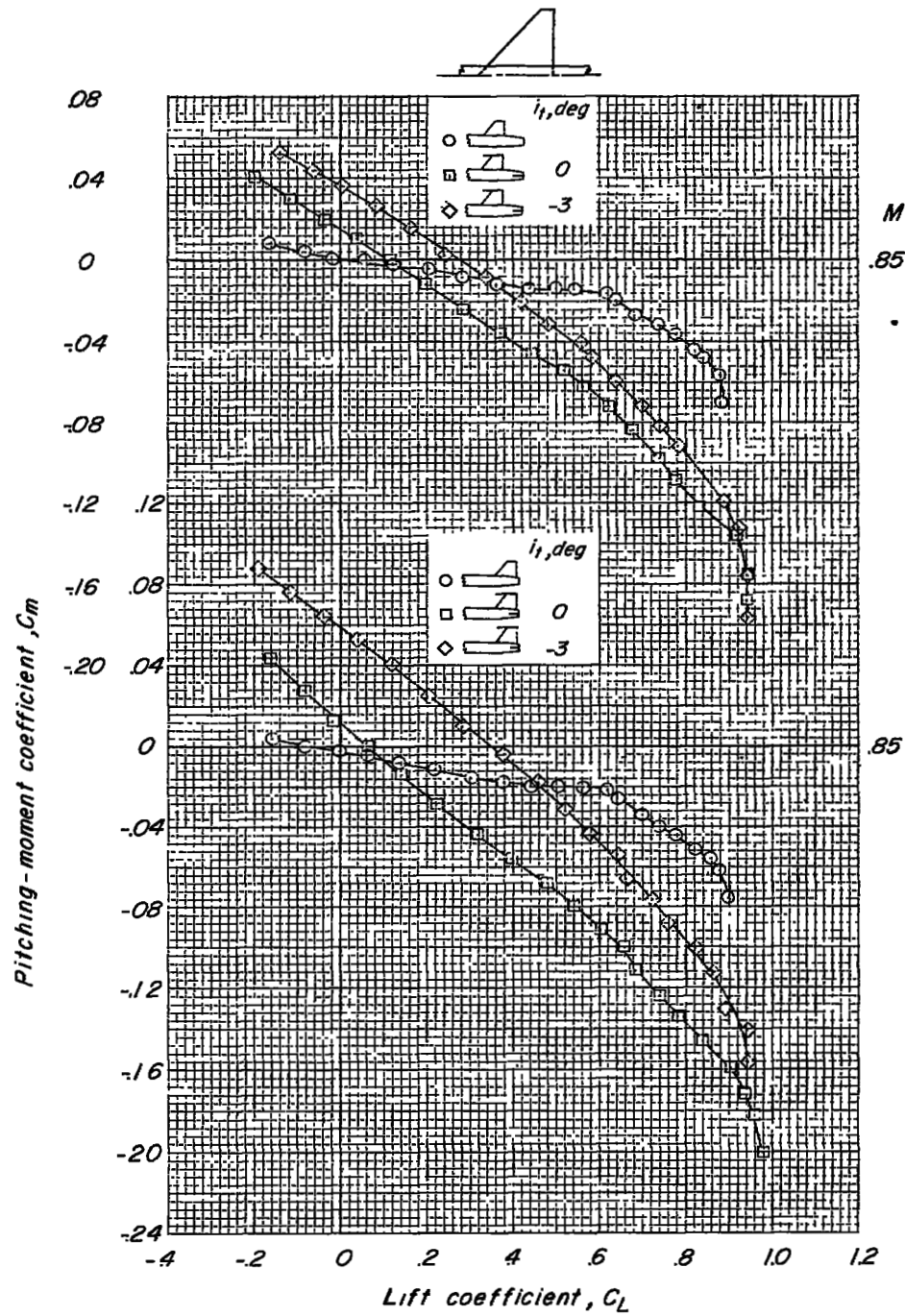
(b)  $M = 0.85$ .

Figure 8.- Continued.

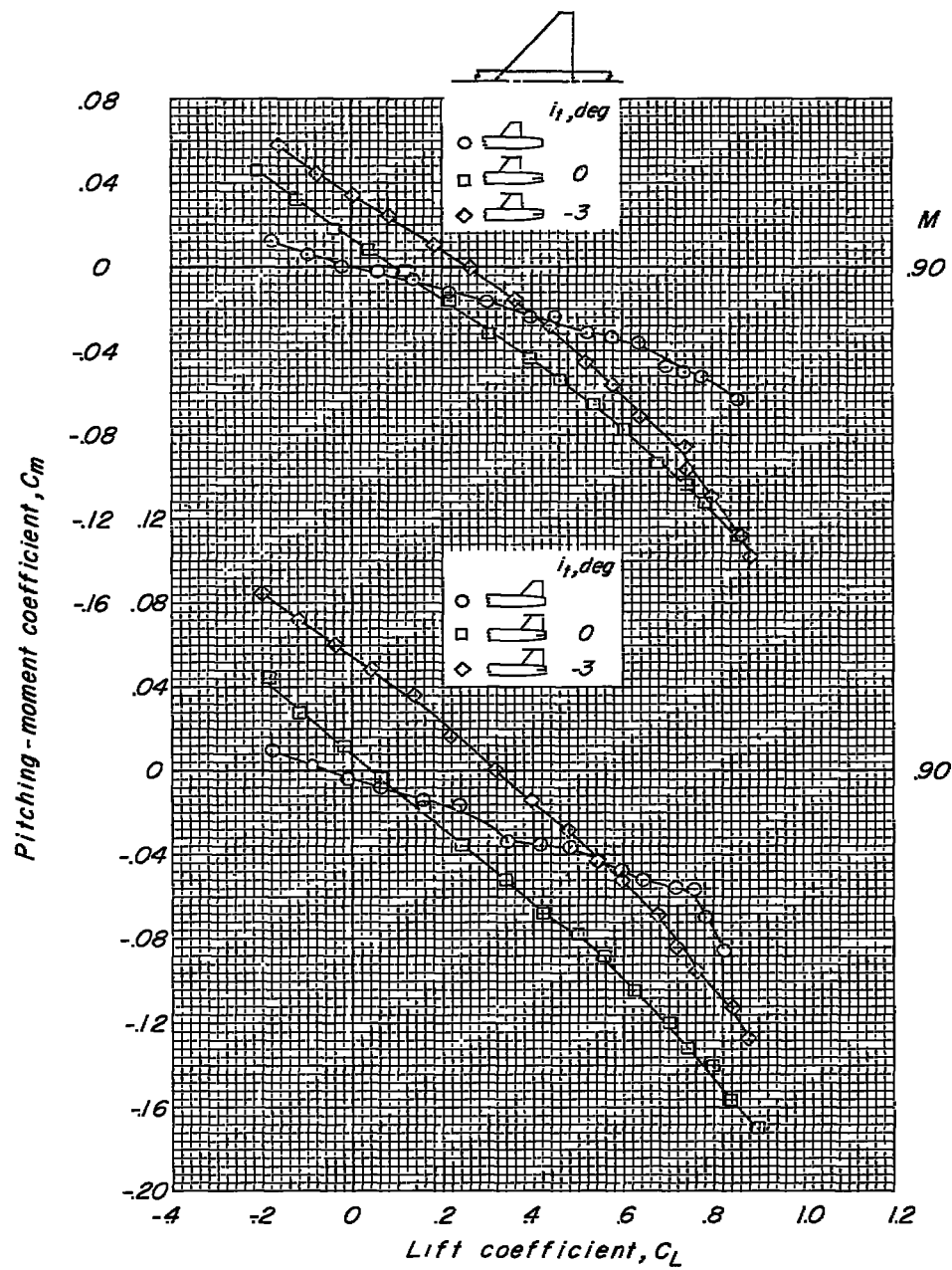
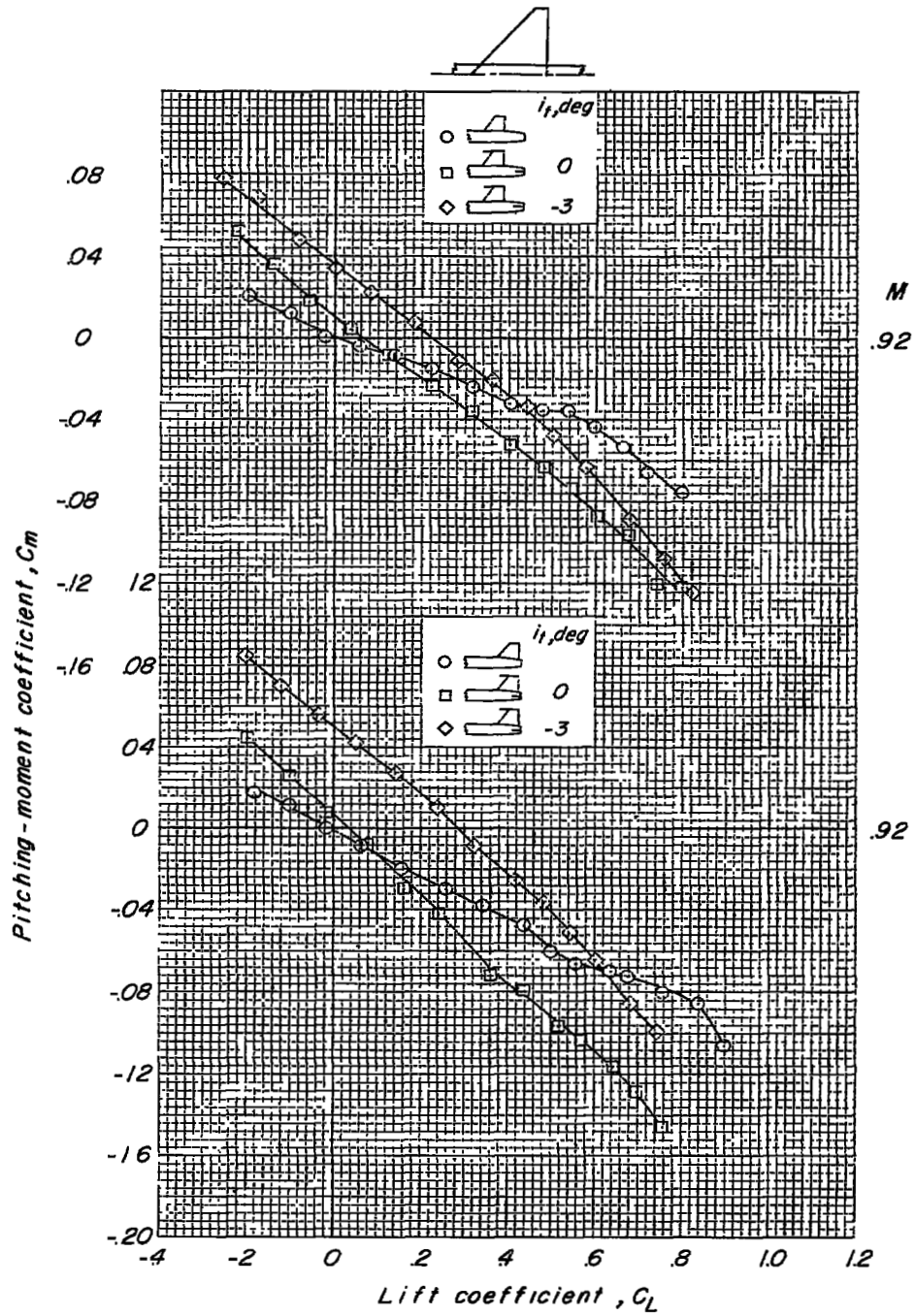
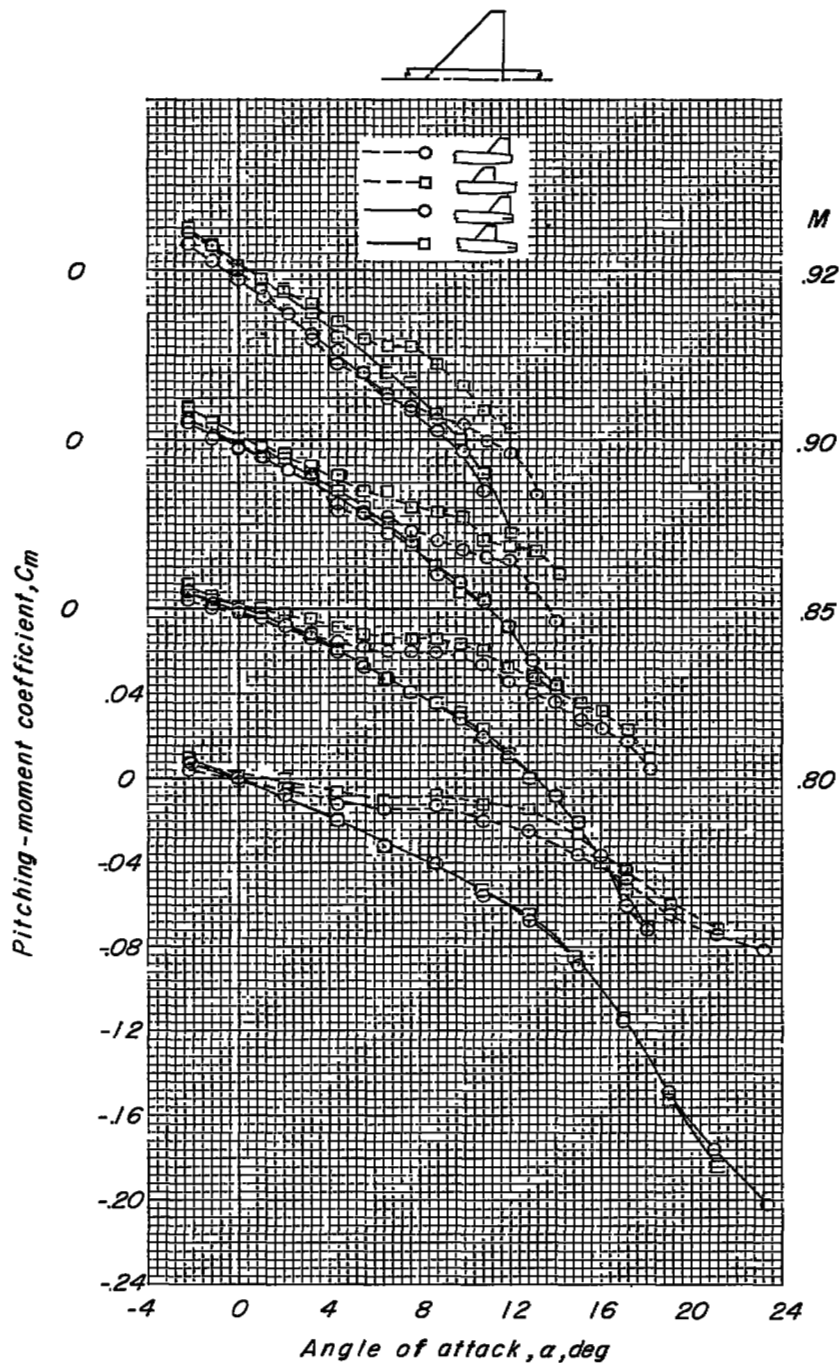
(c)  $M = 0.90$ .

Figure 8.- Continued.



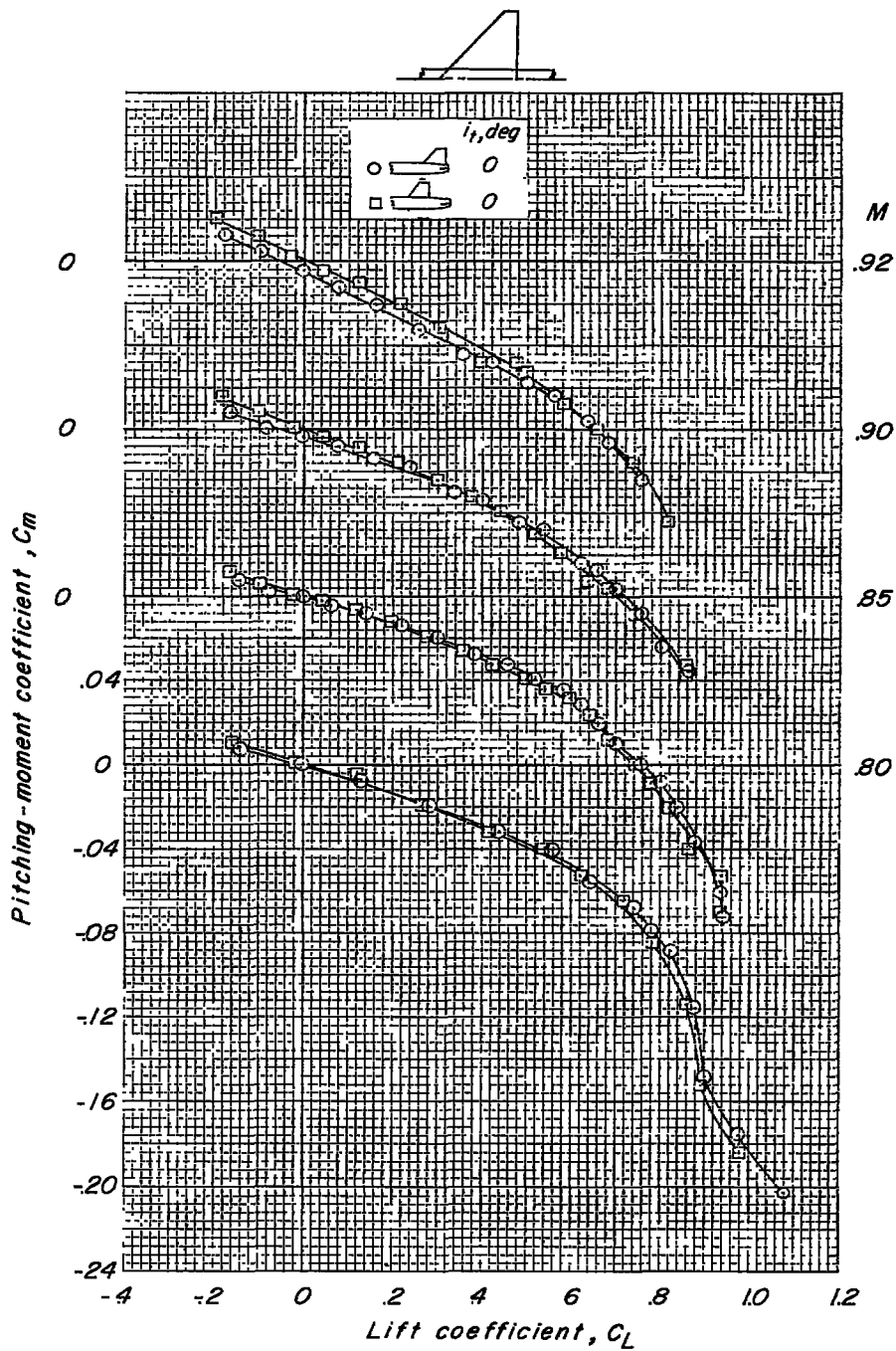
(a)  $M = 0.92$ .

Figure 8.- Concluded.



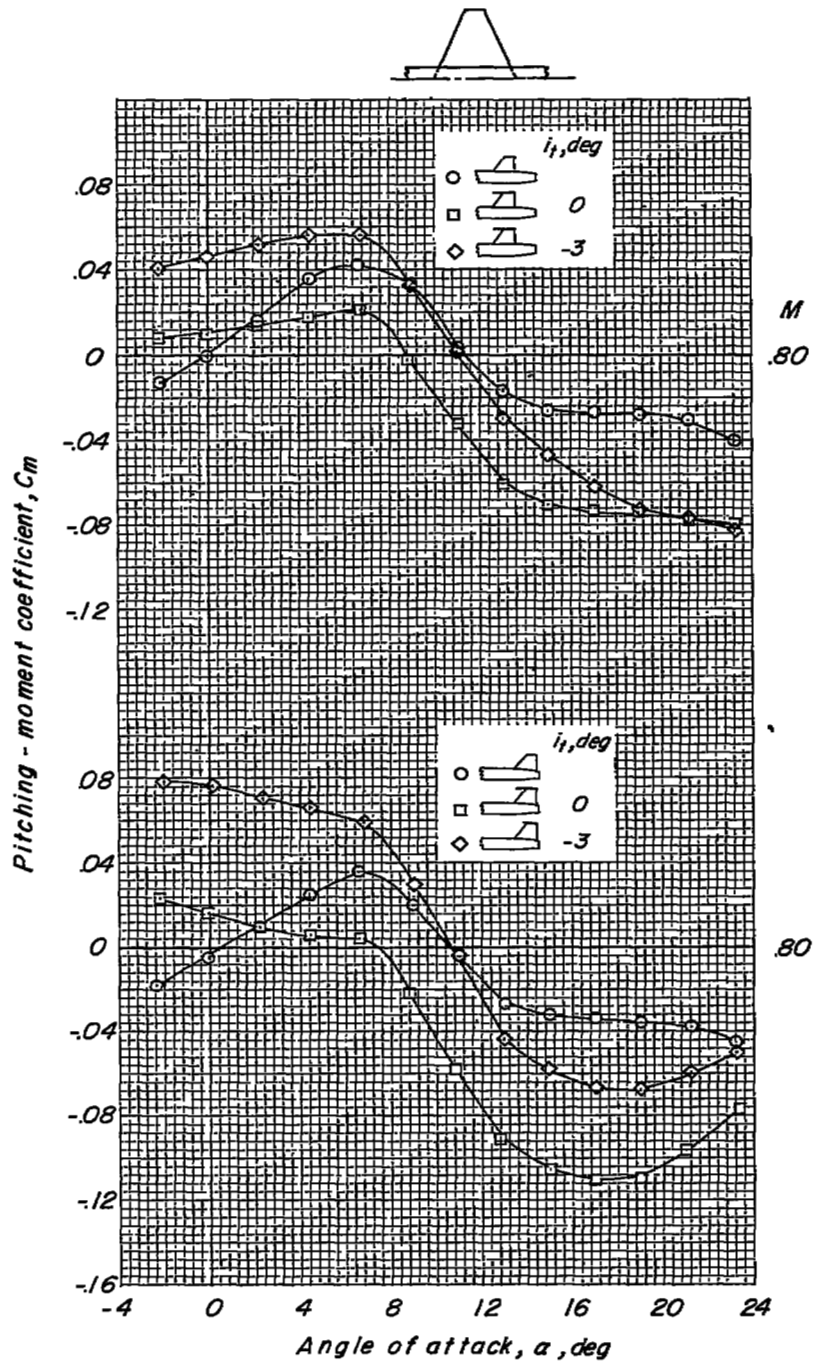
(a)  $C_m$  plotted against  $\alpha$ .

Figure 9.- Variation of pitching-moment coefficient for the model with a low tail and cropped-delta wing.



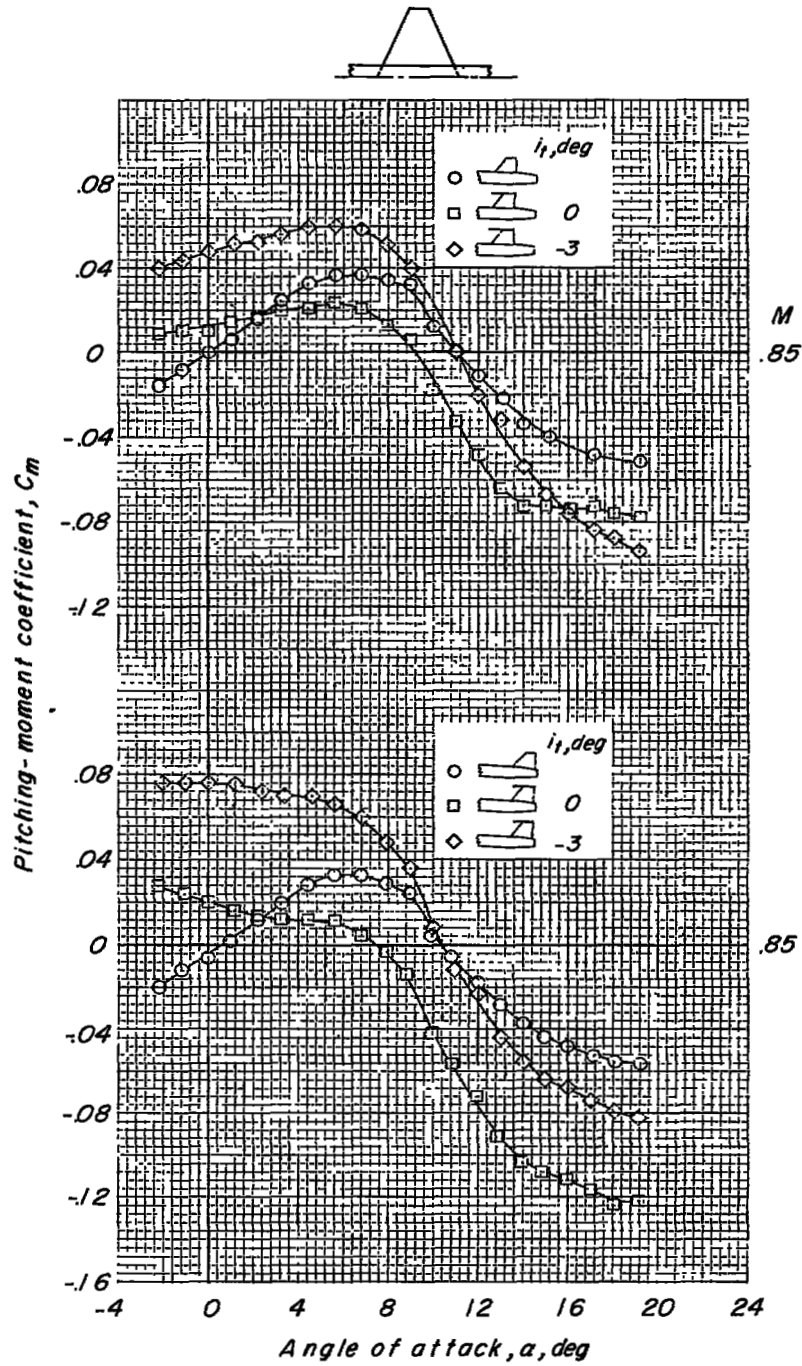
(b)  $C_m$  plotted against  $C_L$ .

Figure 9.- Concluded.



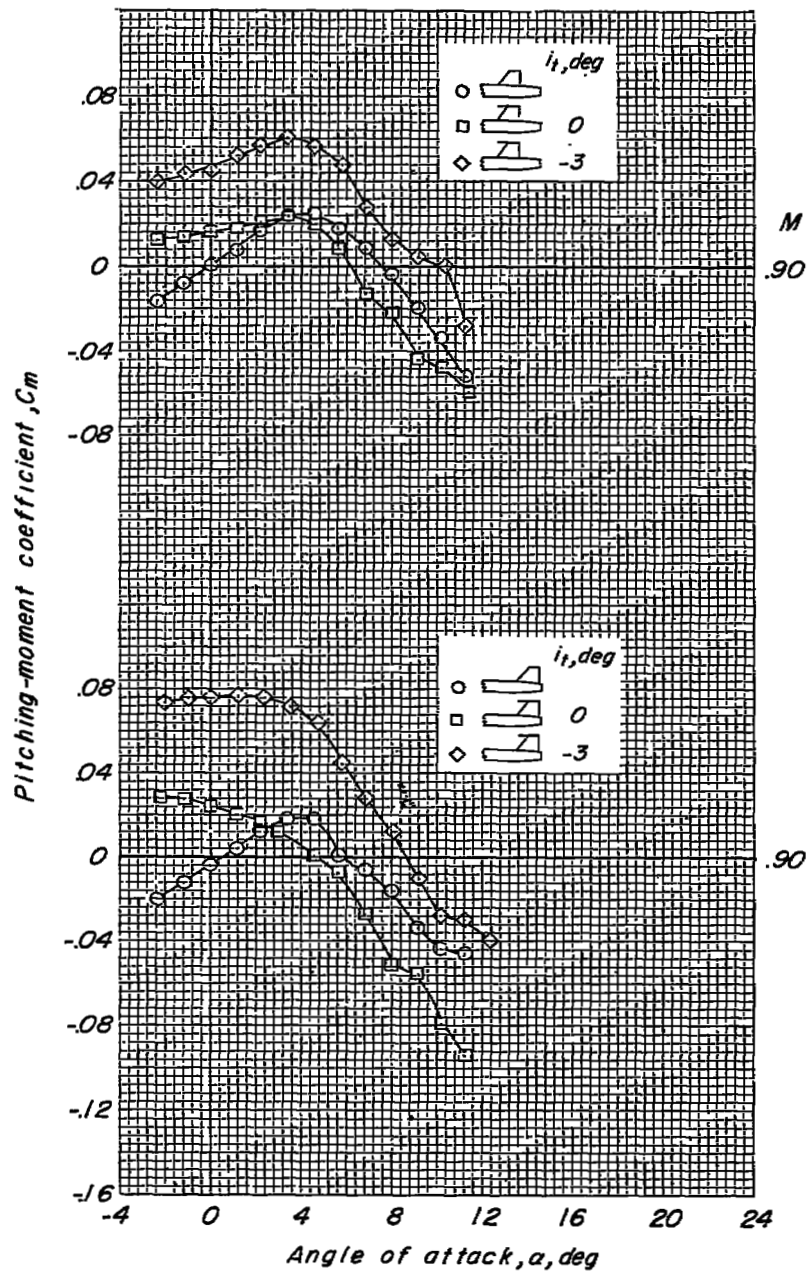
(a)  $M = 0.80$ .

Figure 10.- Variation of pitching-moment coefficient with angle of attack for the model with a high tail and unswept wing.



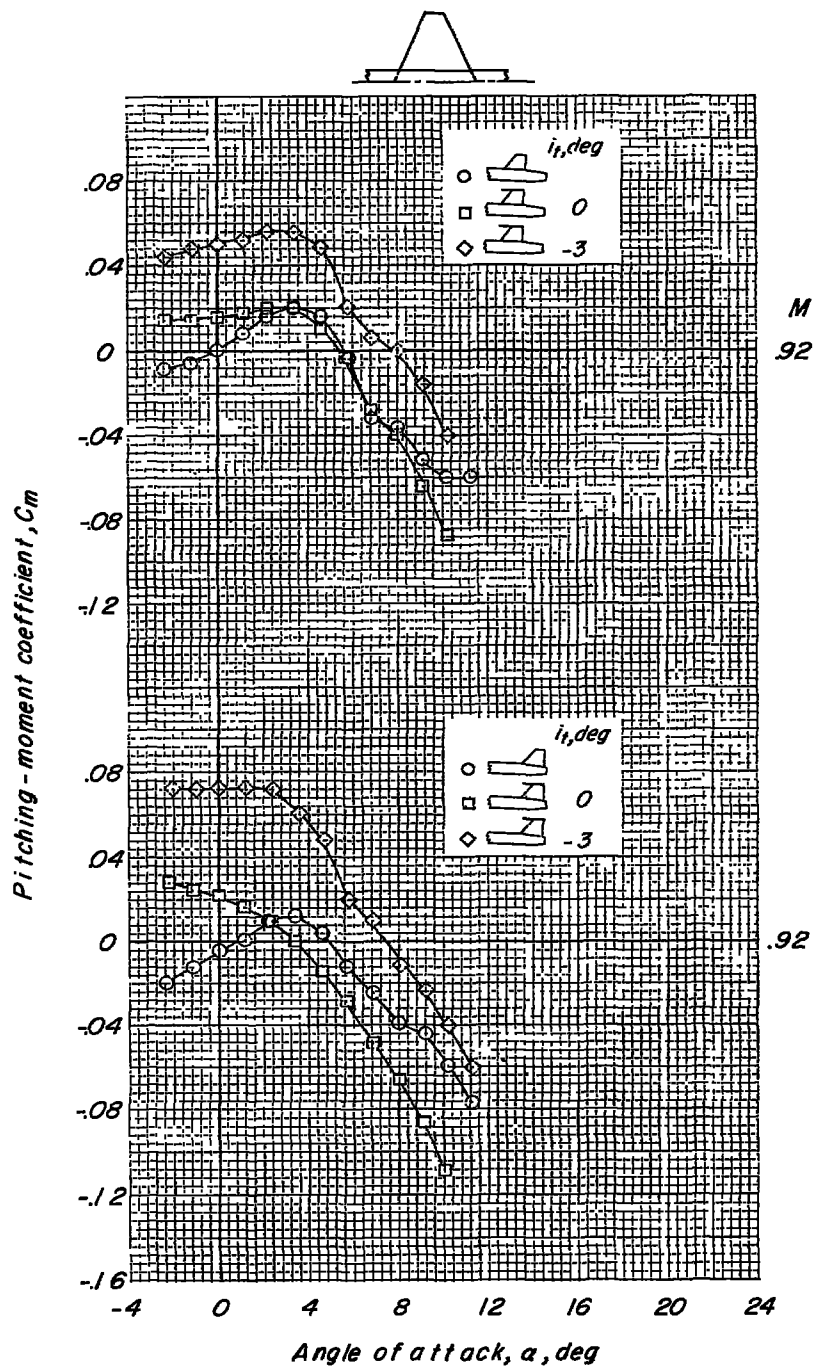
(b)  $M = 0.85$ .

Figure 10.- Continued.



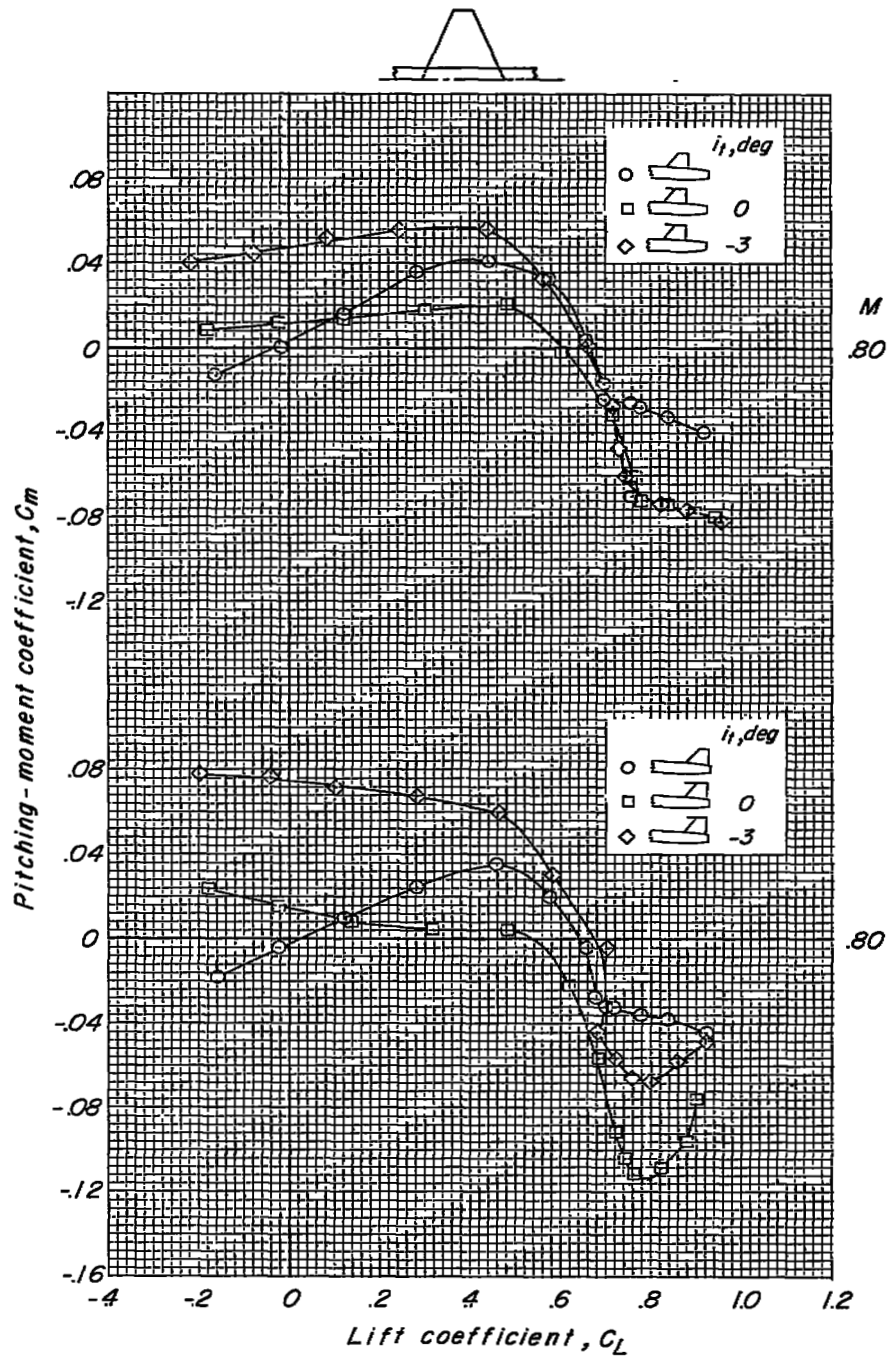
(c)  $M = 0.90$ .

Figure 10.- Continued.



(a)  $M = 0.92$ .

Figure 10.- Concluded.



(a)  $M = 0.80$ .

Figure 11.- Variation of pitching-moment coefficient with lift coefficient for the model with a high tail and unswept wing.

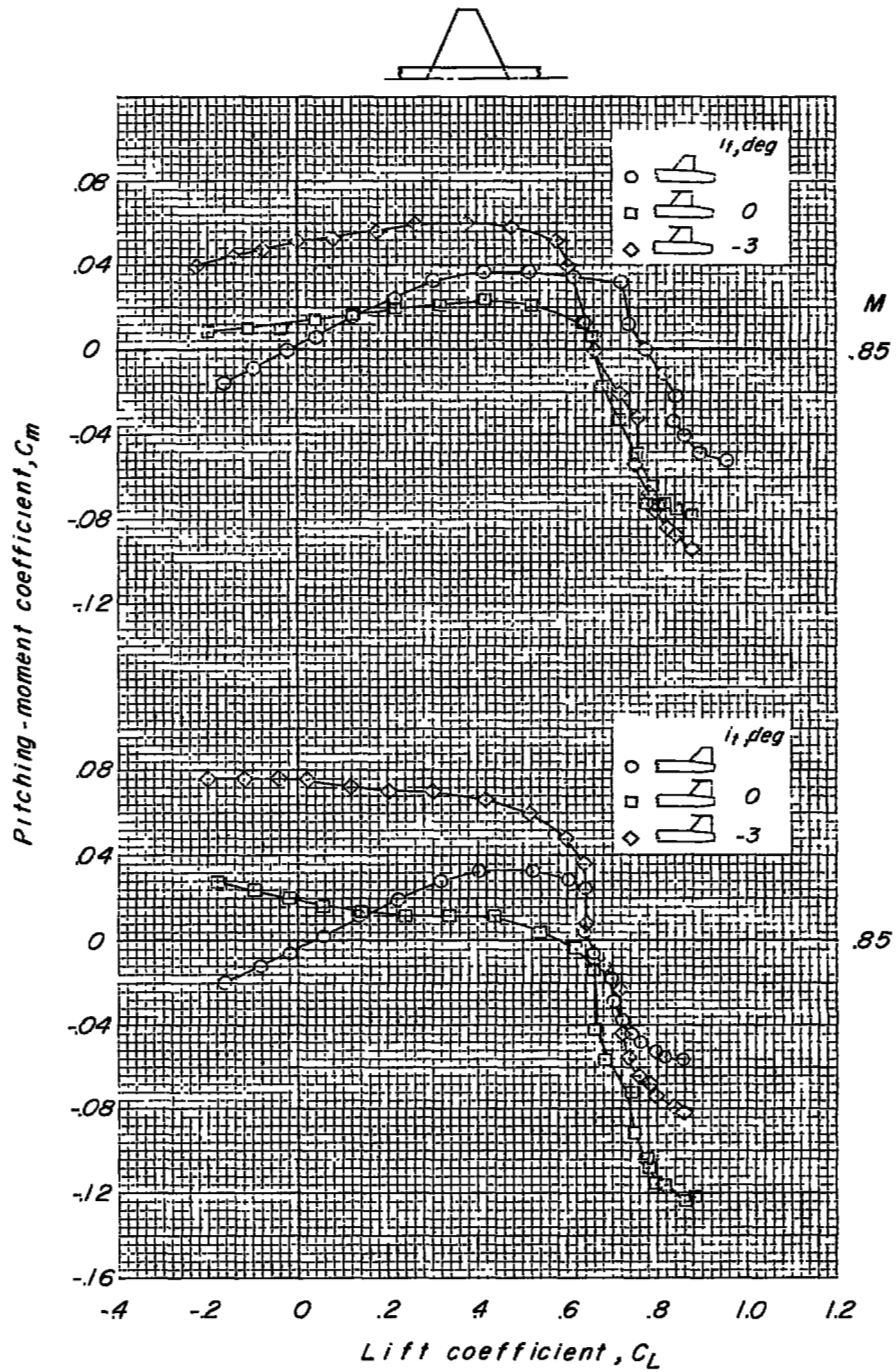
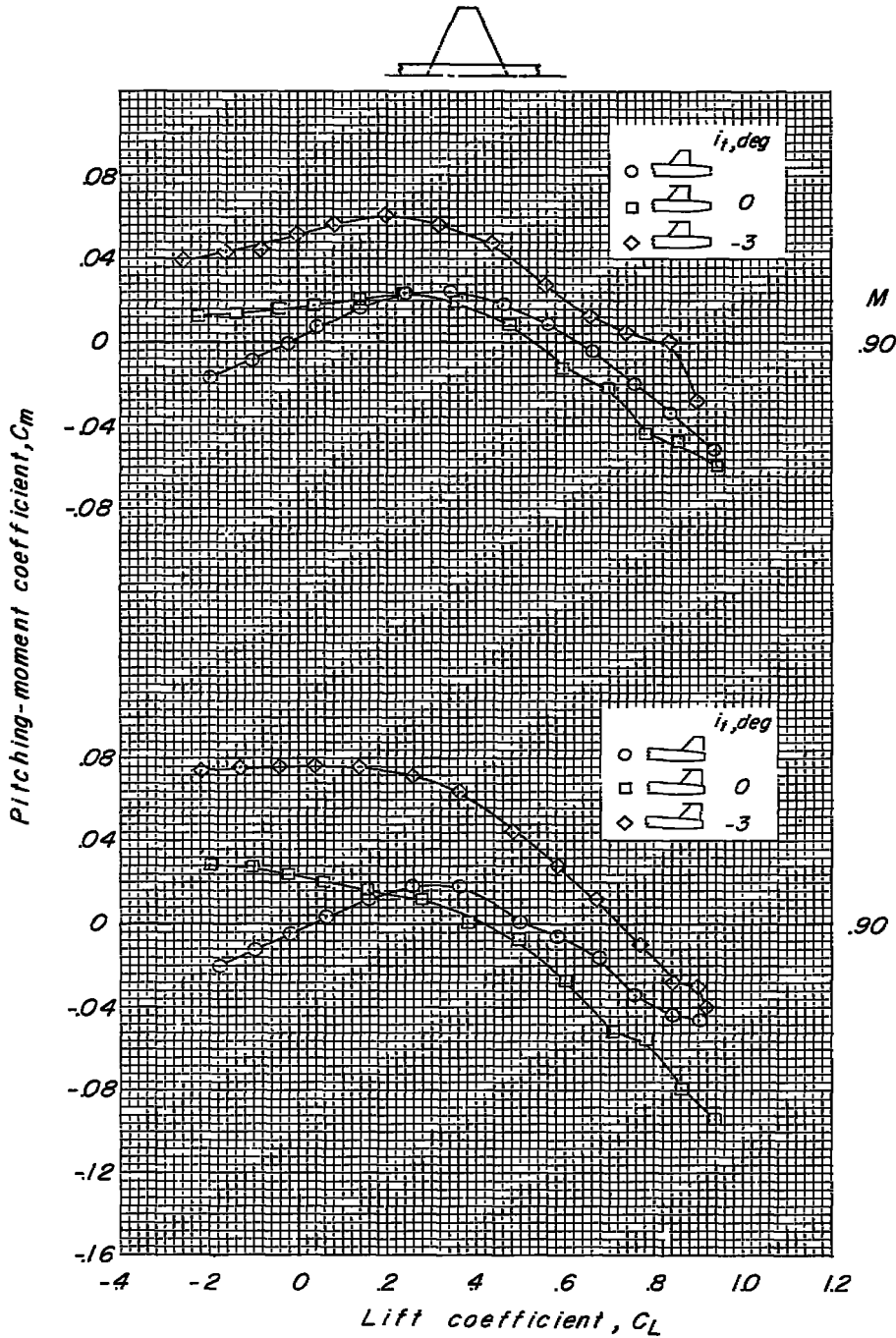
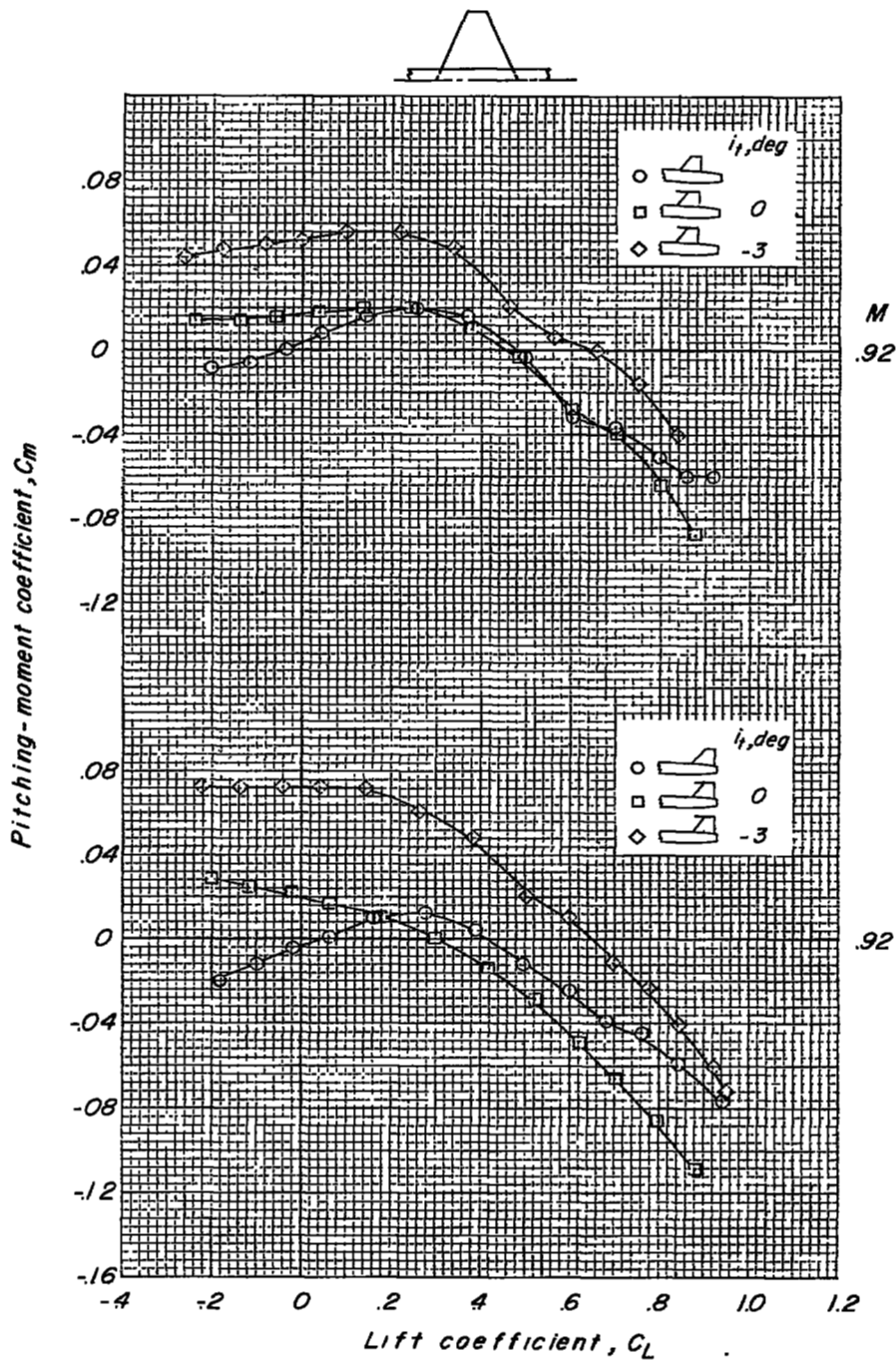
(b)  $M = 0.85$ .

Figure 11.- Continued.



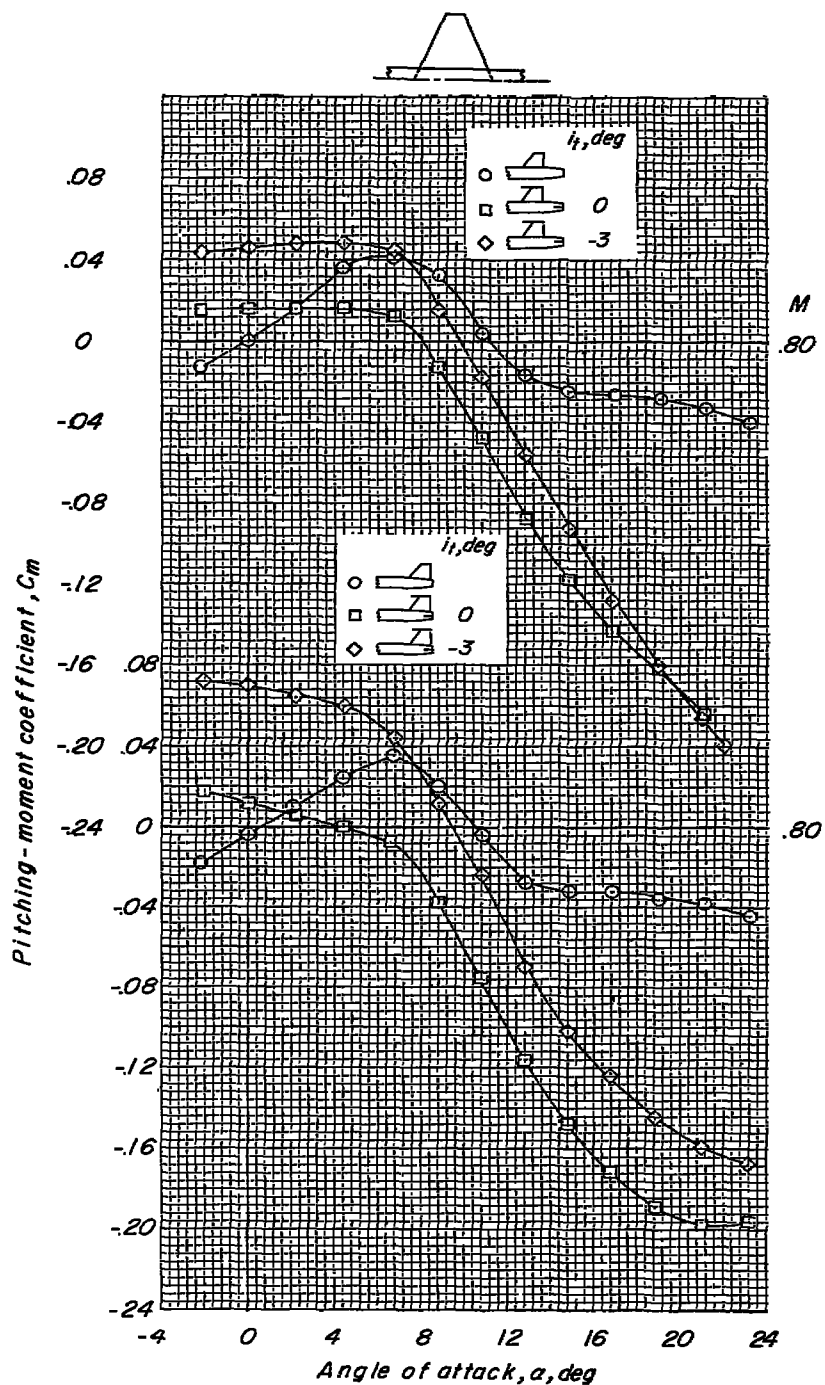
(c)  $M = 0.90$ .

Figure 11.- Continued.



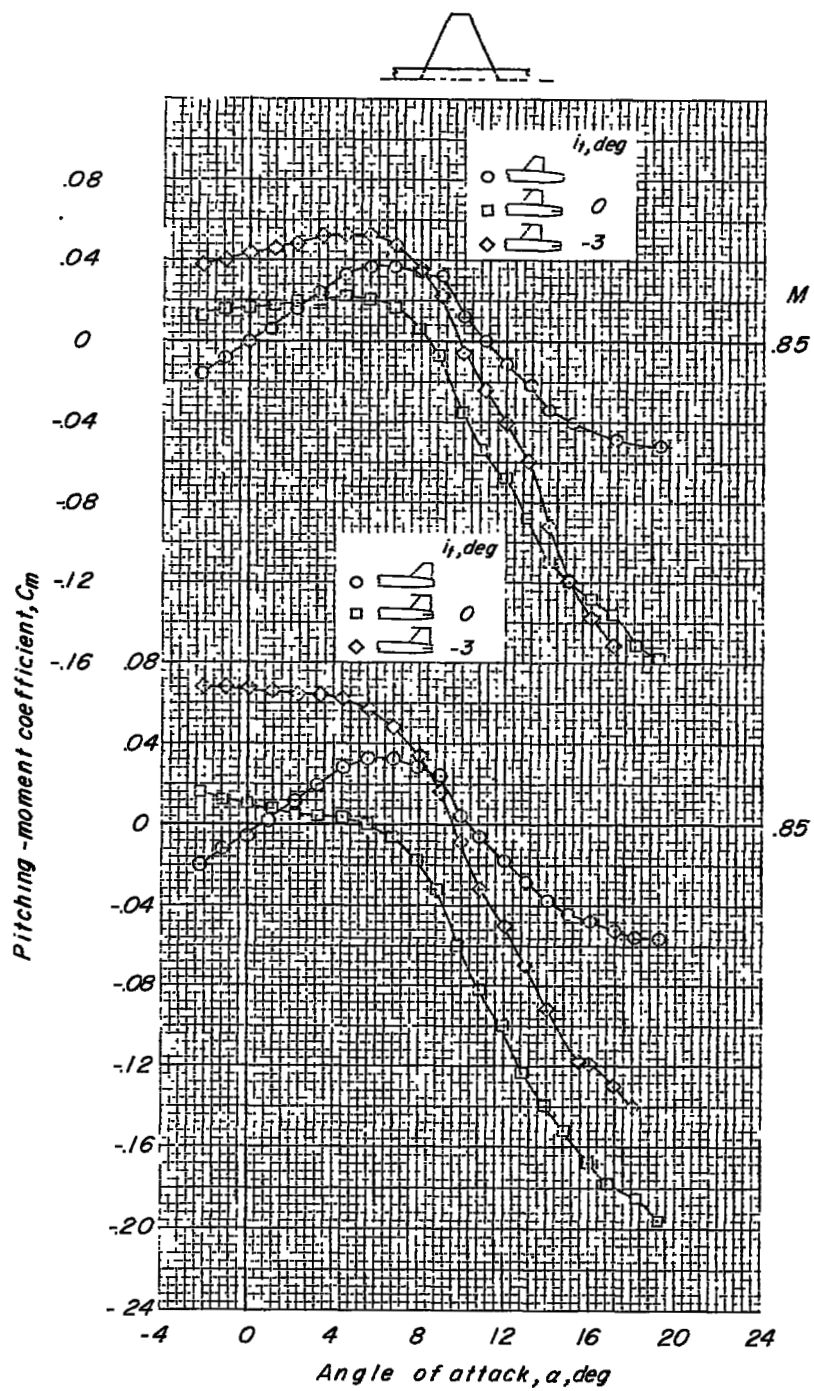
(d)  $M = 0.92$ .

Figure 11.- Concluded.



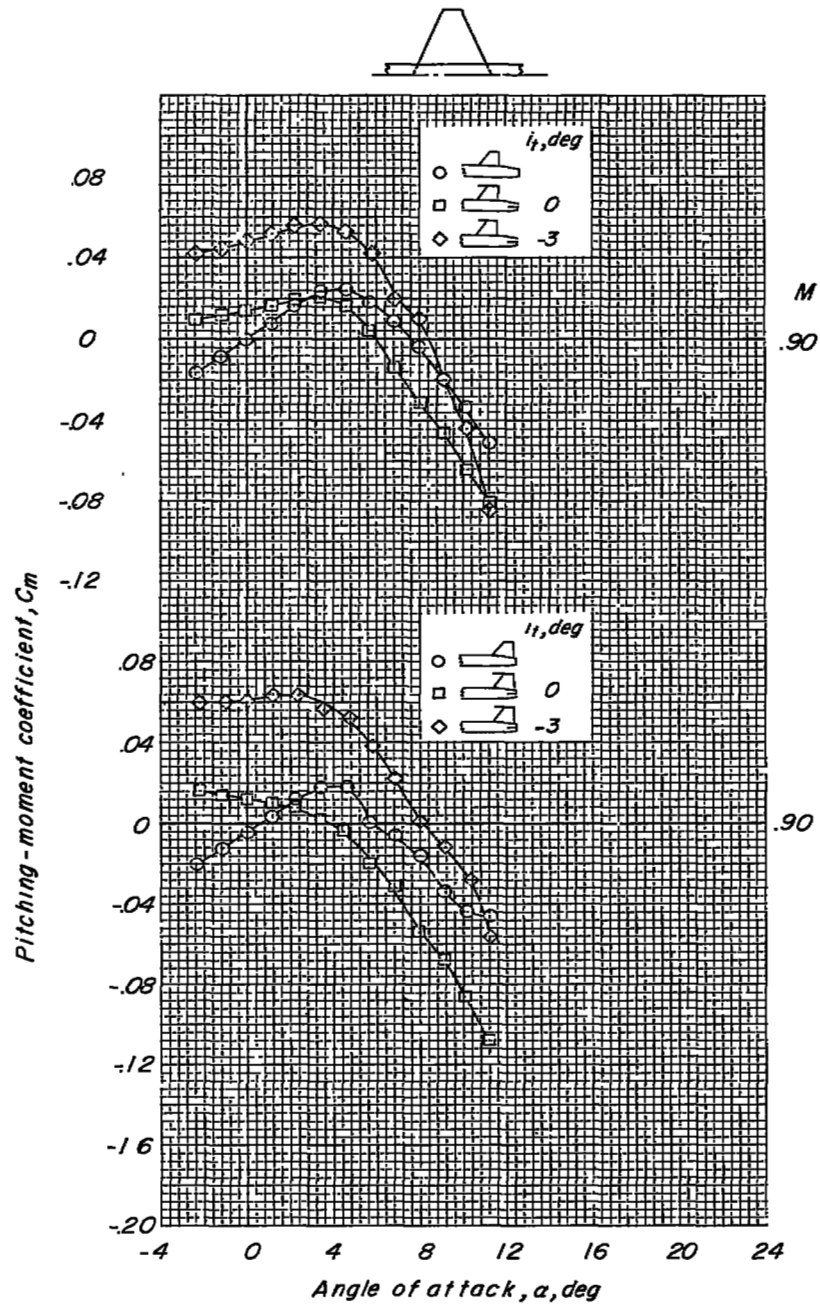
(a)  $M = 0.80$ .

Figure 12.- Variation of pitching-moment coefficient with angle of attack for the model with a bitail and unswept wing.



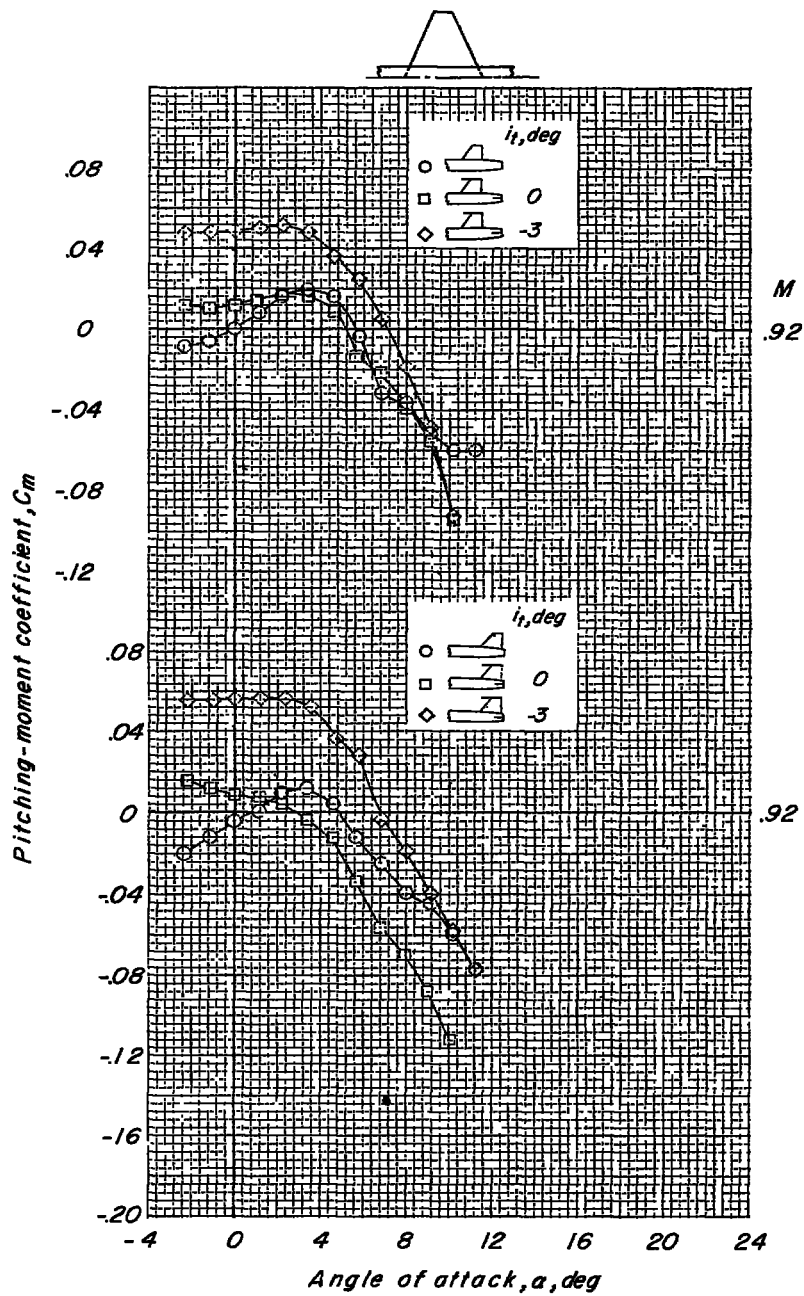
(b)  $M = 0.85$ .

Figure 12.- Continued.



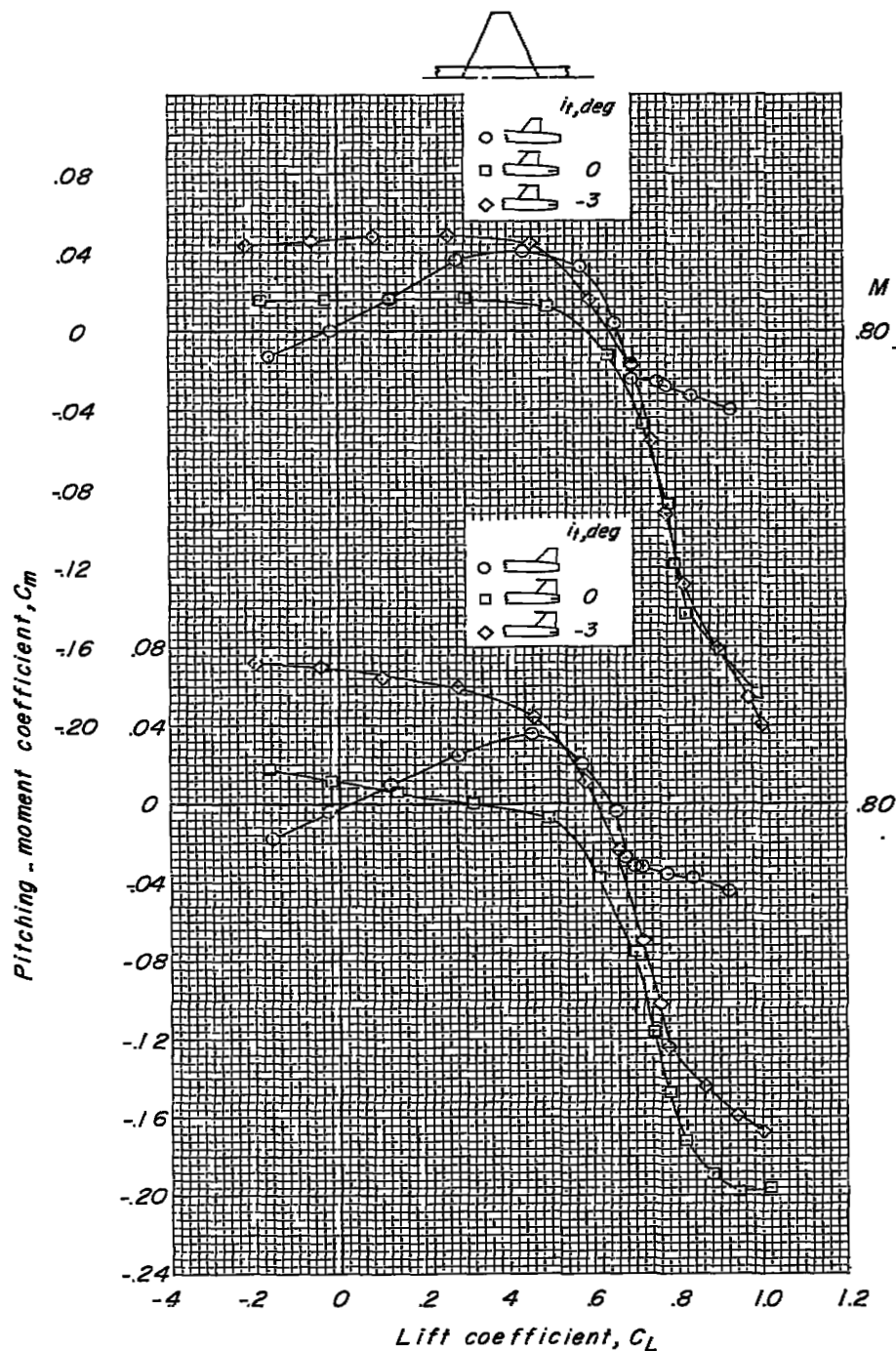
(c)  $M = 0.90$ .

Figure 12.- Continued.



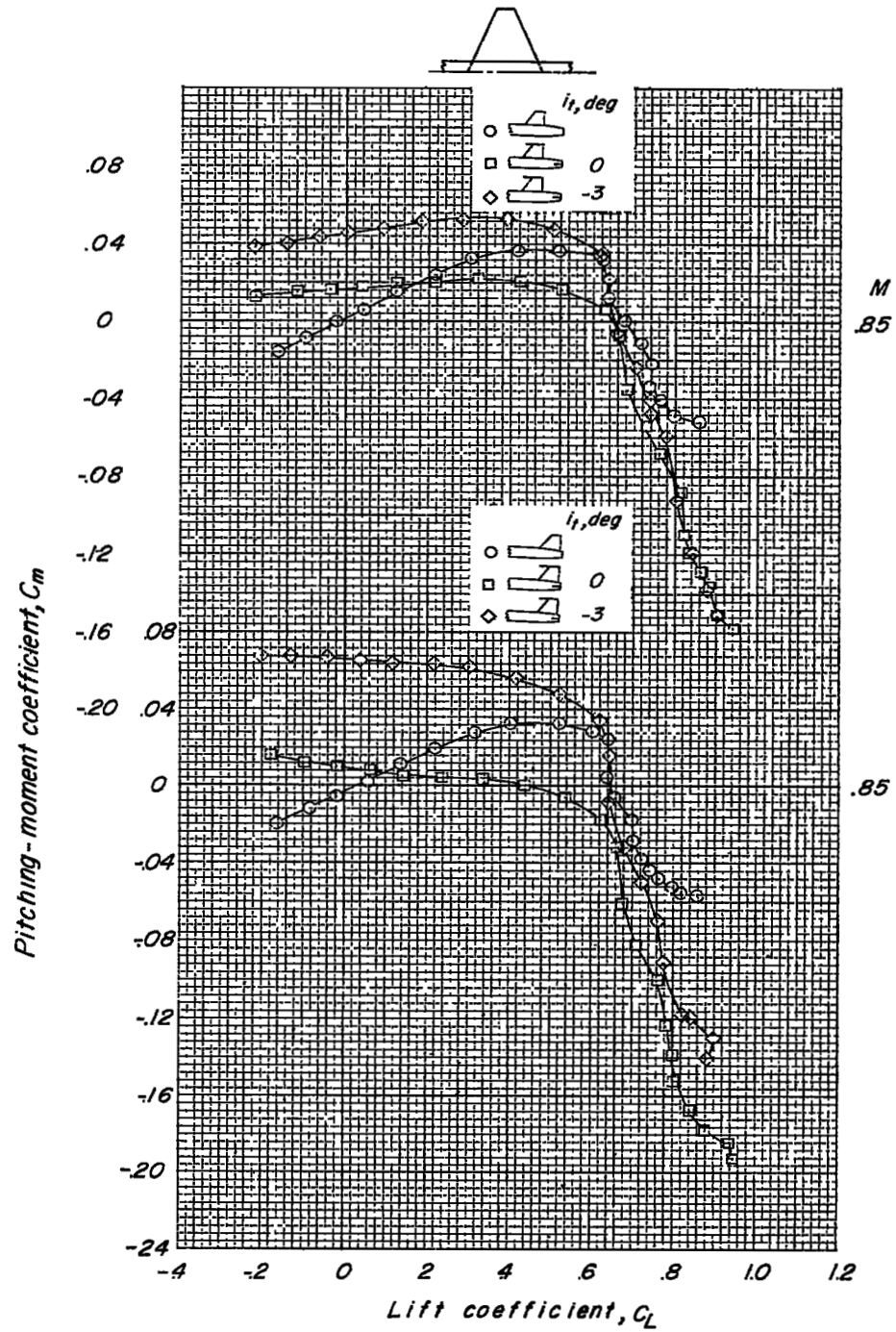
(d)  $M = 0.92$ .

Figure 12.- Concluded.



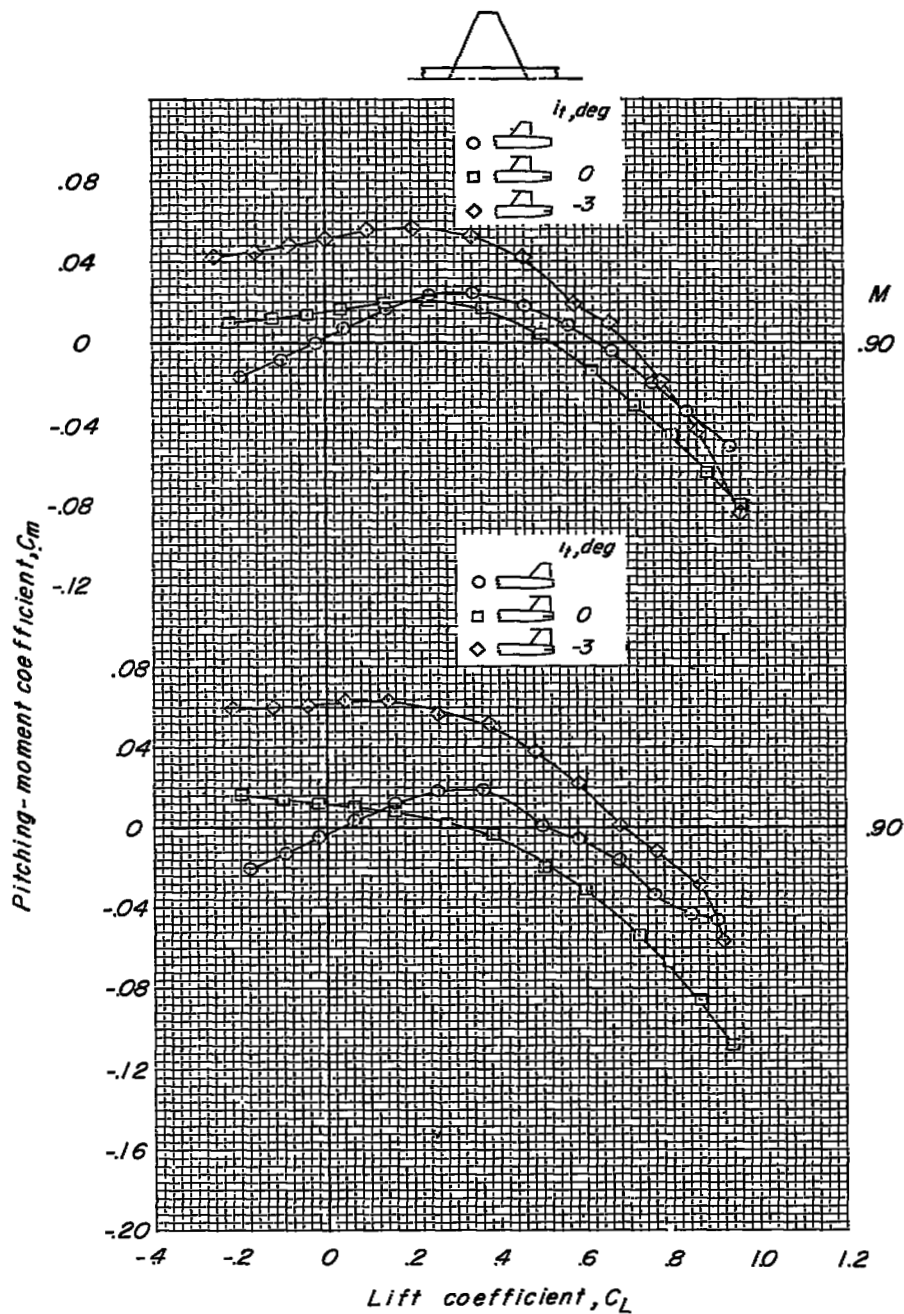
(a)  $M = 0.80$ .

Figure 13.- Variation of pitching-moment coefficient with lift coefficient for the model with a bitail and unswept wing.



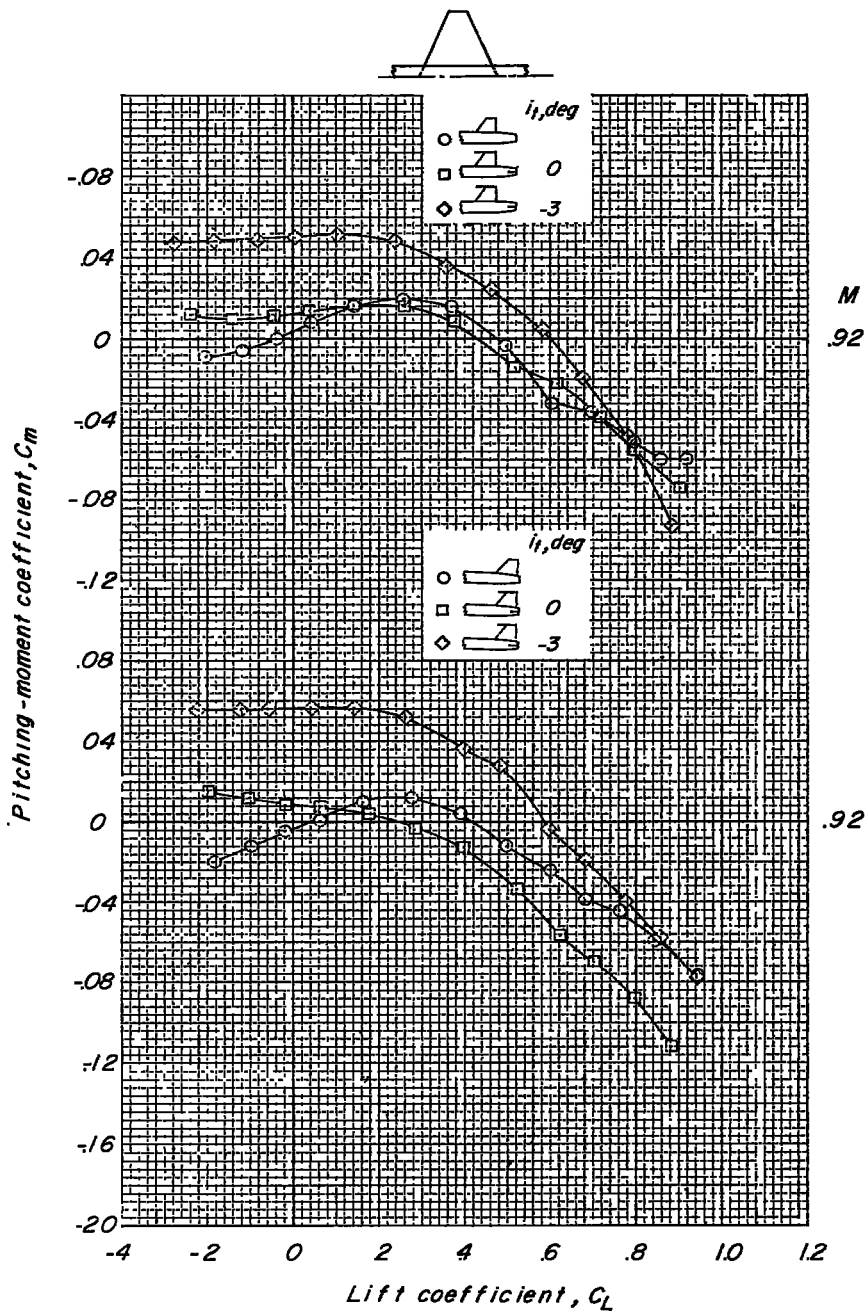
(b)  $M = 0.85$ .

Figure 13.- Continued.



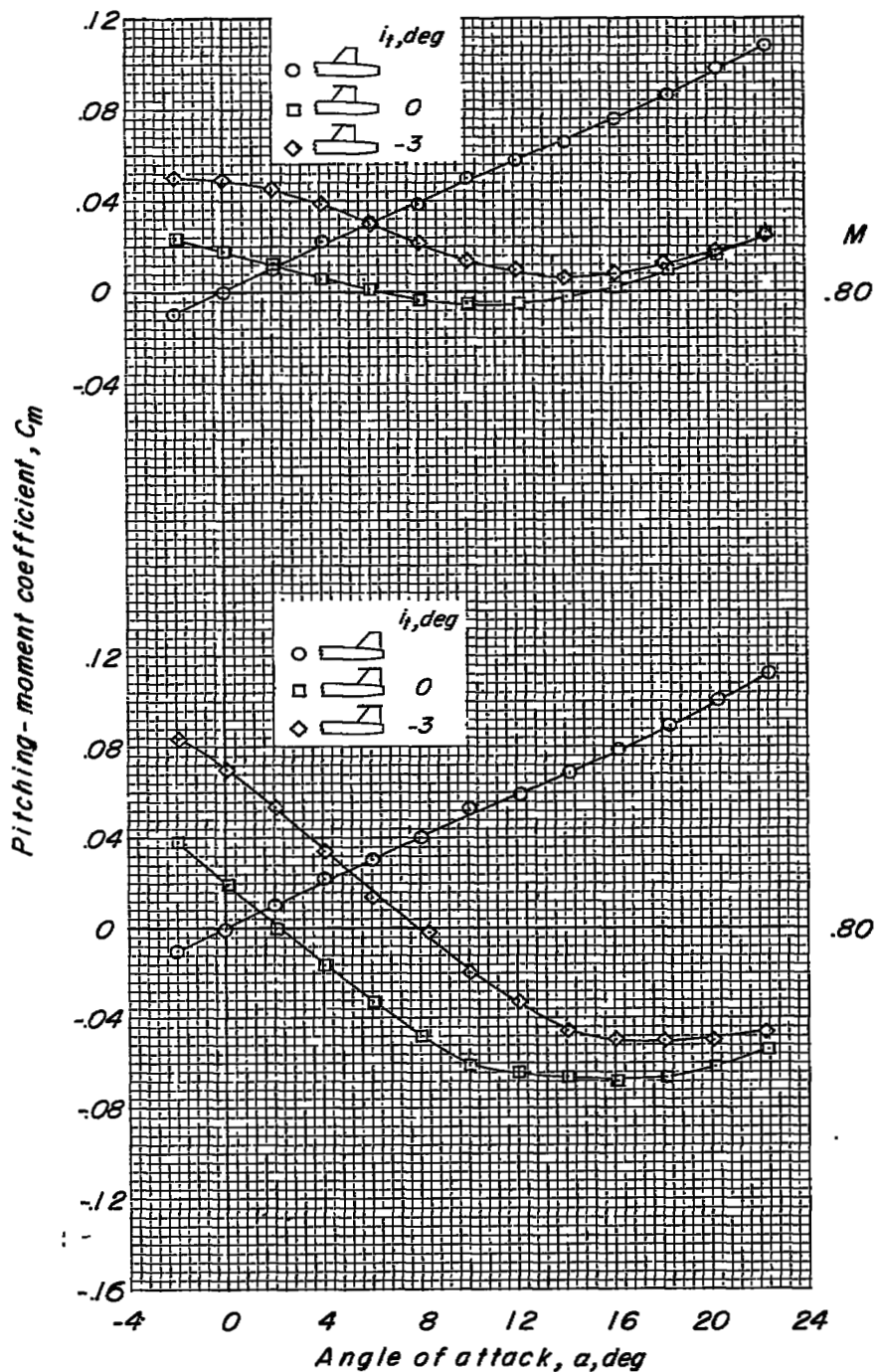
(c)  $M = 0.90$ .

Figure 13.- Continued.



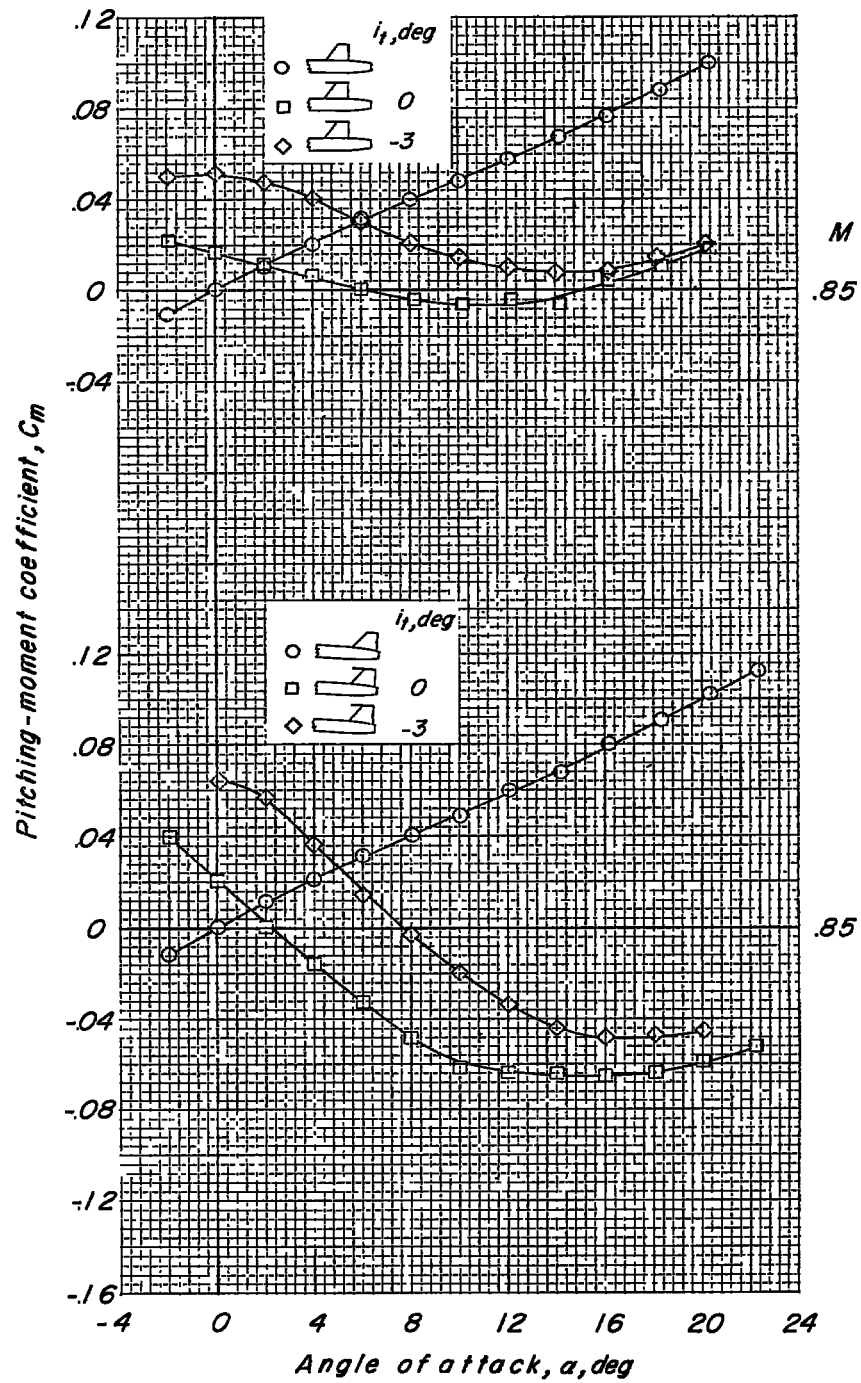
(a)  $M = 0.92$ .

Figure 13.- Concluded.



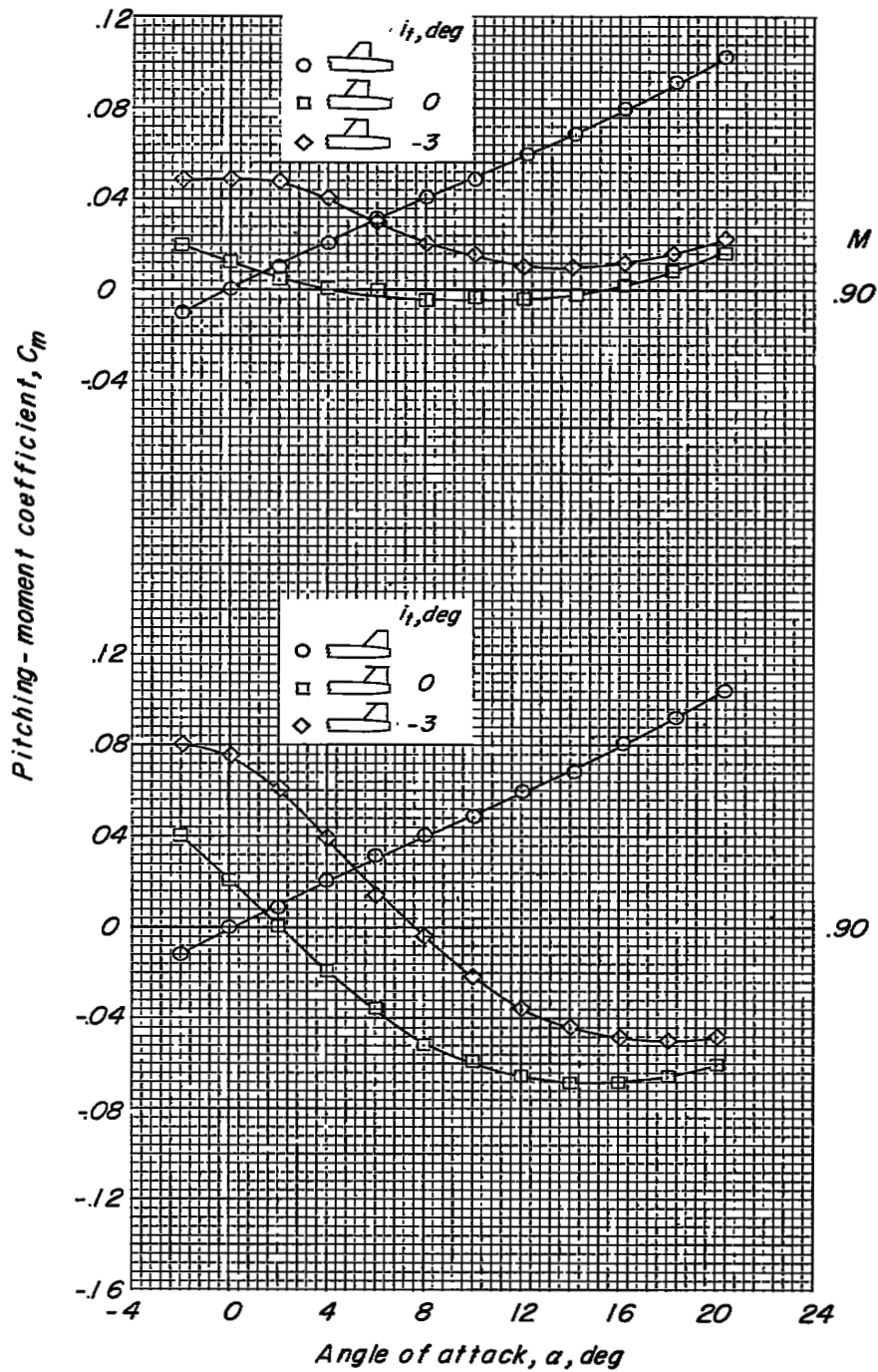
(a)  $M = 0.80$ .

Figure 14.- Variation of pitching-moment coefficient with angle of attack for the model with a high tail and wing off.



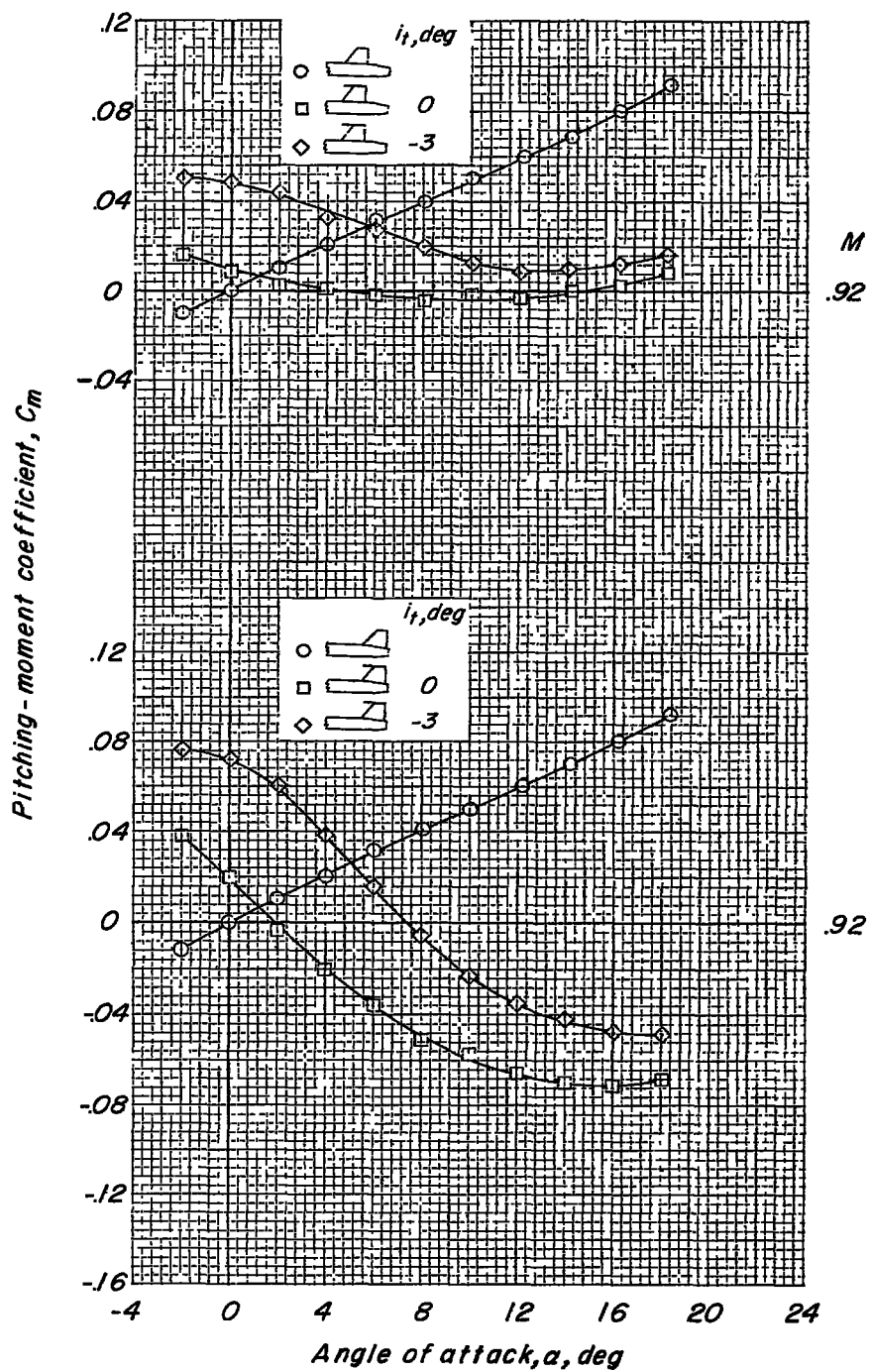
(b)  $M = 0.85$ .

Figure 14.- Continued.



(c)  $M = 0.90$ .

Figure 14.- Continued.



(d)  $M = 0.92$ .

Figure 14.- Concluded.

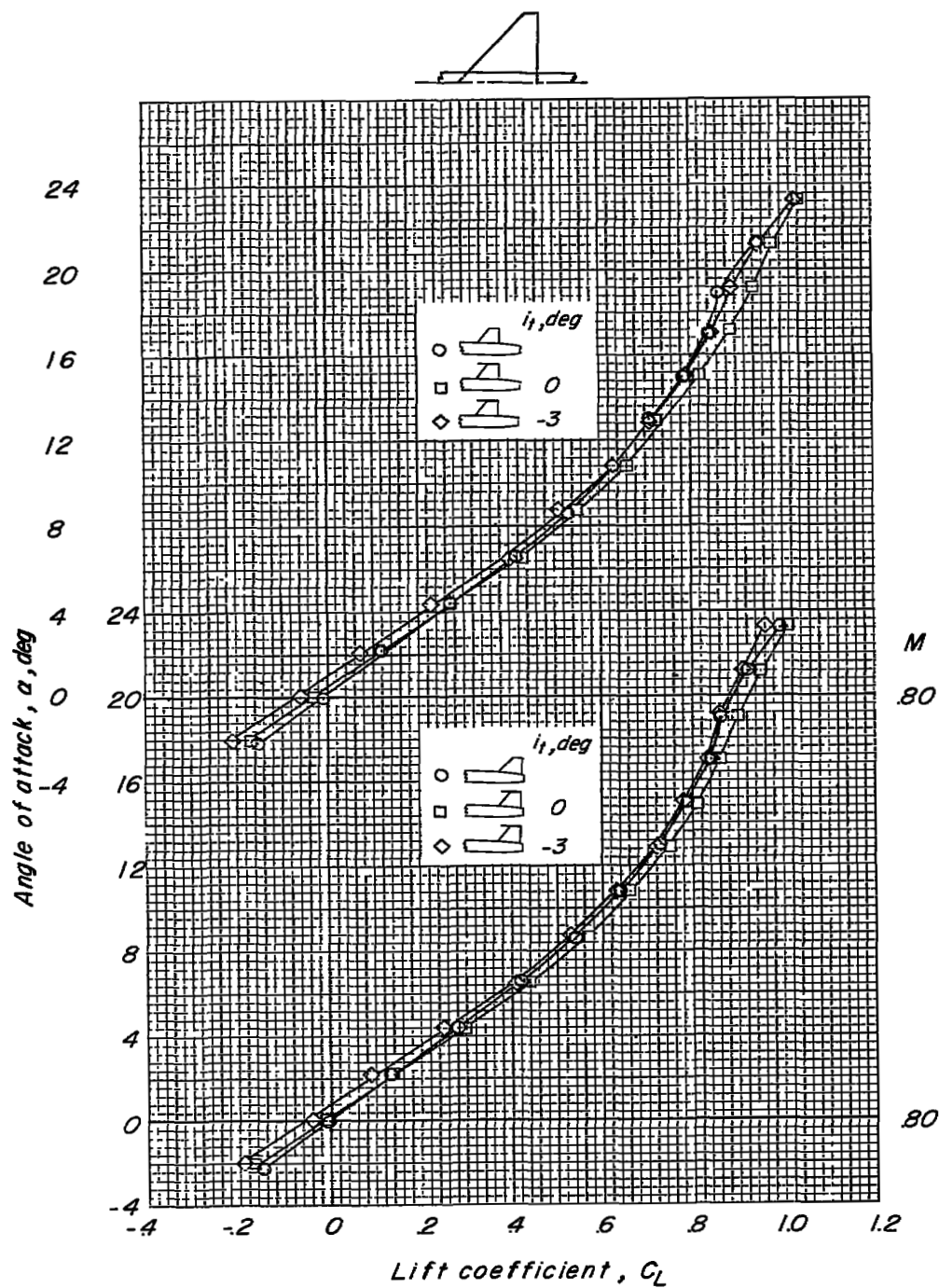
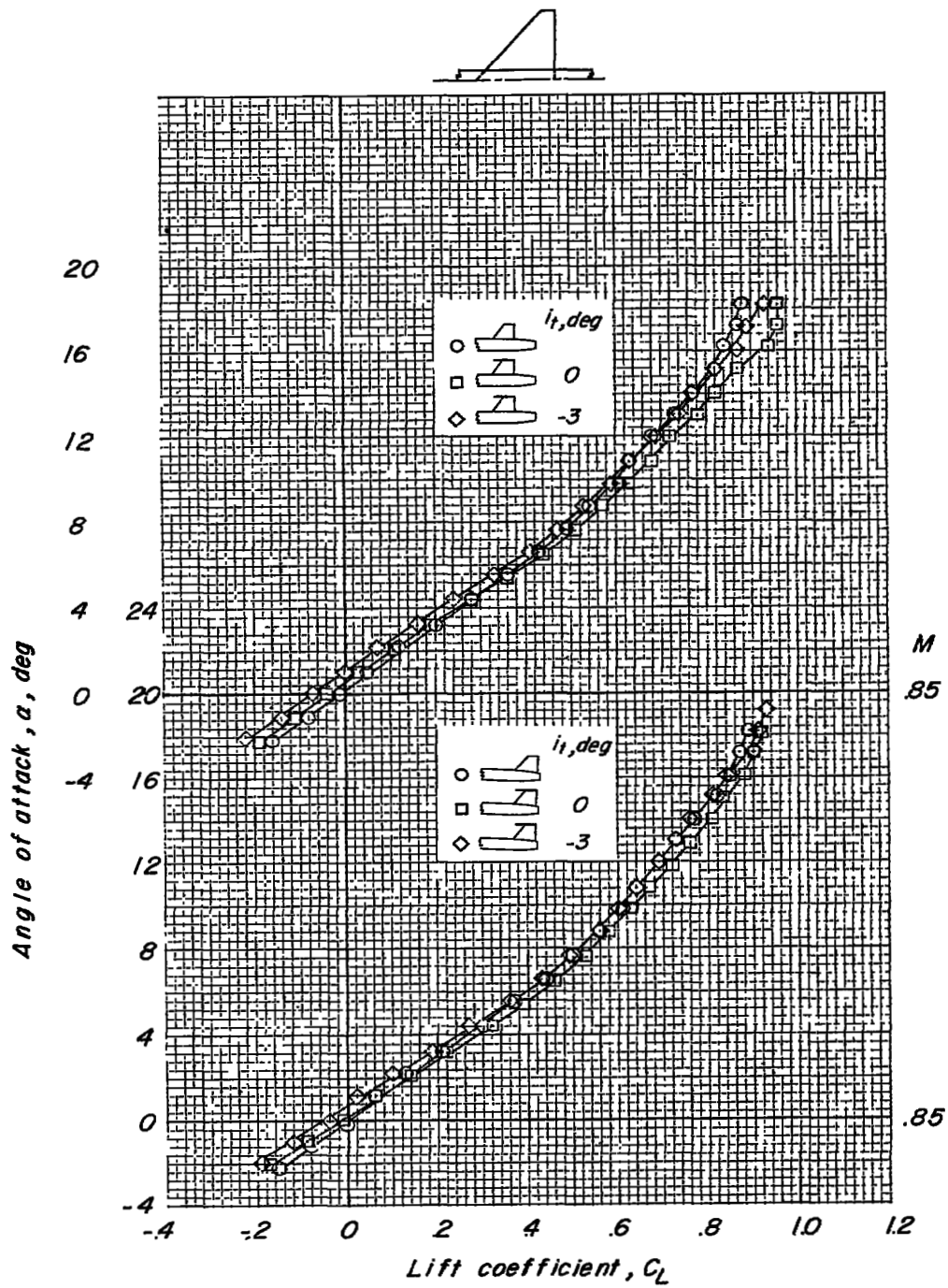
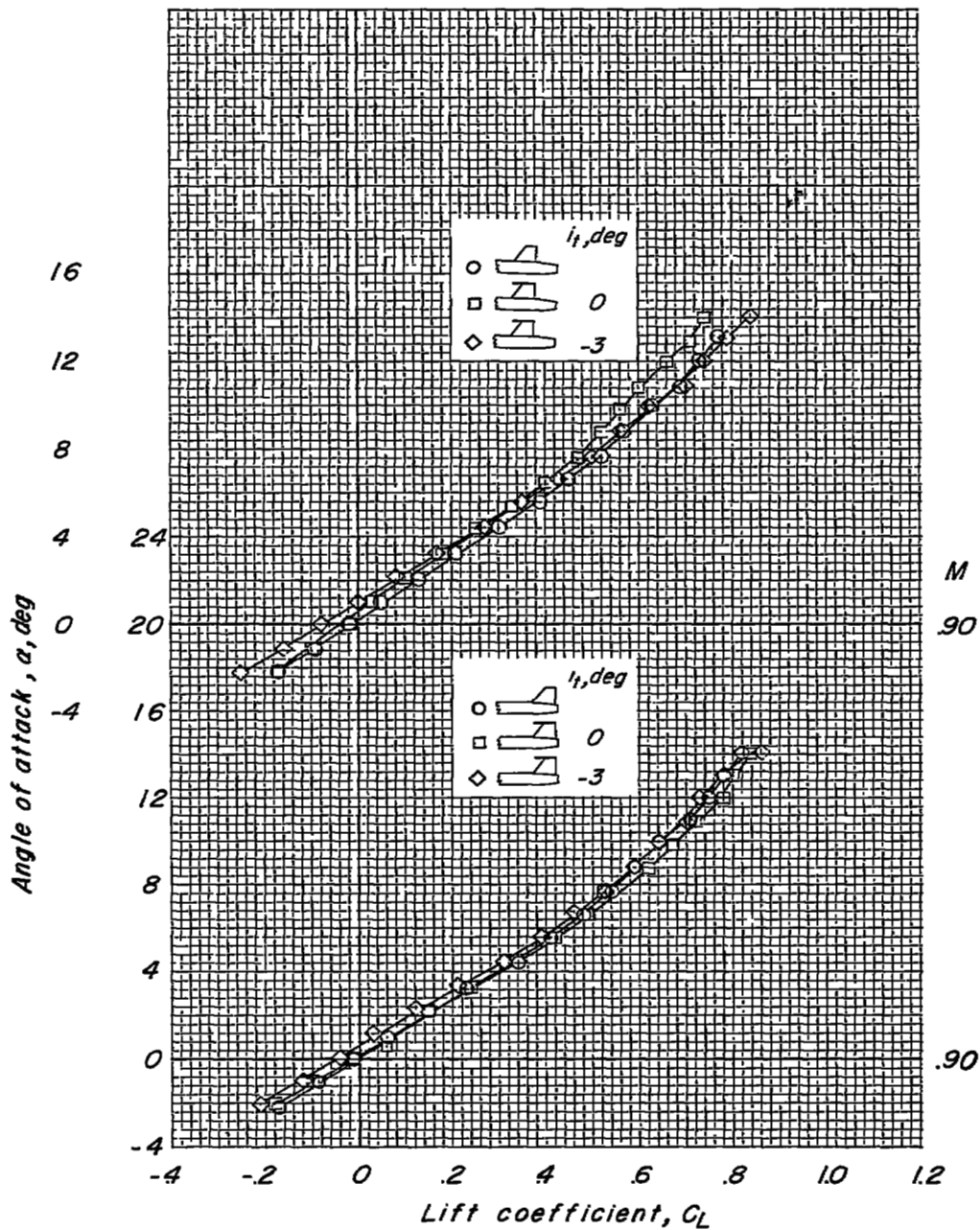
(a)  $M = 0.80$ .

Figure 15.- Variation of lift coefficient with angle of attack for the model with a high tail and cropped-delta wing.



(b)  $M = 0.85$ .

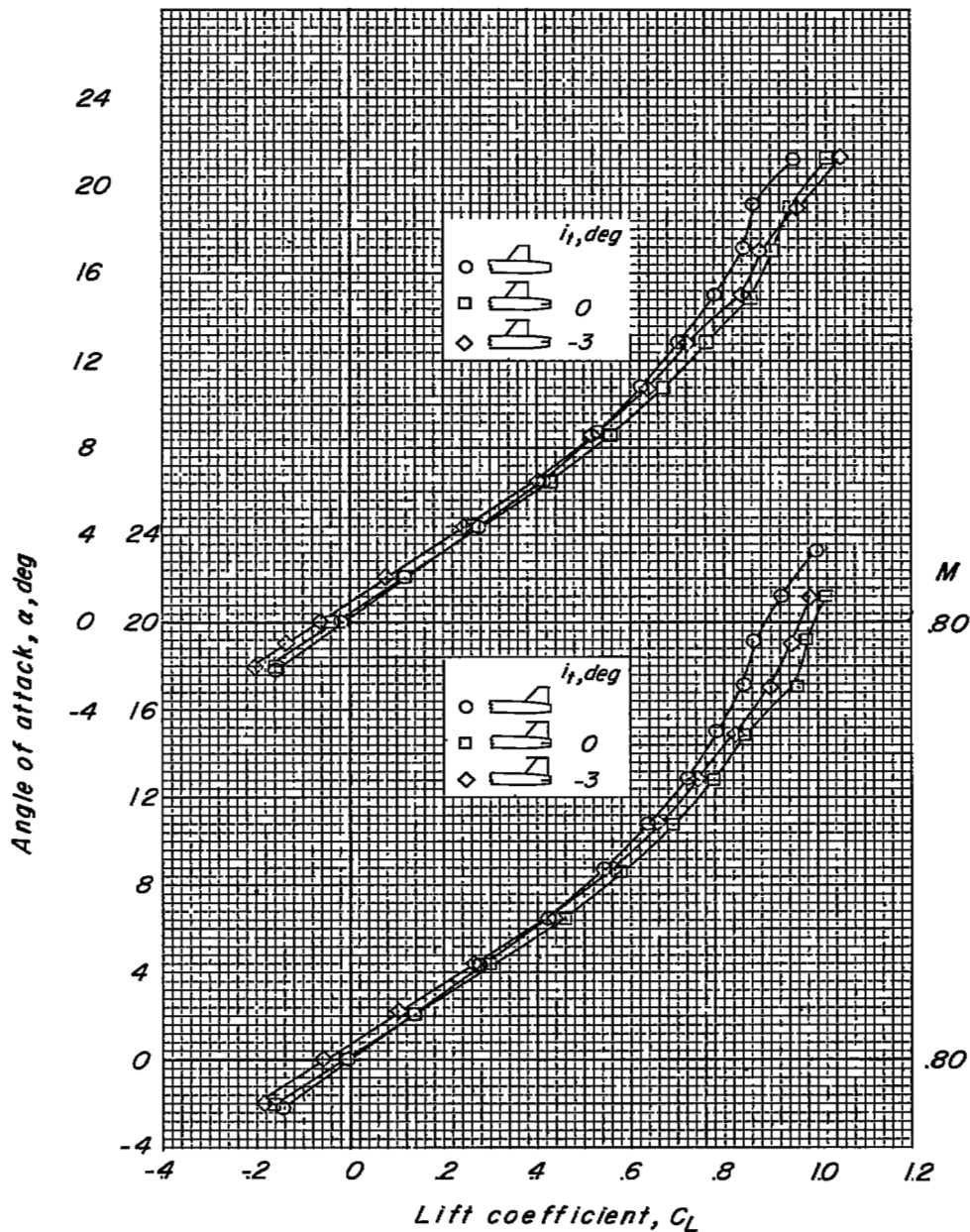
Figure 15.- Continued.



(c)  $M = 0.90$ .

Figure 15.- Continued.





(a)  $M = 0.80$ .

Figure 16.- Variation of lift coefficient with angle of attack for the model with a bitail and cropped-delta wing.

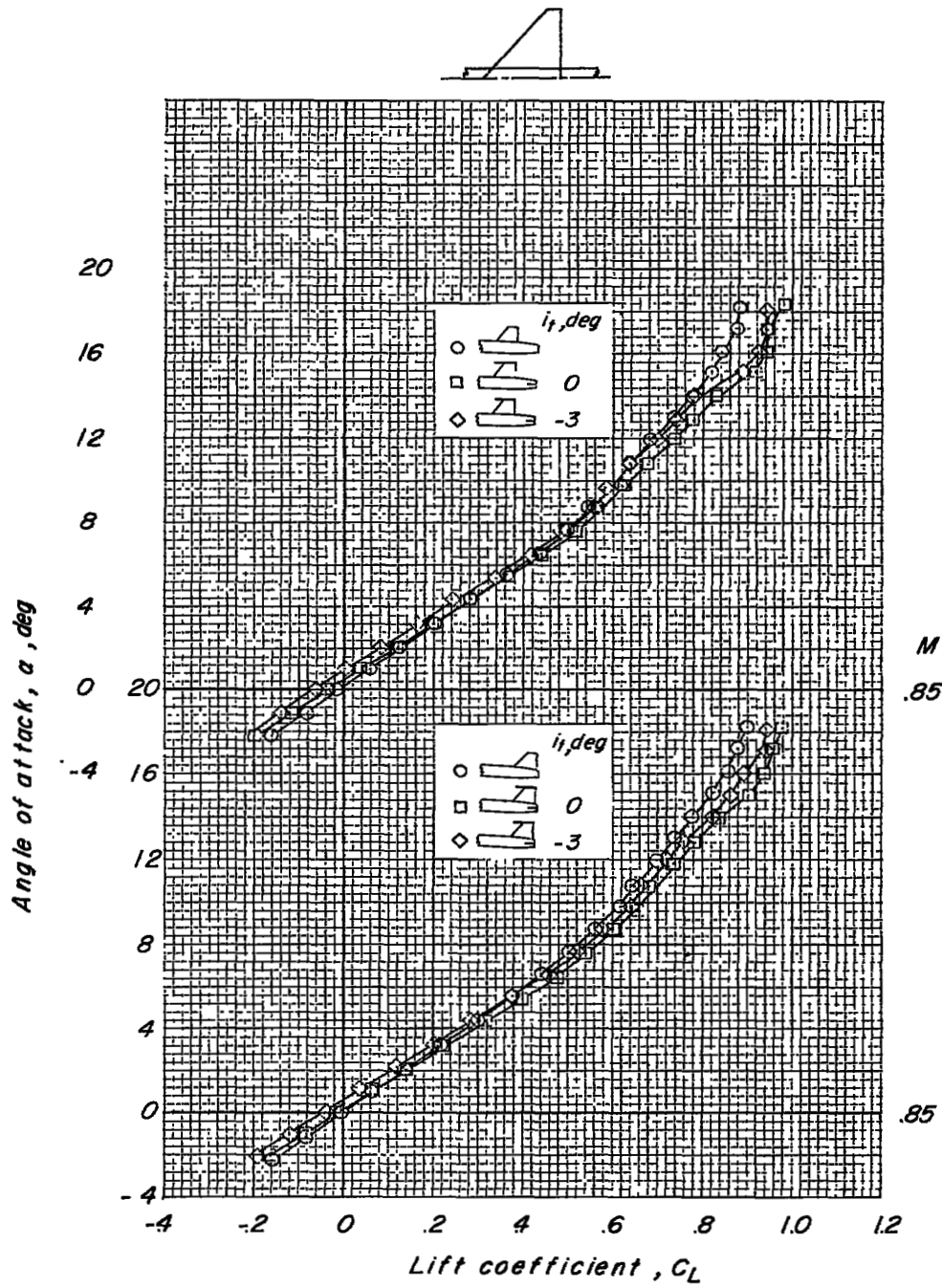
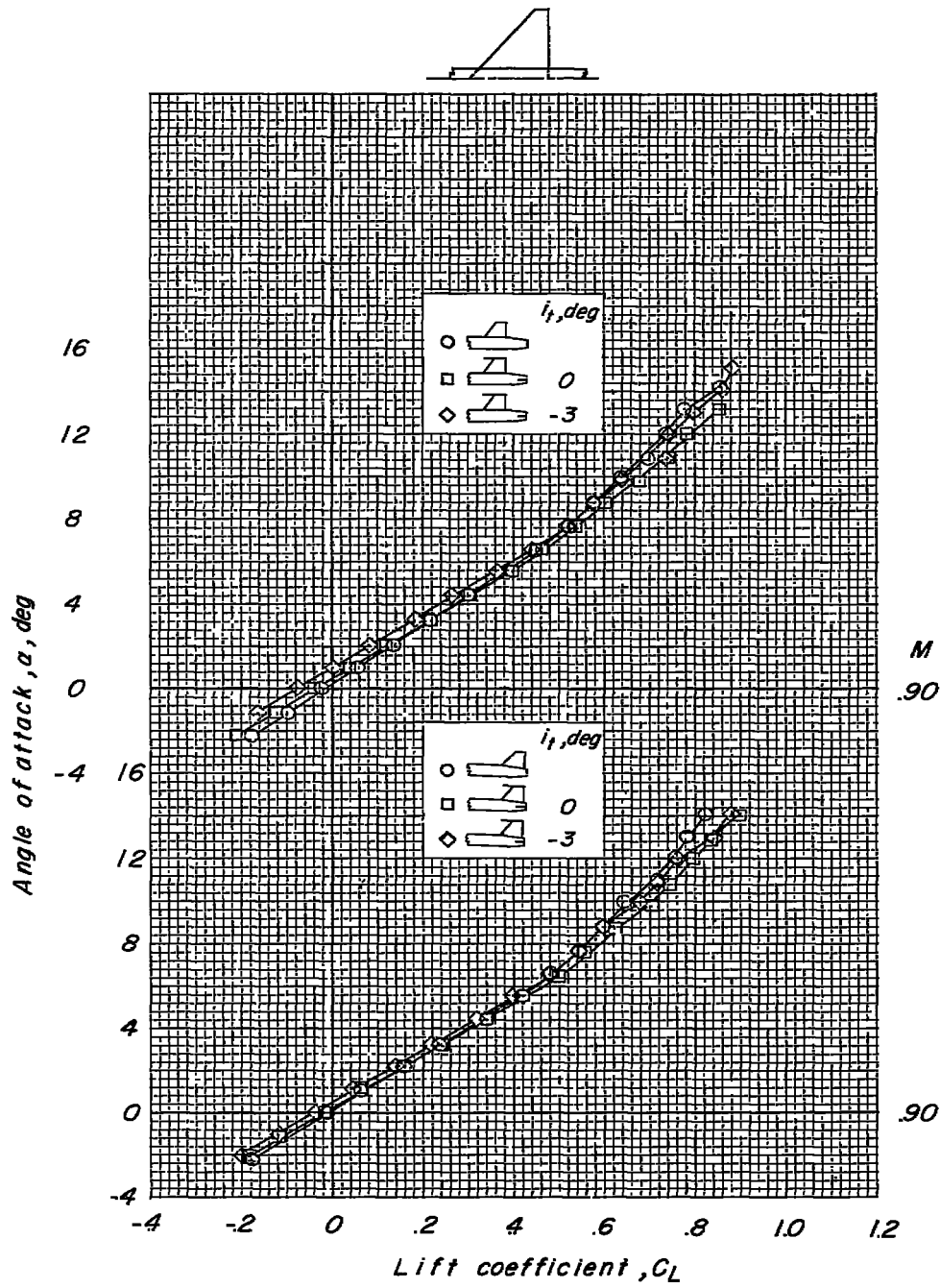
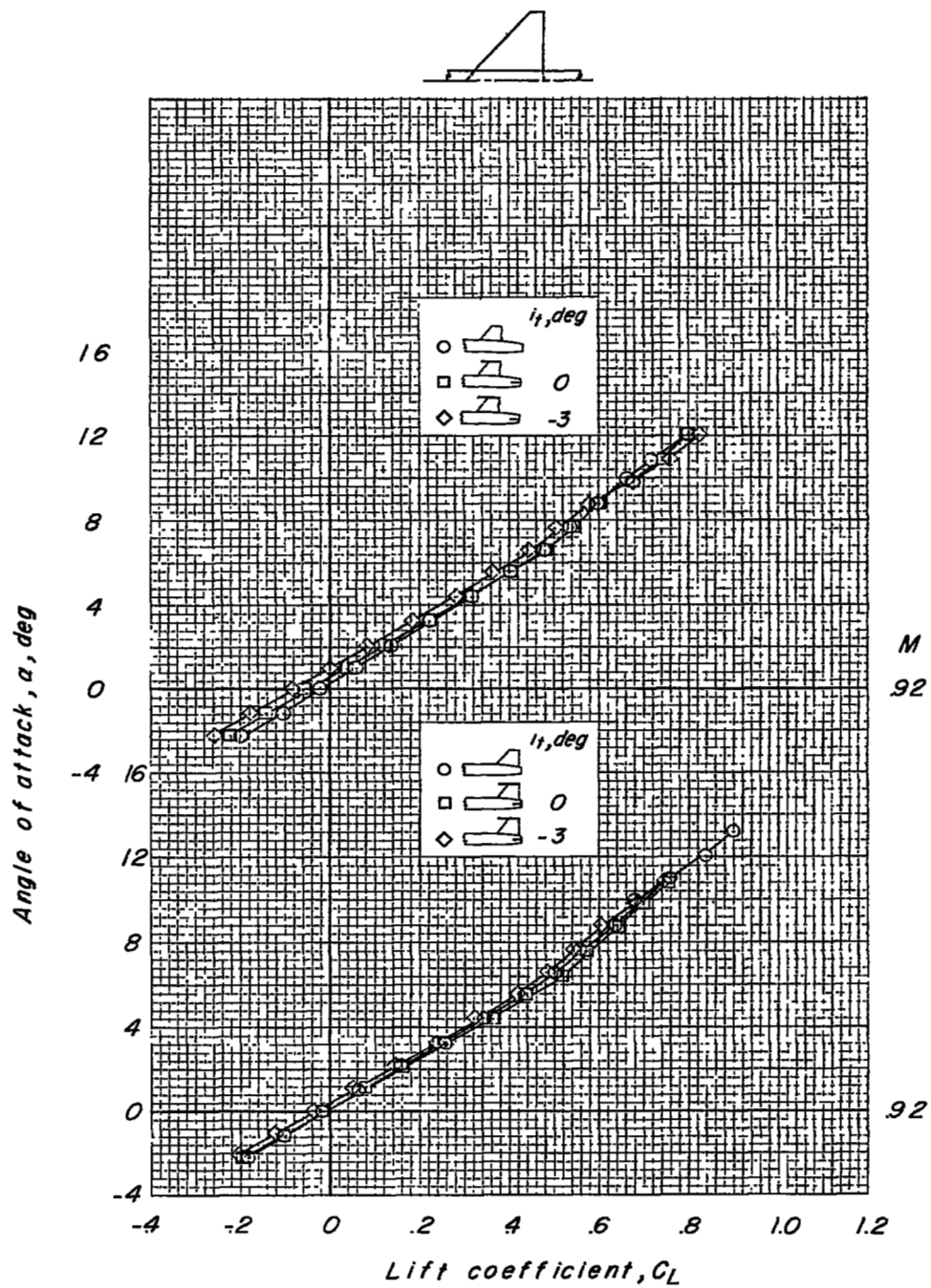
(b)  $M = 0.85$ .

Figure 16.- Continued.



(c)  $M = 0.90$ .

Figure 16.- Continued.



(d)  $M = 0.92$ .

Figure 16.- Concluded.

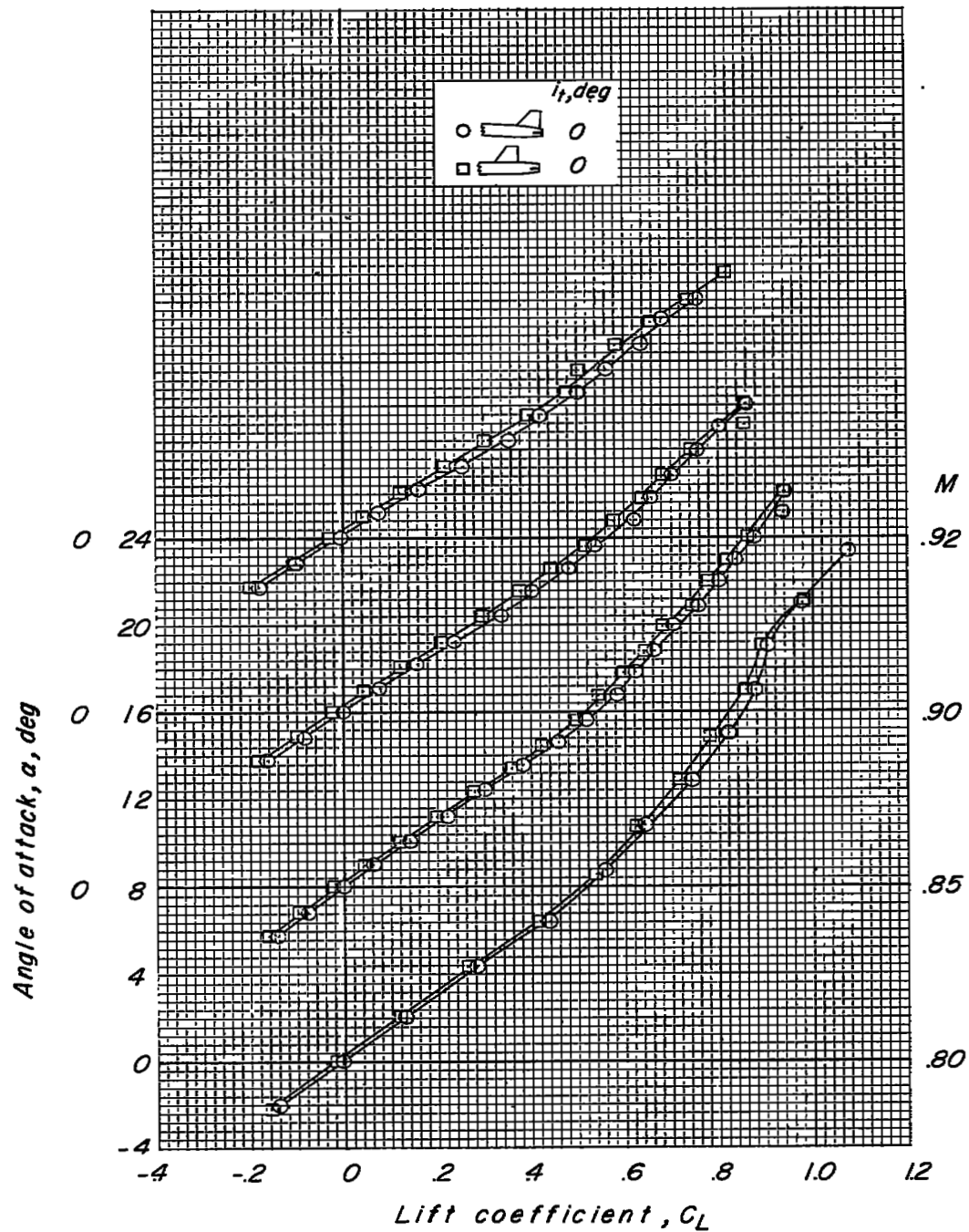


Figure 17.- Variation of lift coefficient with angle of attack for the model with a low tail and cropped-delta wing.

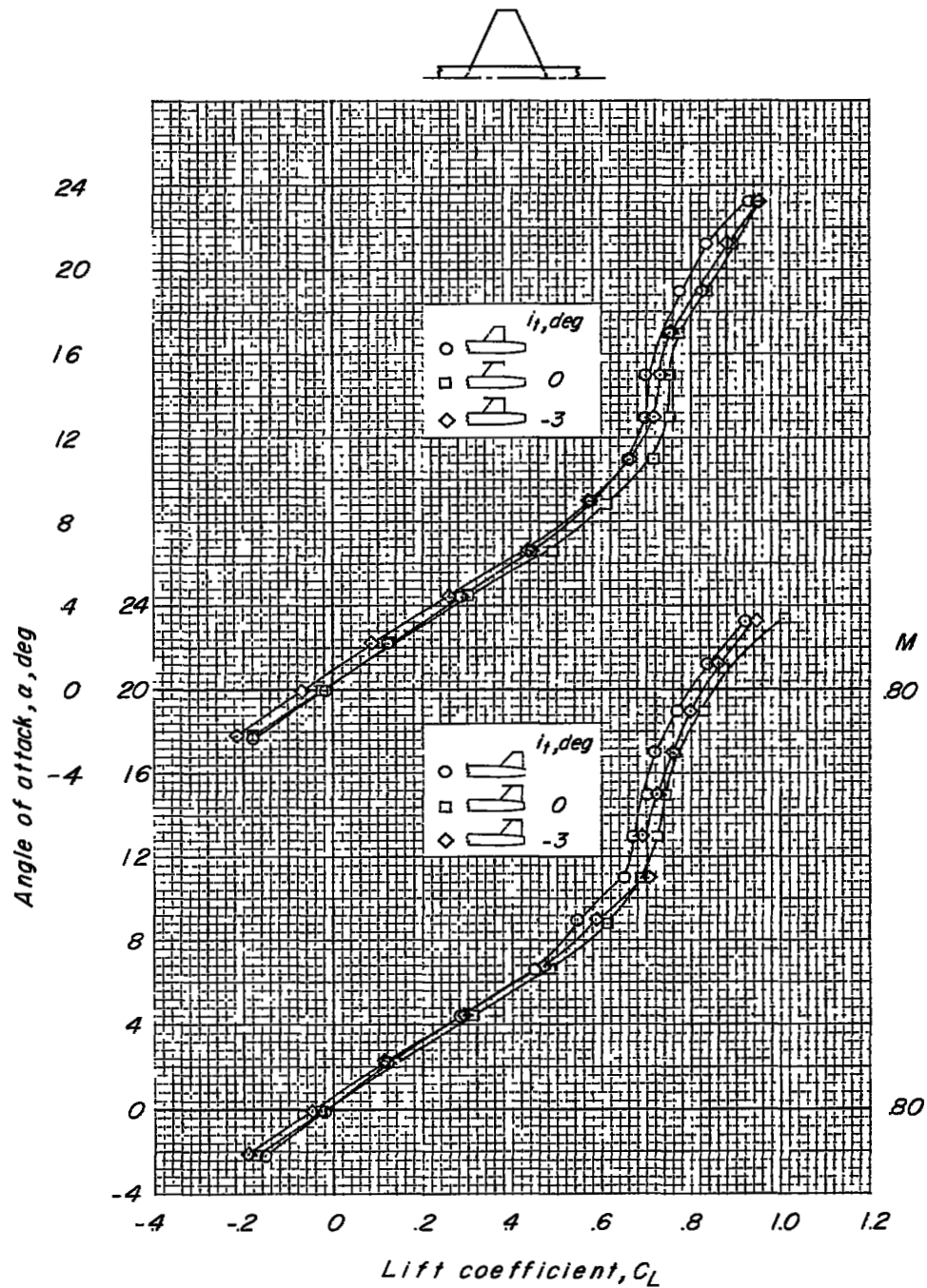
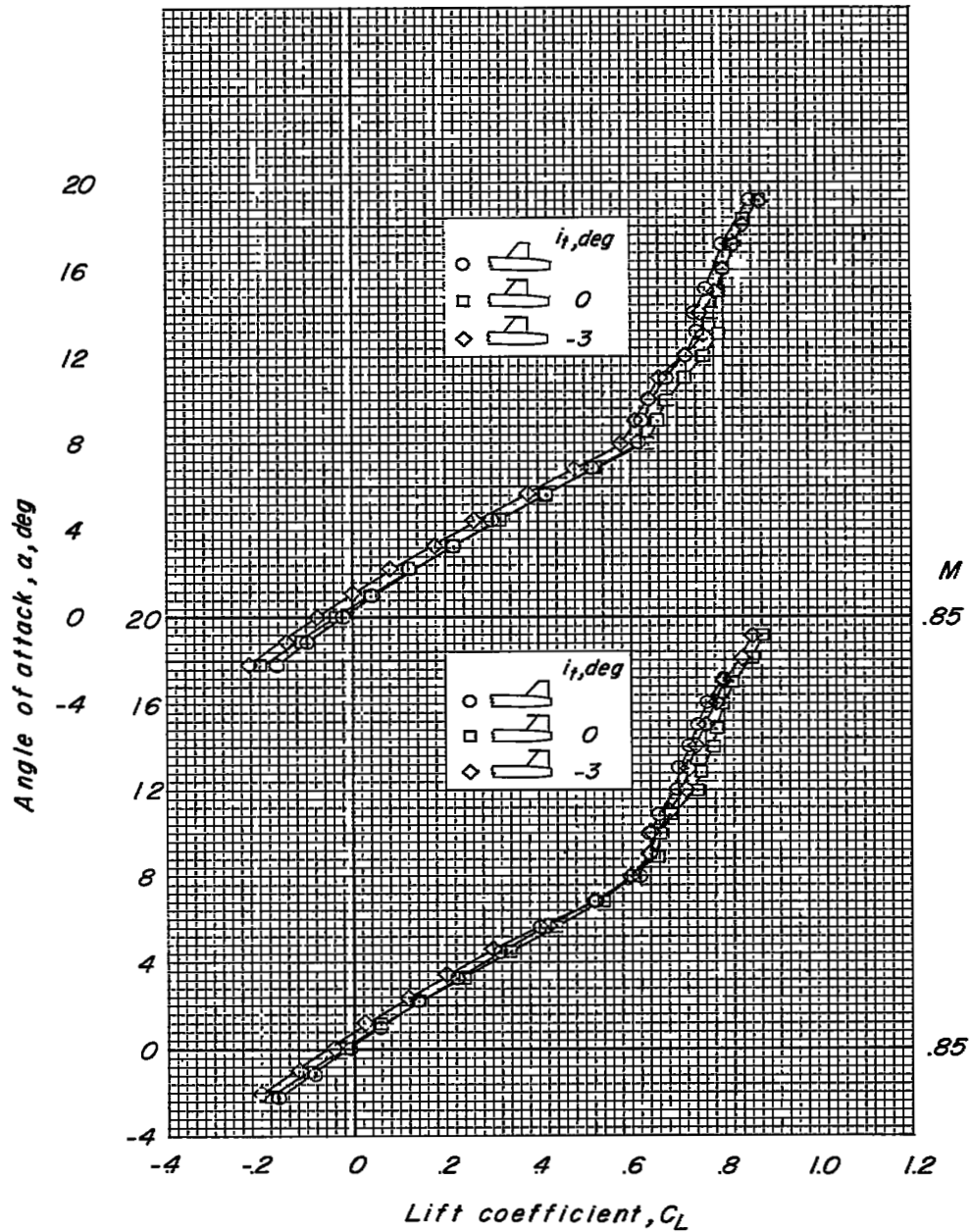
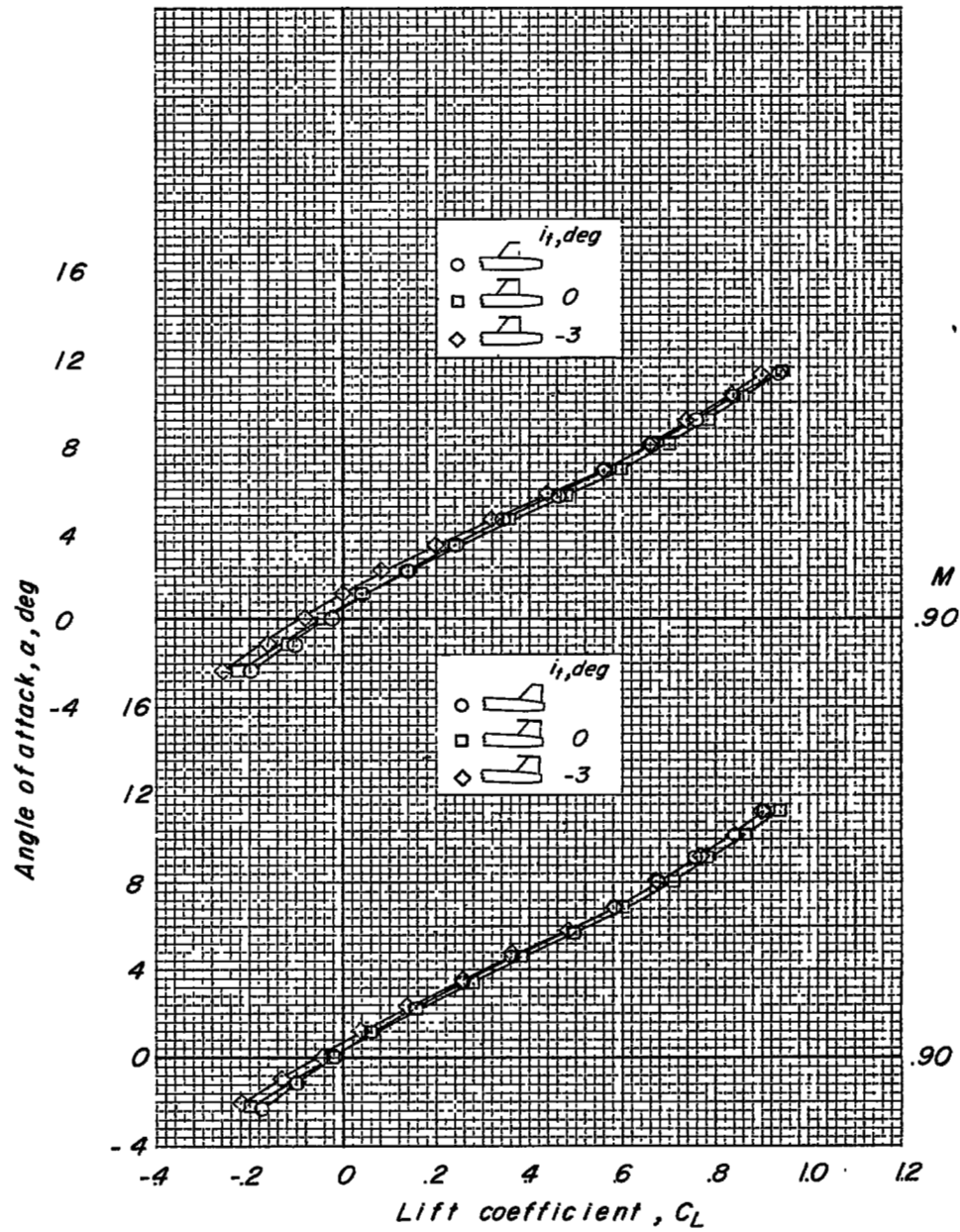
(a)  $M = 0.80$ .

Figure 18.- Variation of lift coefficient with angle of attack for the model with a high tail and unswept wing.



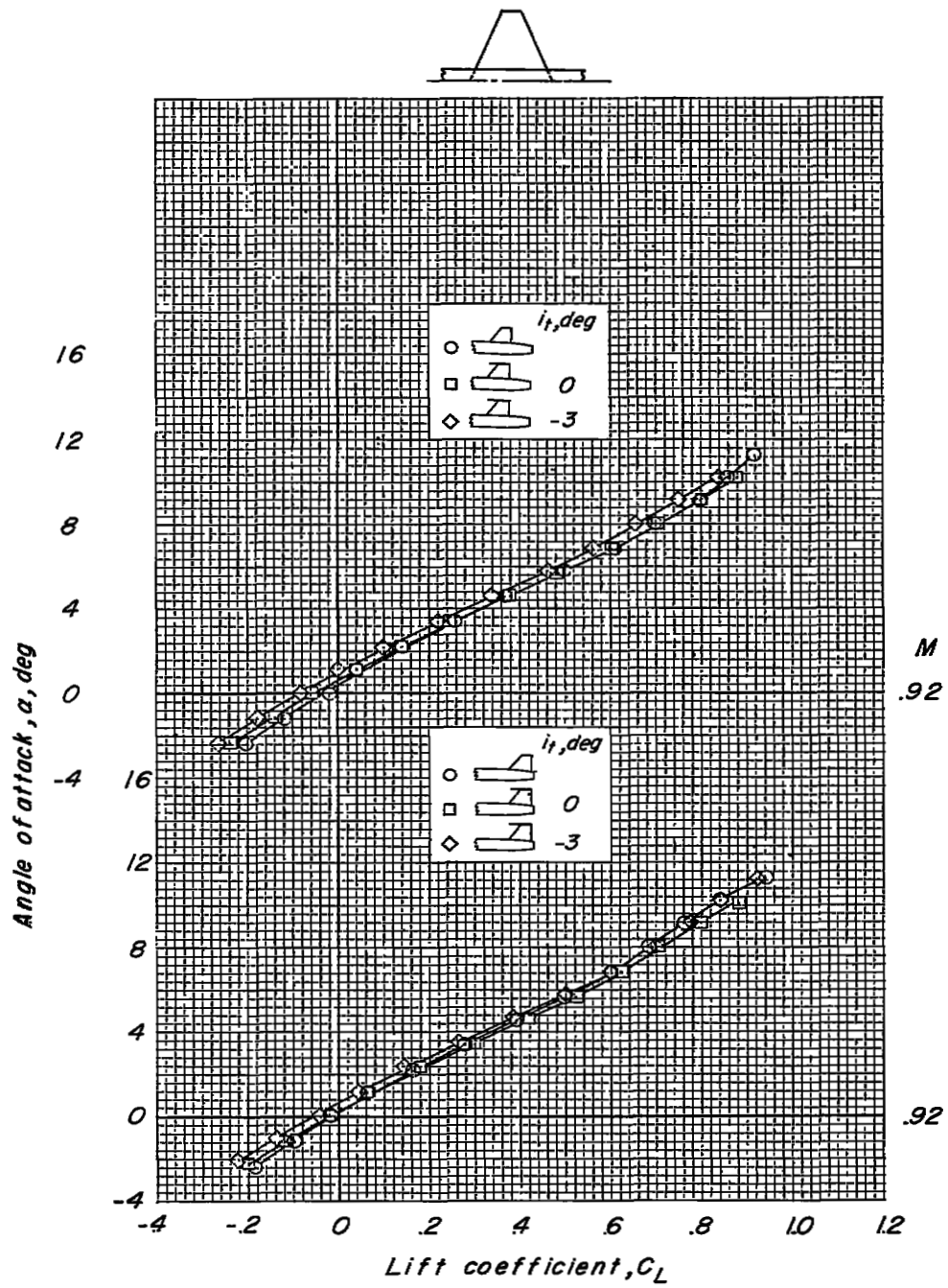
(b)  $M = 0.85$ .

Figure 18.- Continued.



(c)  $M = 0.90$ .

Figure 18.- Continued.



(d)  $M = 0.92$ .

Figure 18.- Concluded.

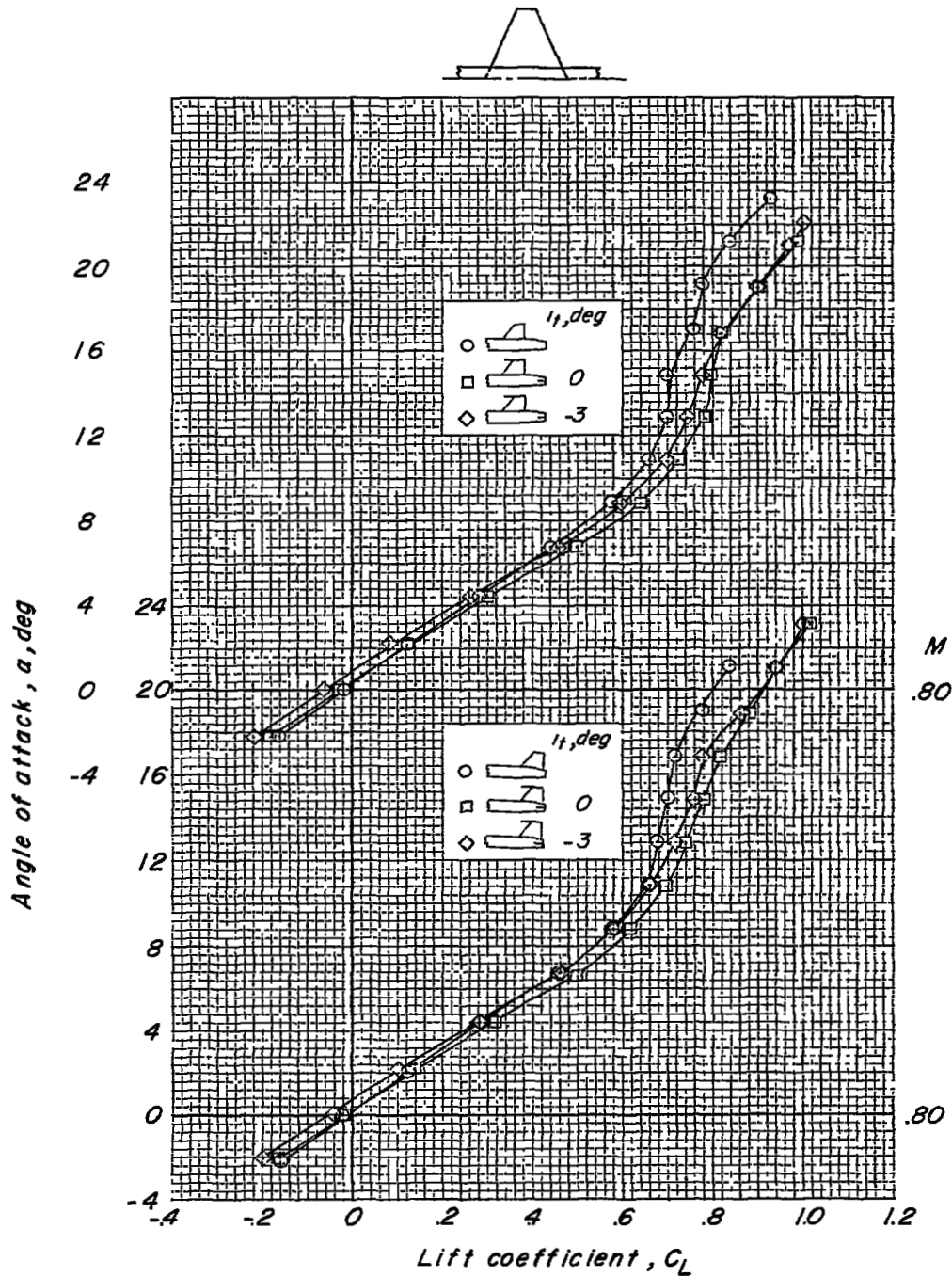
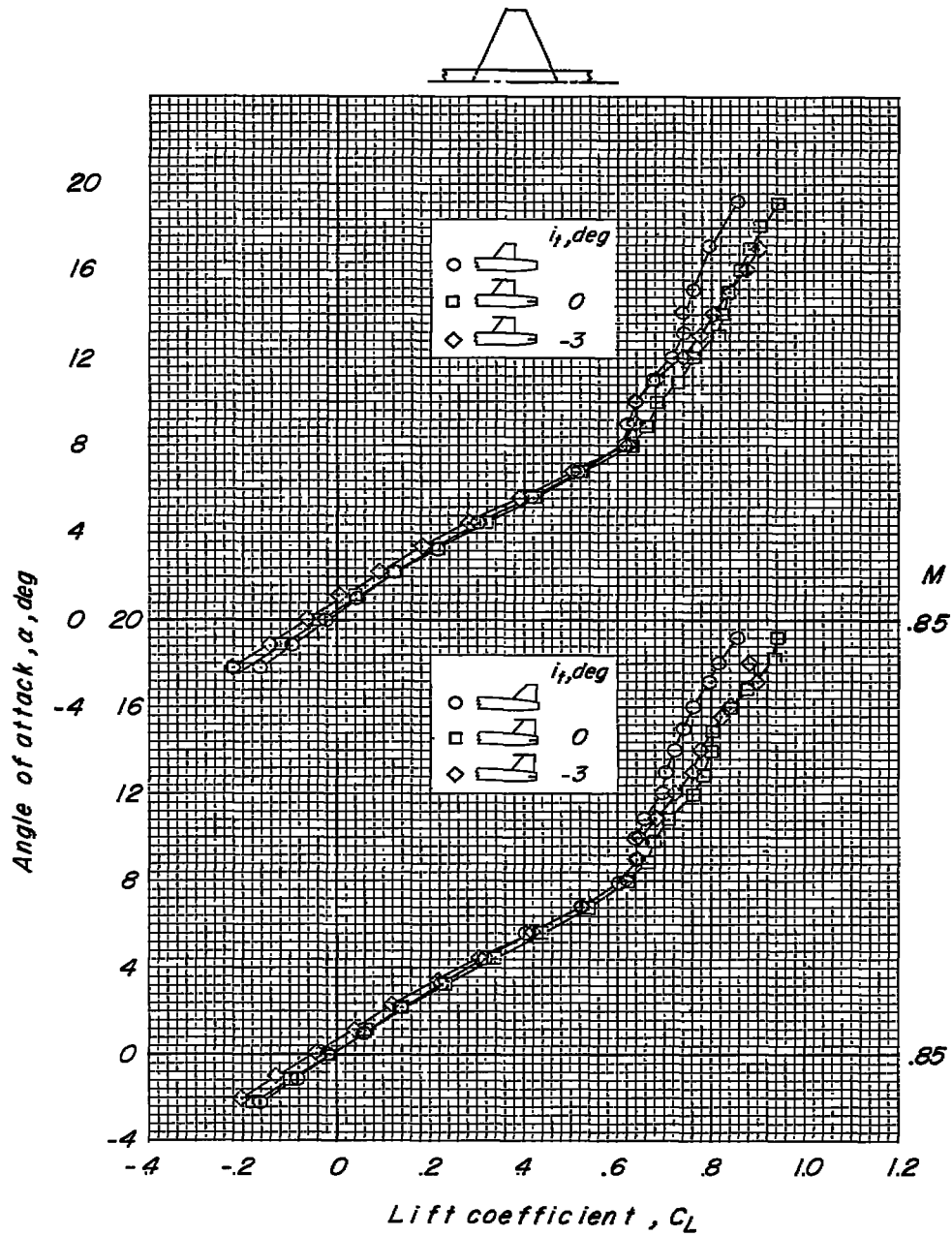
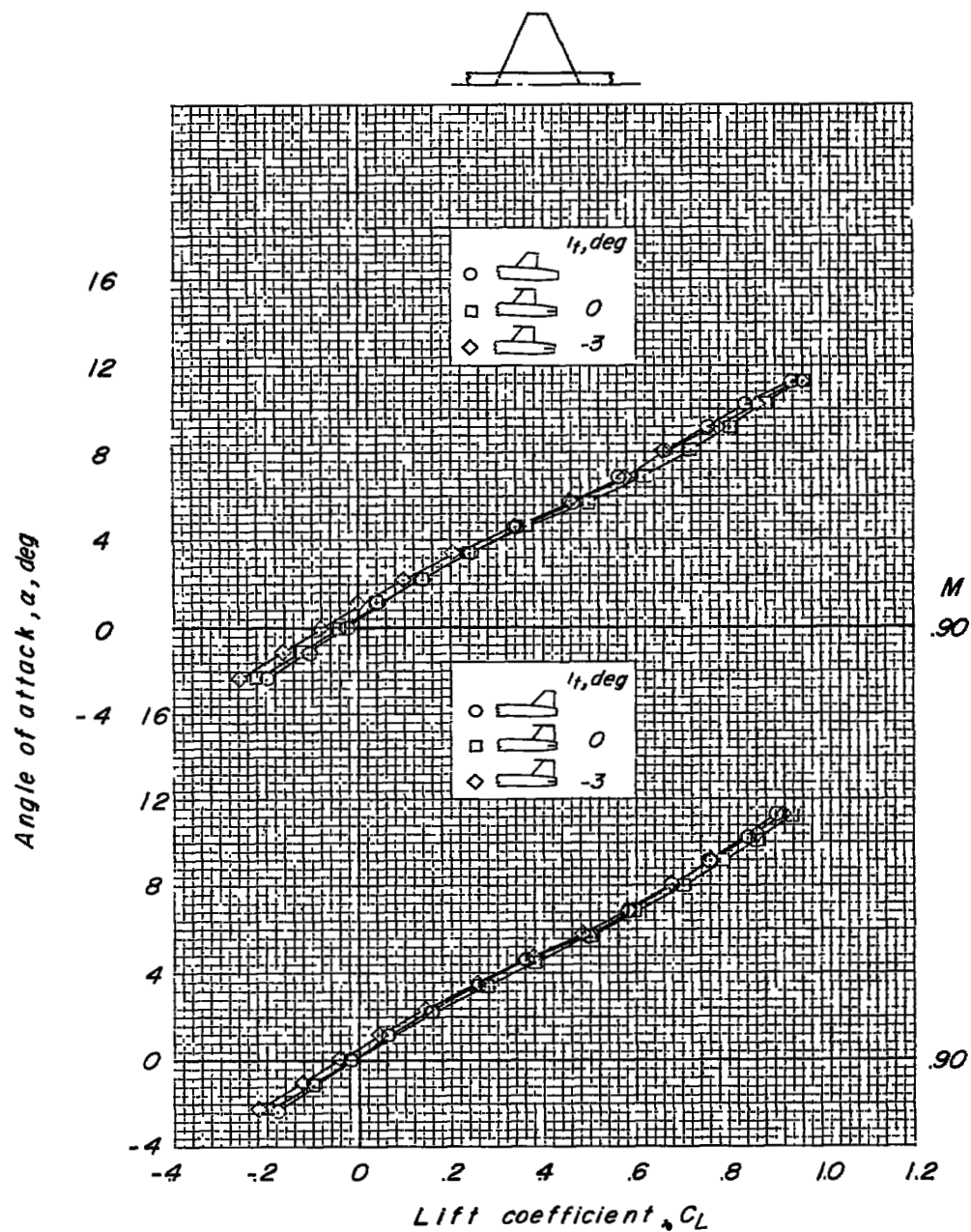
(a)  $M = 0.80$ .

Figure 19.- Variation of lift coefficient with angle of attack for the model with a bitail and unswept wing.



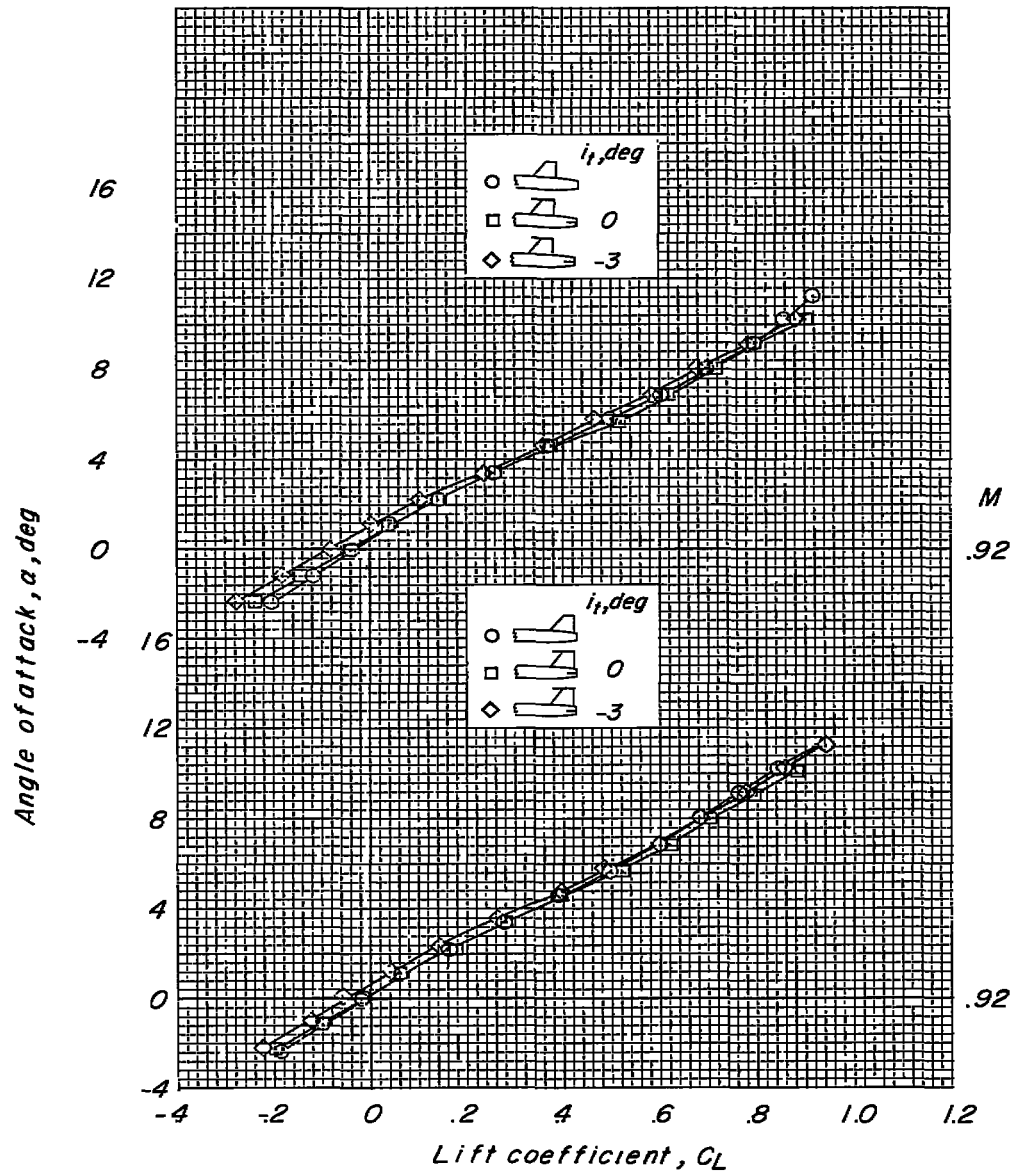
(b)  $M = 0.85$ .

Figure 19.- Continued.



(c)  $M = 0.90$ .

Figure 19.- Continued.



(d)  $M = 0.92$ .

Figure 19.- Concluded.

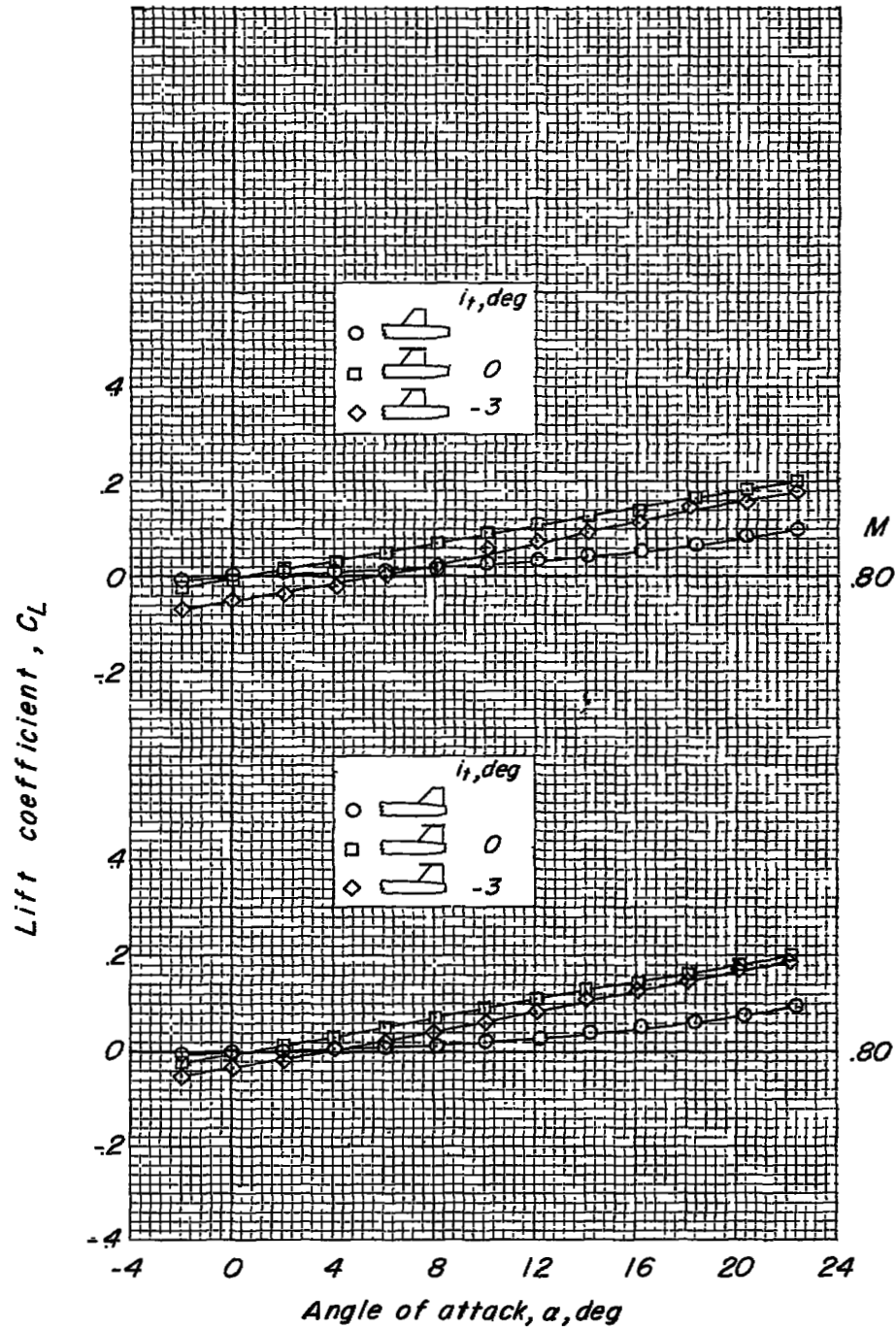
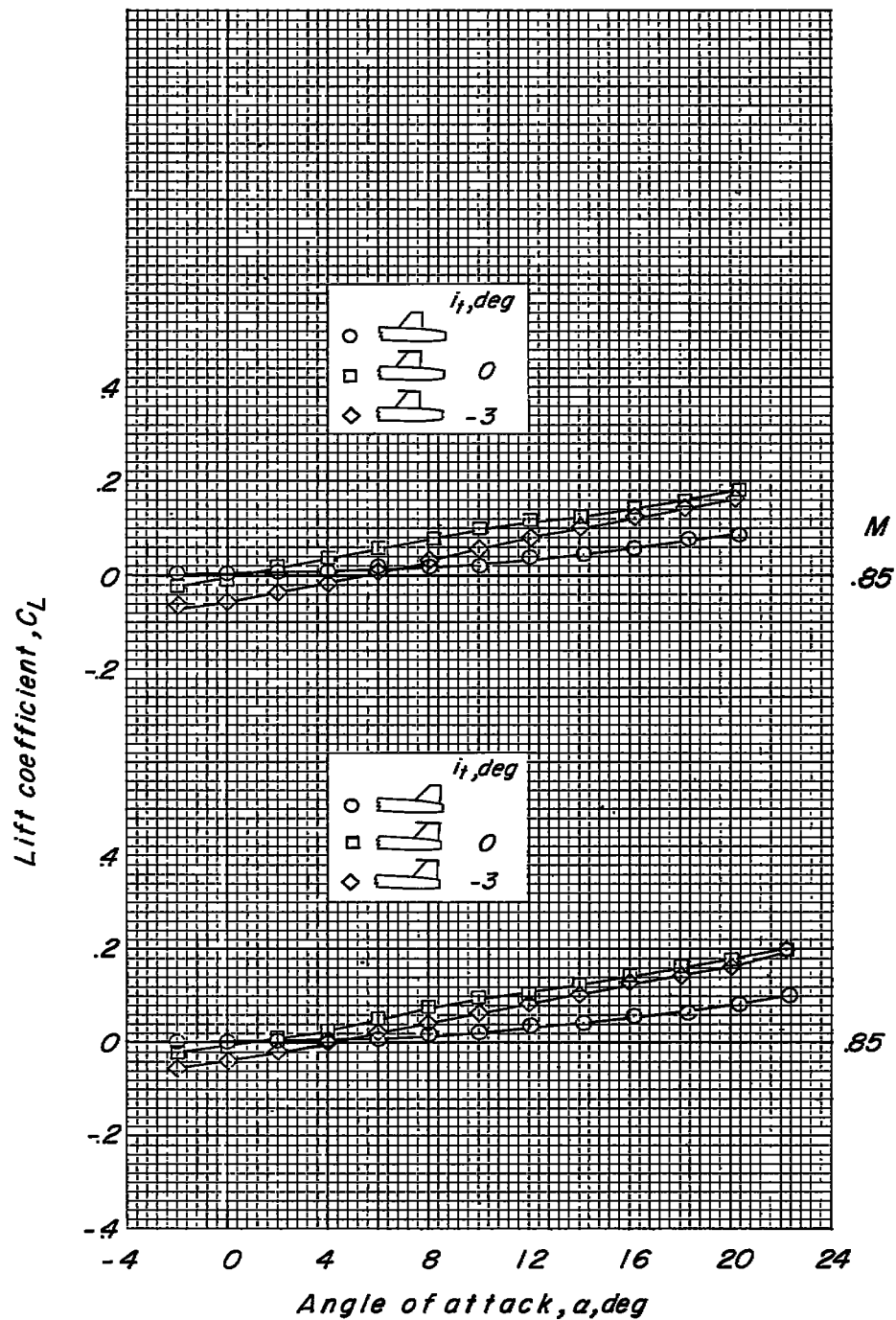
(a)  $M = 0.80$ .

Figure 20.- Variation of lift coefficient with angle of attack for the model with a high tail and wing off.



(b)  $M = 0.85$ .

Figure 20.- Continued.

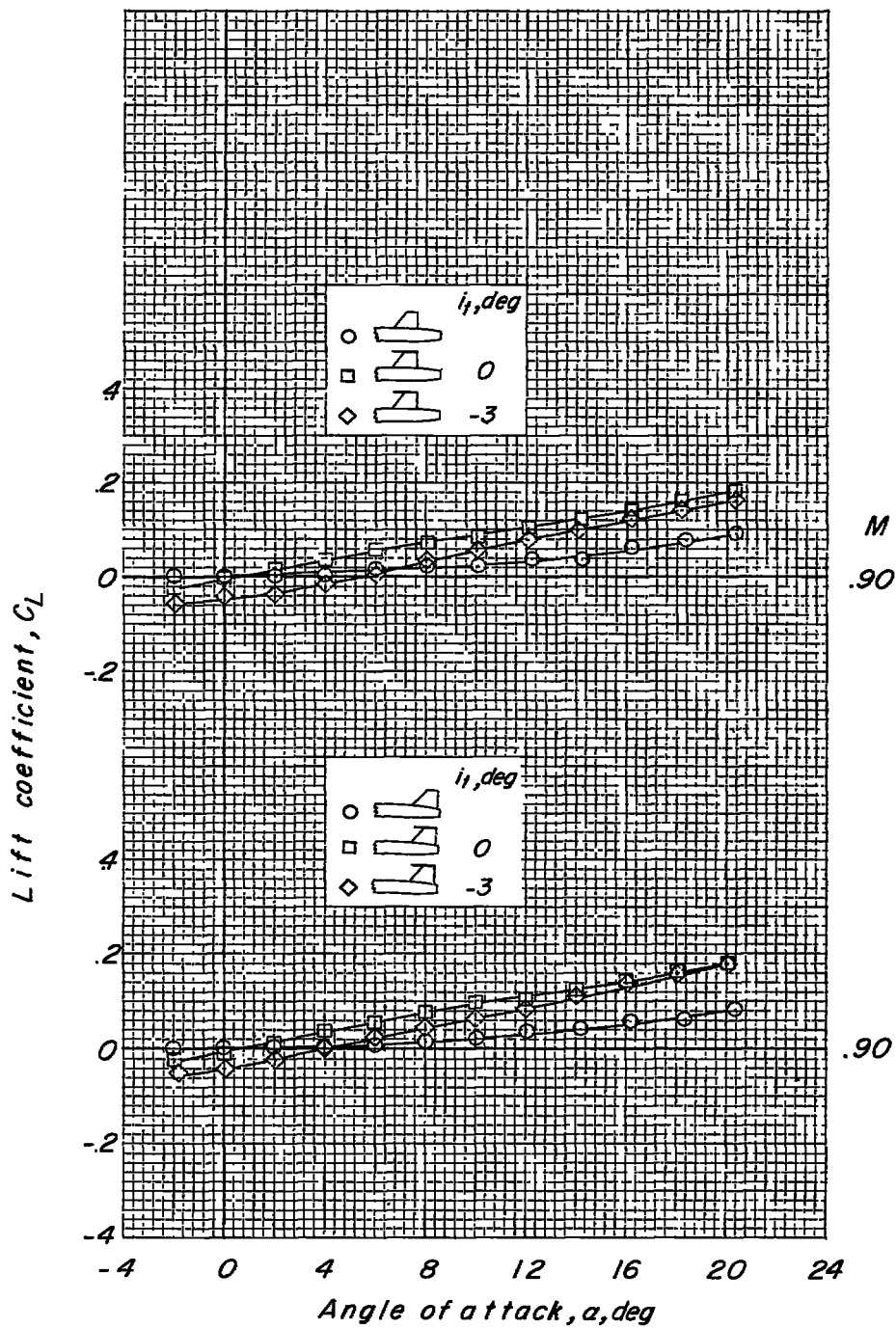
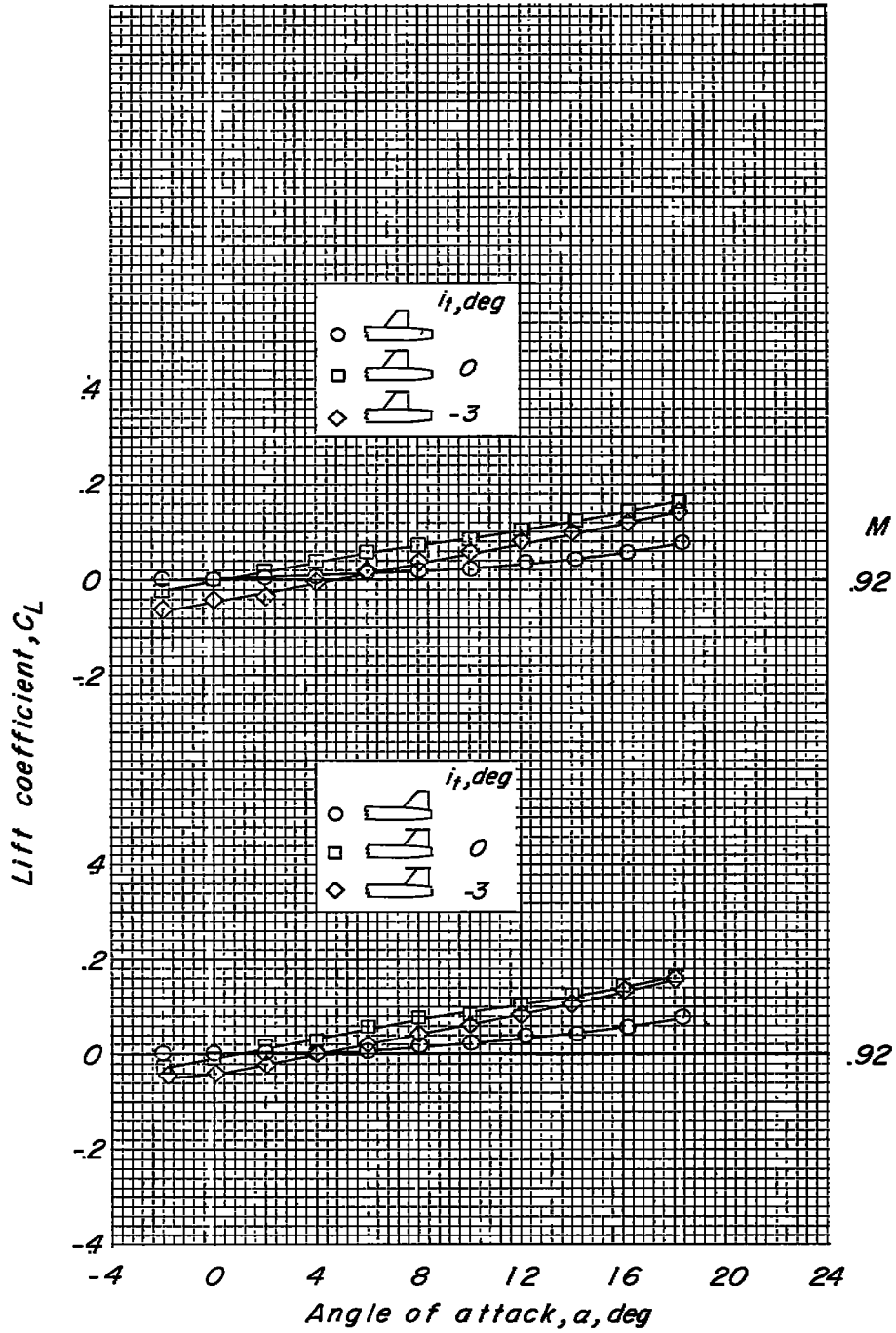
(c)  $M = 0.90$ .

Figure 20.- Continued.



(d)  $M = 0.92$ .

Figure 20.- Concluded.

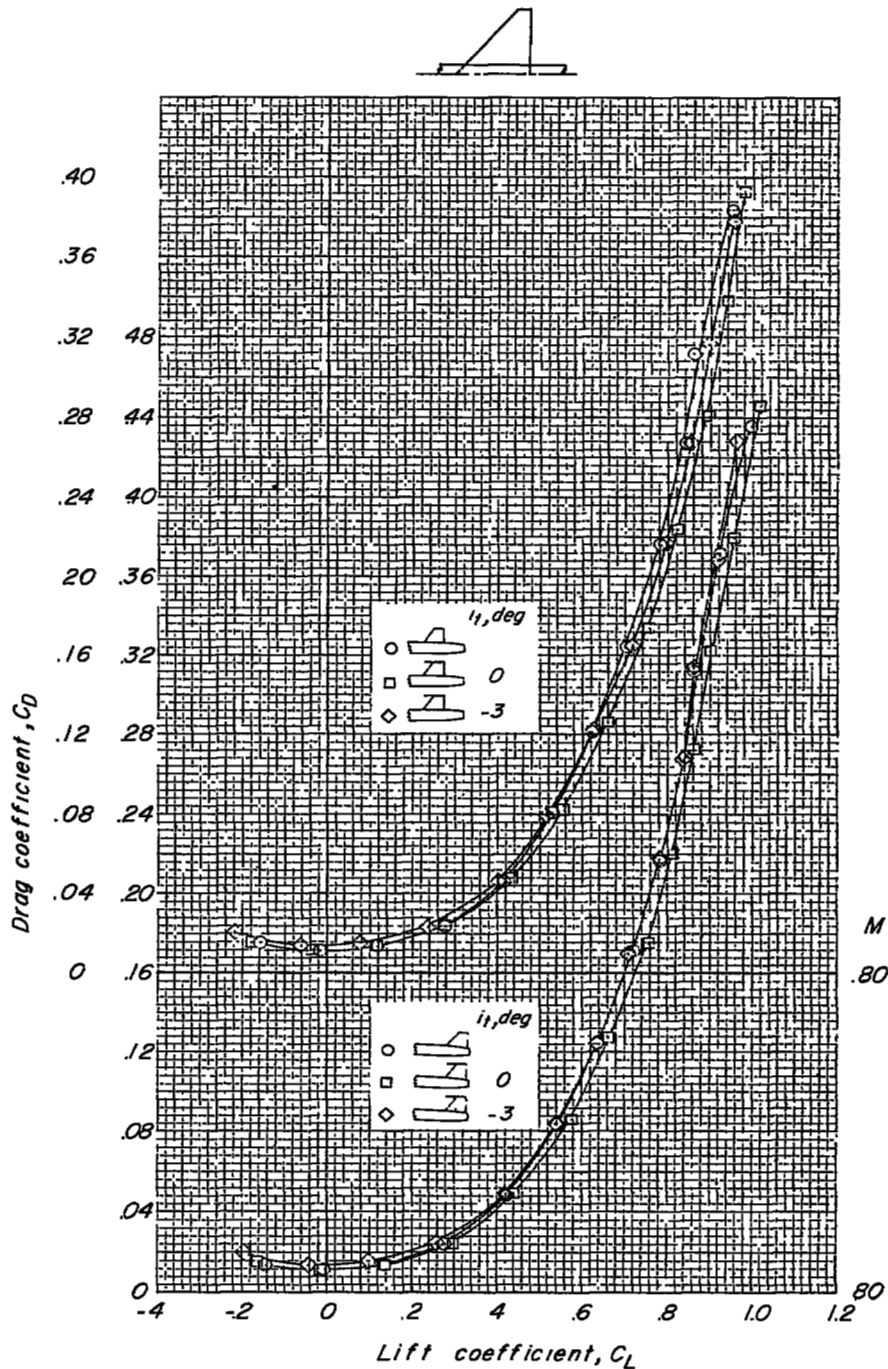
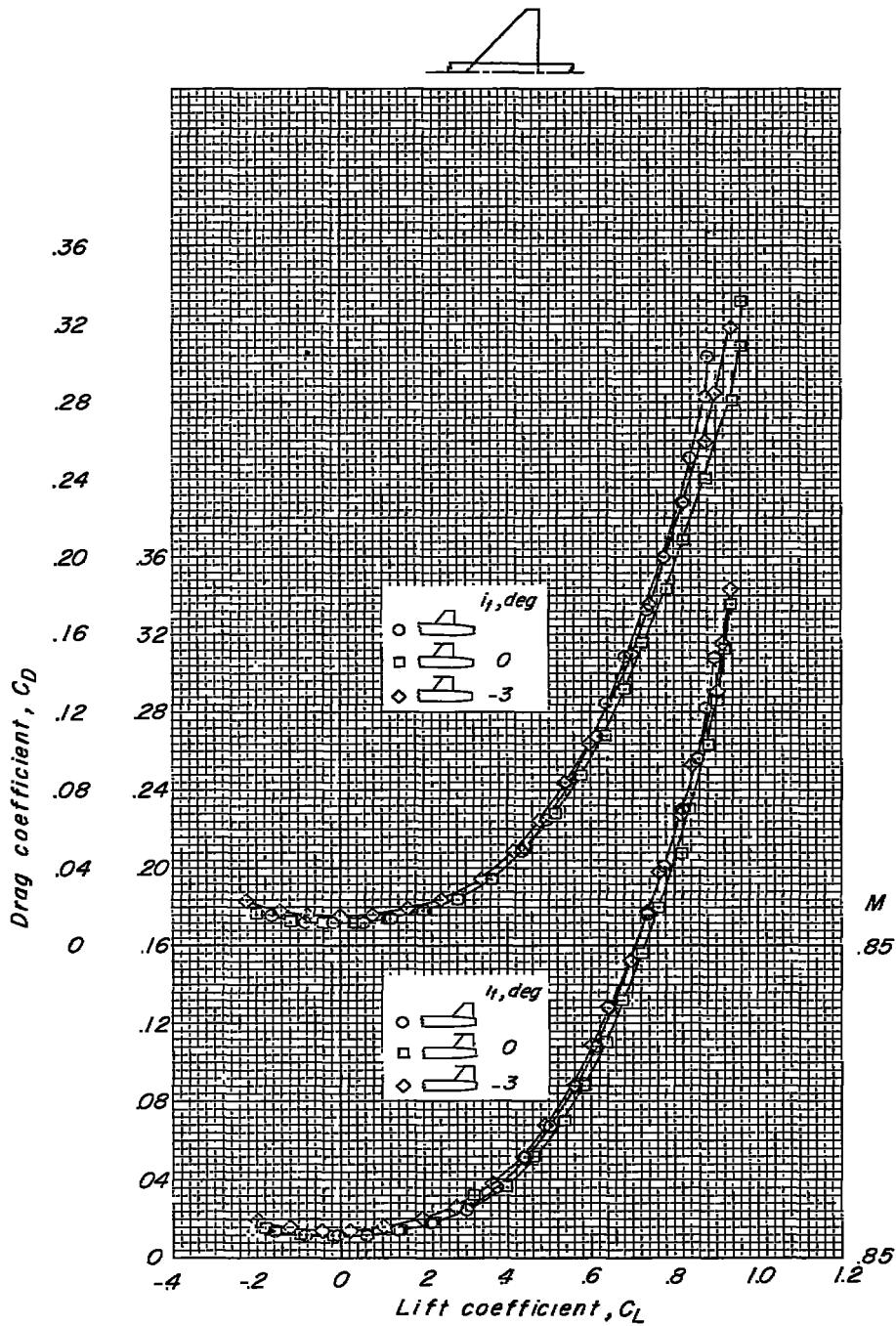
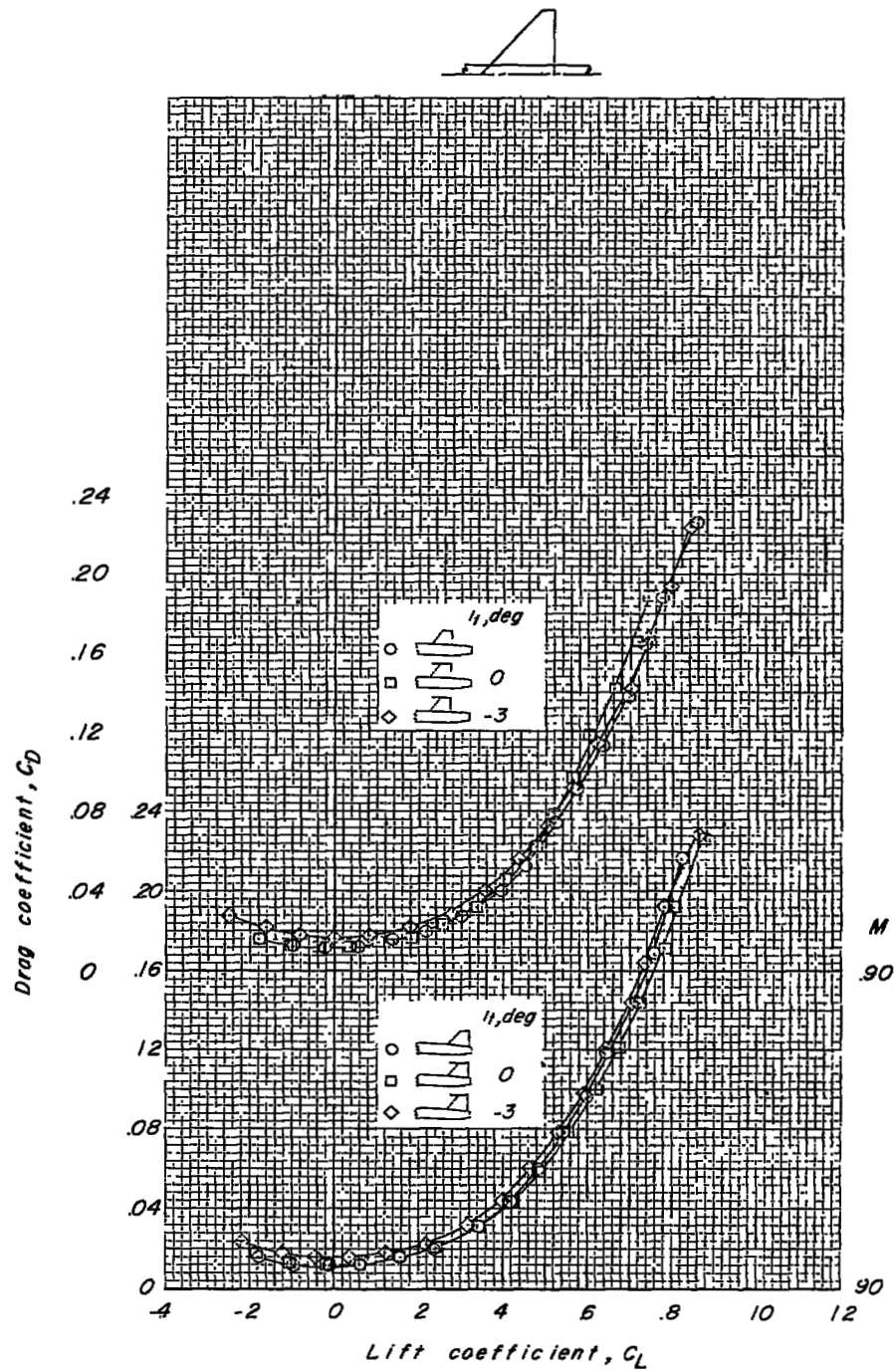
(a)  $M = 0.80$ .

Figure 21.- Variation of drag coefficient with lift coefficient for the model with a high tail and cropped-delta wing.



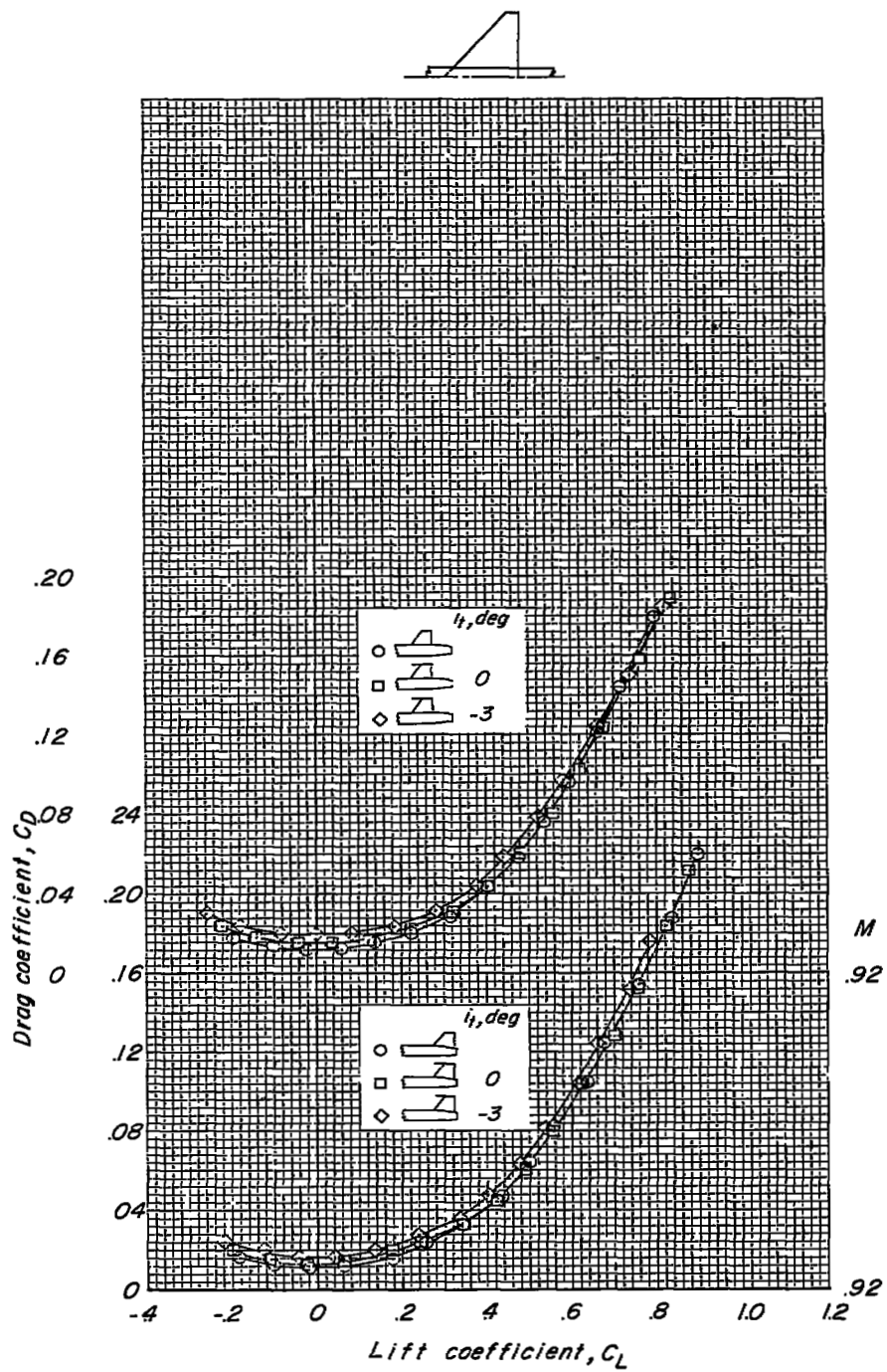
(b)  $M = 0.85$ .

Figure 21.- Continued.



(c)  $M = 0.90$ .

Figure 21.- Continued.



(d)  $M = 0.92$ .

Figure 21.- Concluded.

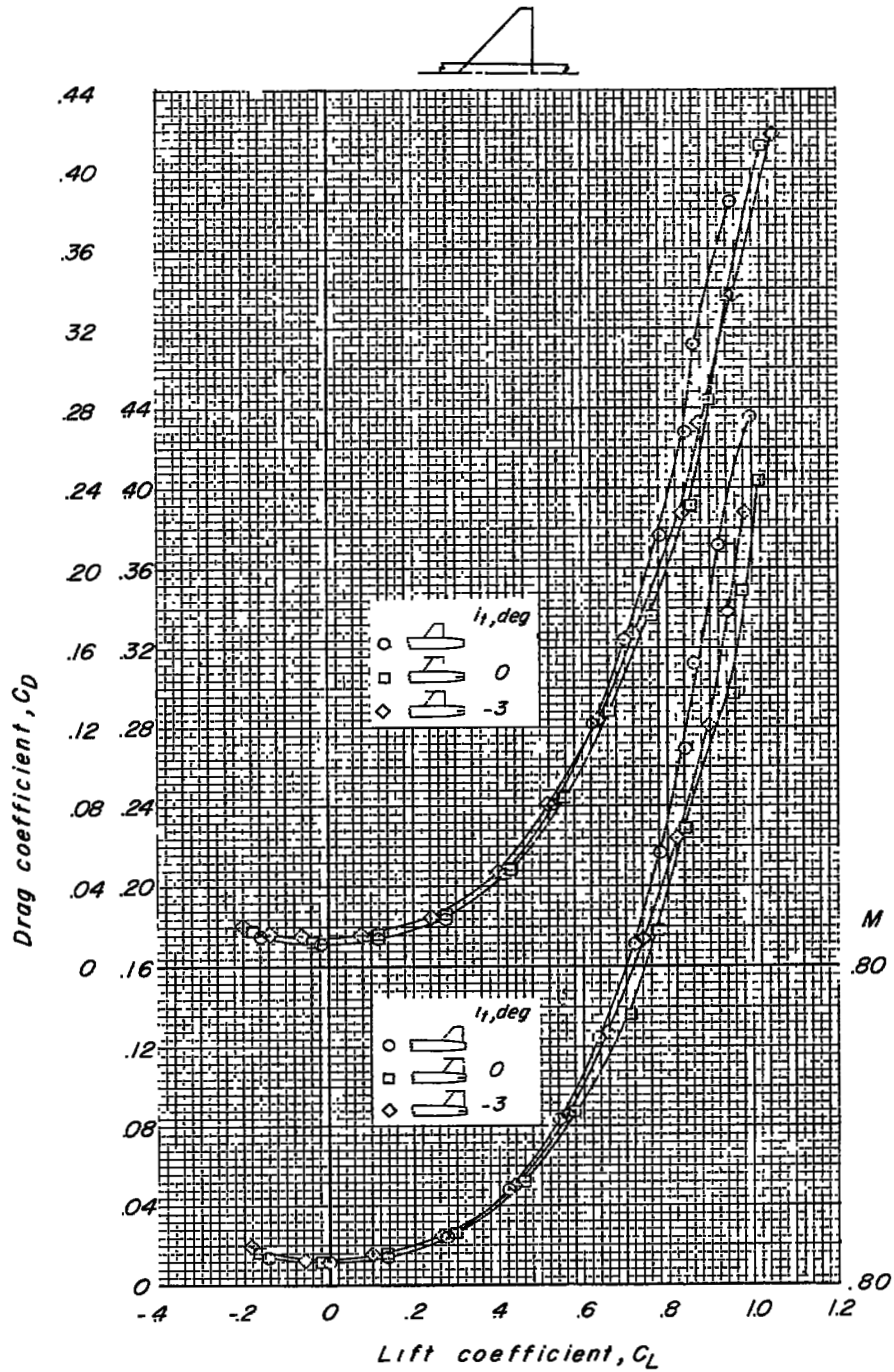
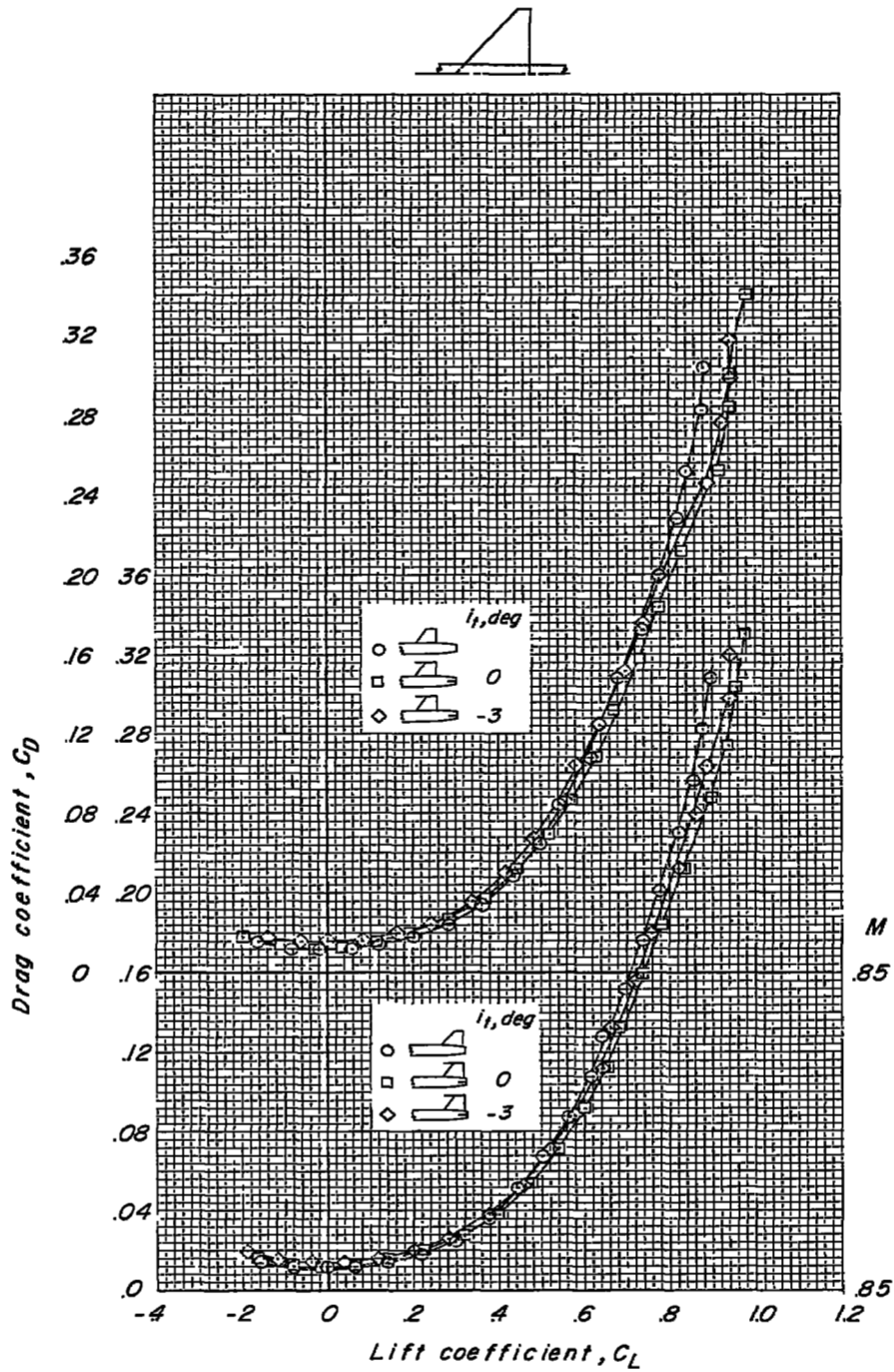
(a)  $M = 0.80$ .

Figure 22.- Variation of drag coefficient with lift coefficient for the model with a bitail and cropped-delta wing.



(b)  $M = 0.85$ .

Figure 22.- Continued.

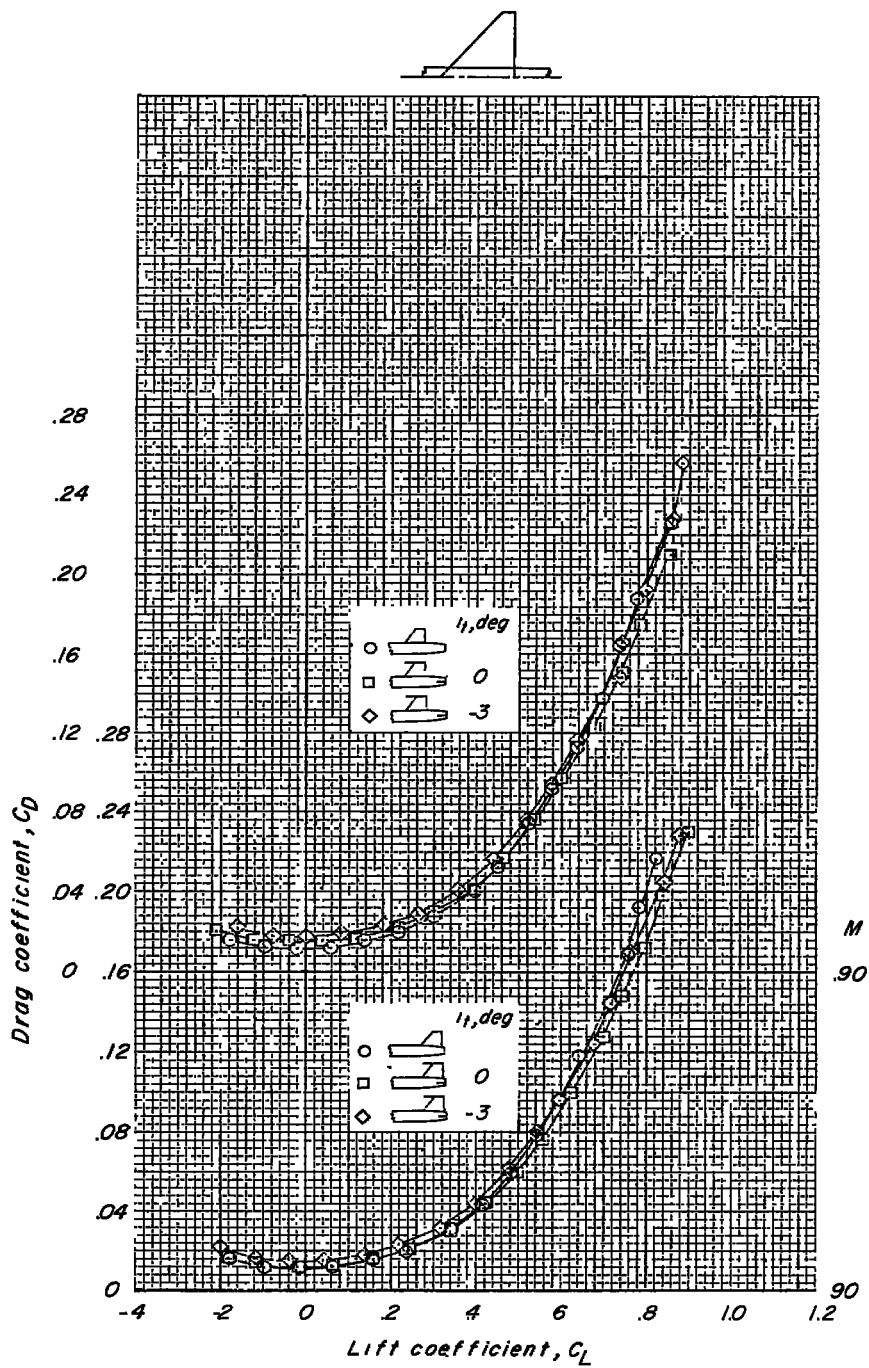
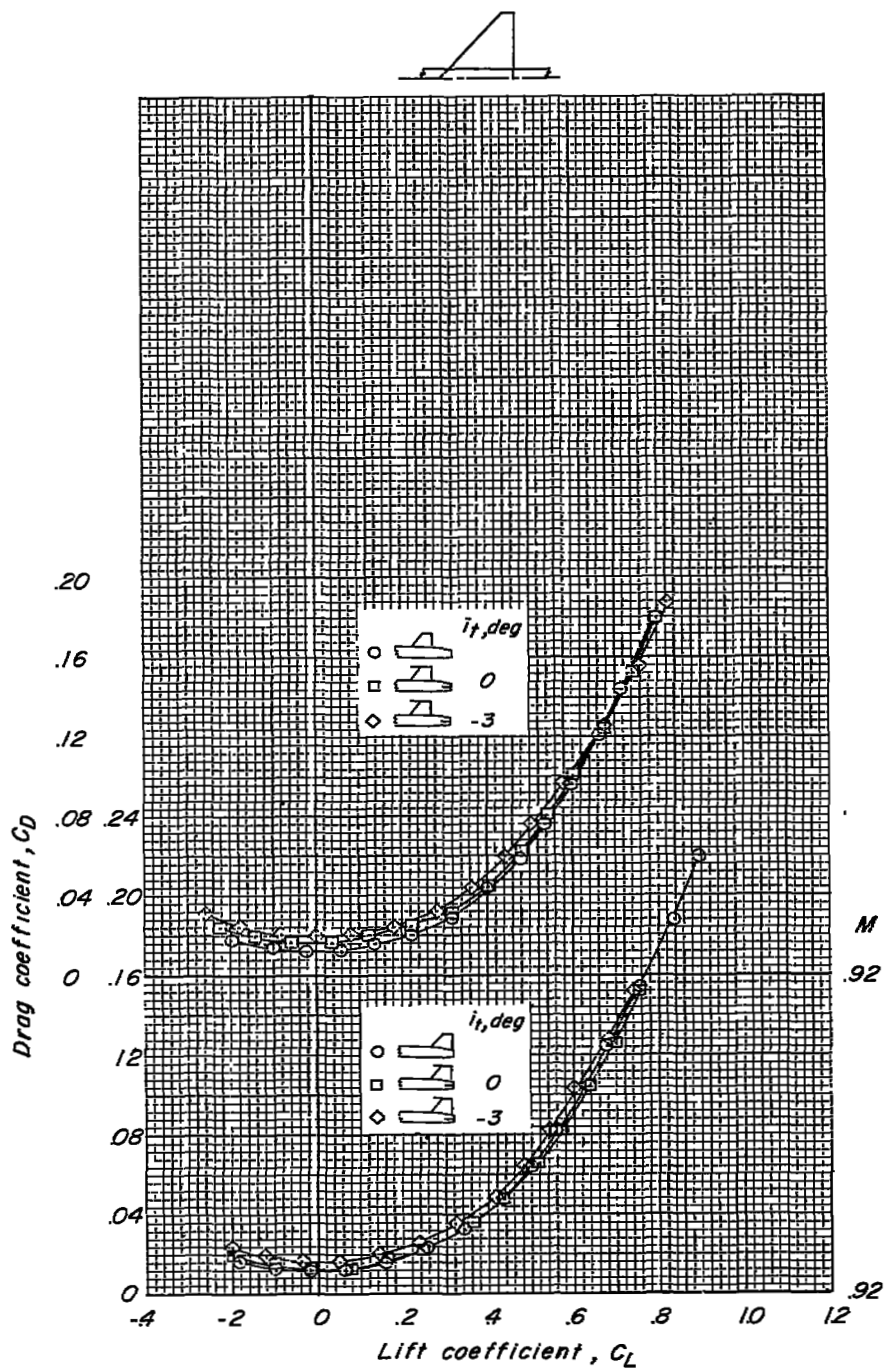
(c)  $M = 0.90$ .

Figure 22.- Continued.



(d)  $M = 0.92$ .

Figure 22.- Concluded.

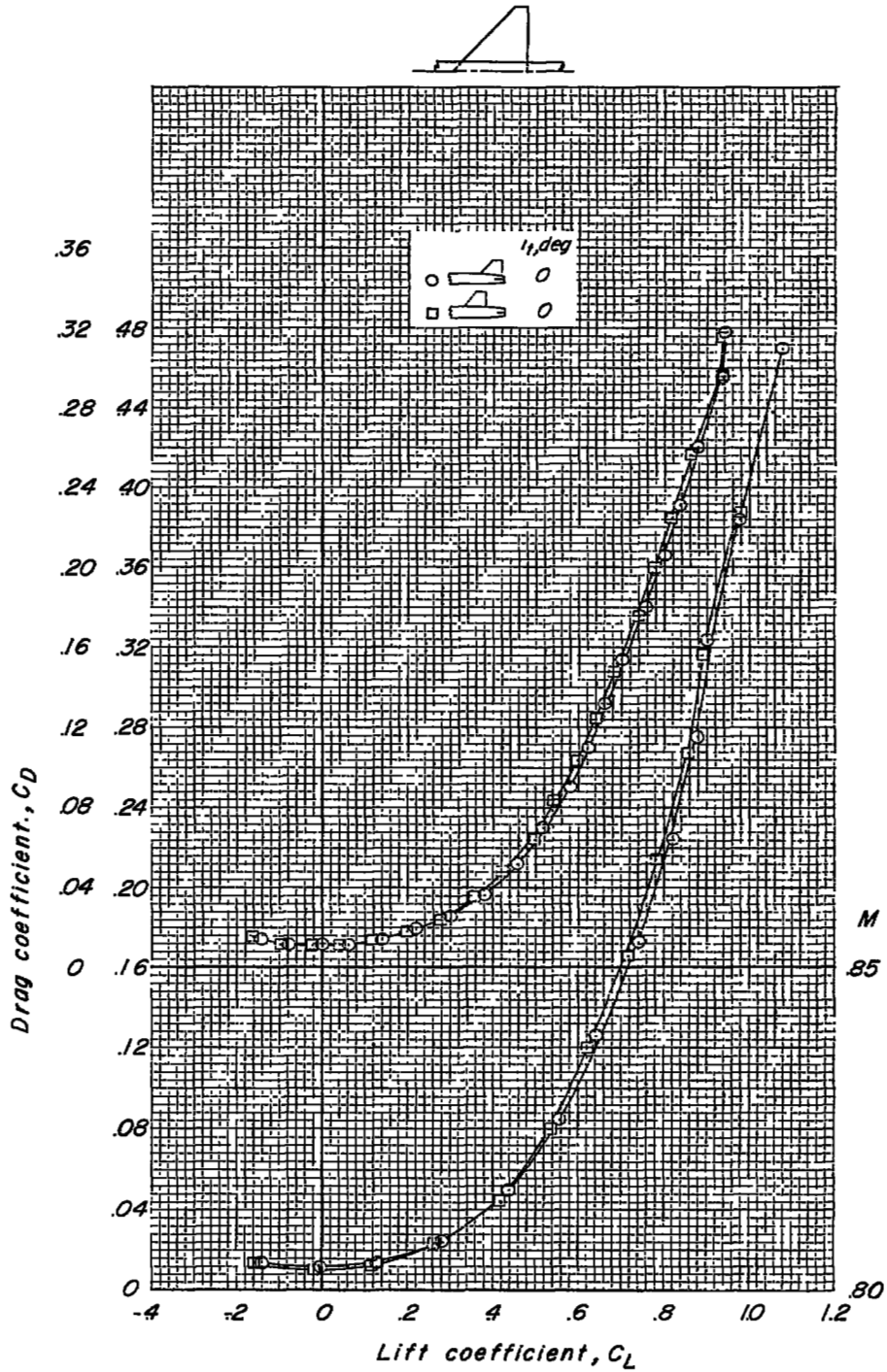


Figure 23.- Variation of drag coefficient with lift coefficient for the model with a low tail and cropped-delta wing.

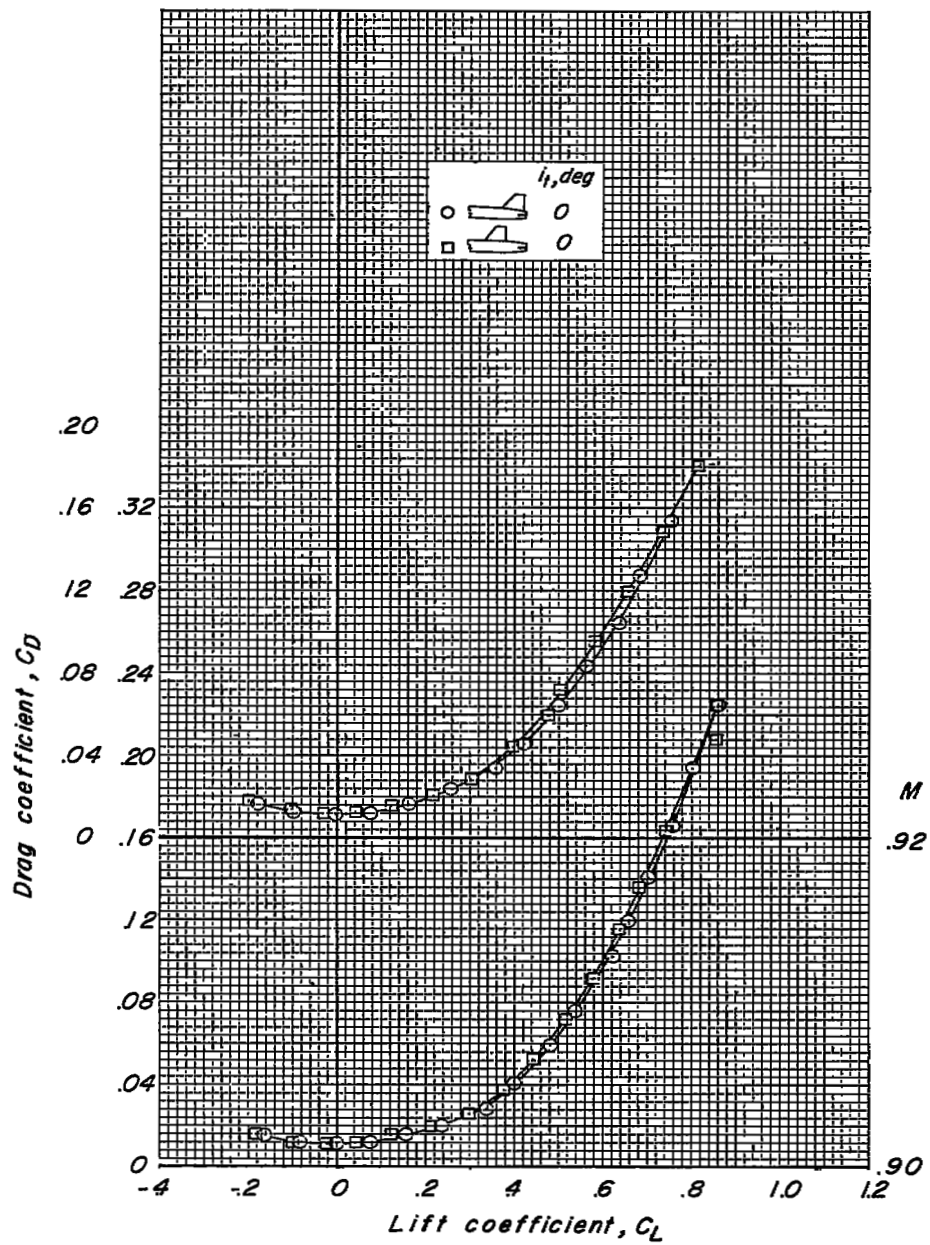


Figure 23.- Concluded.

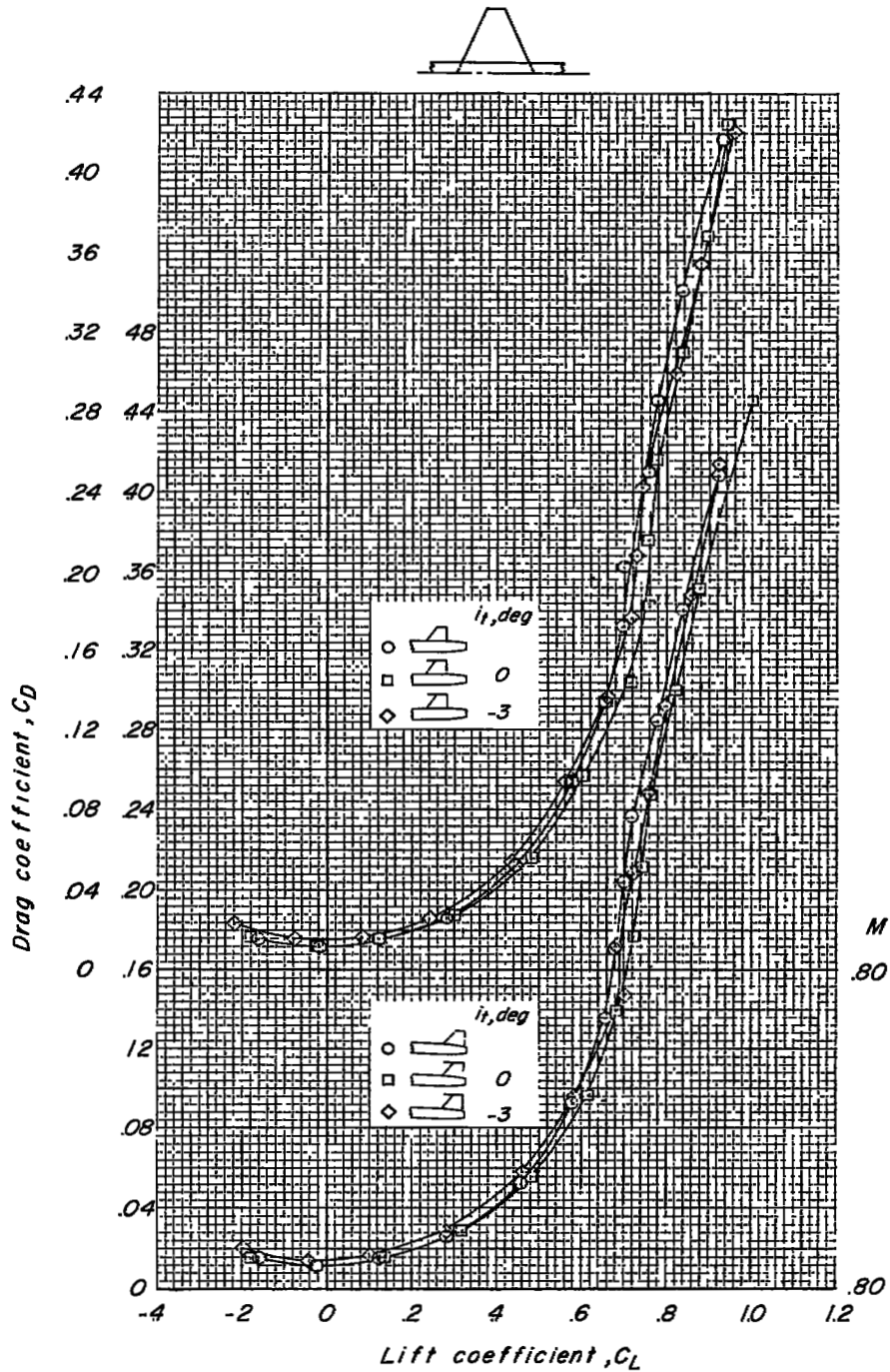
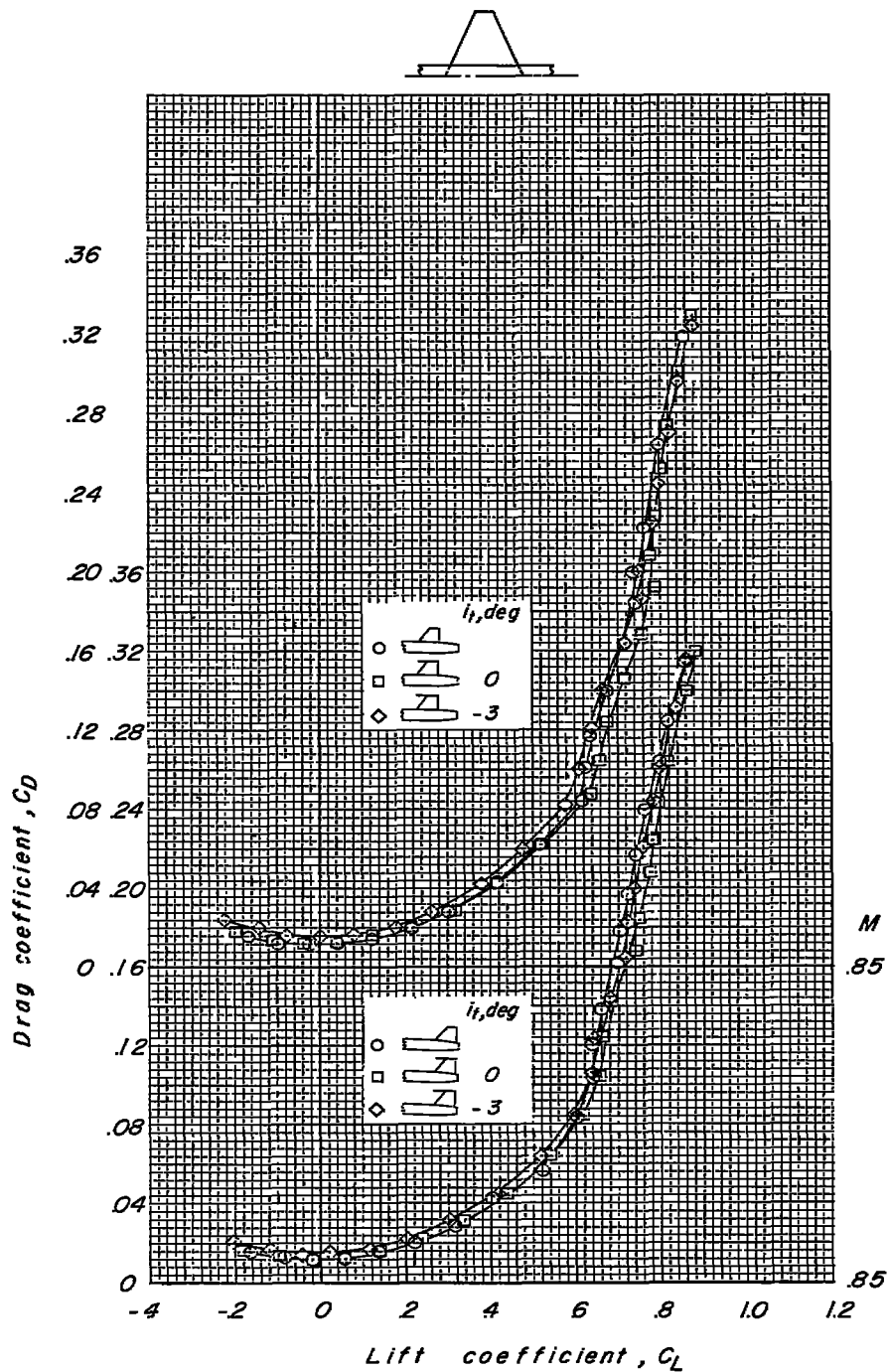
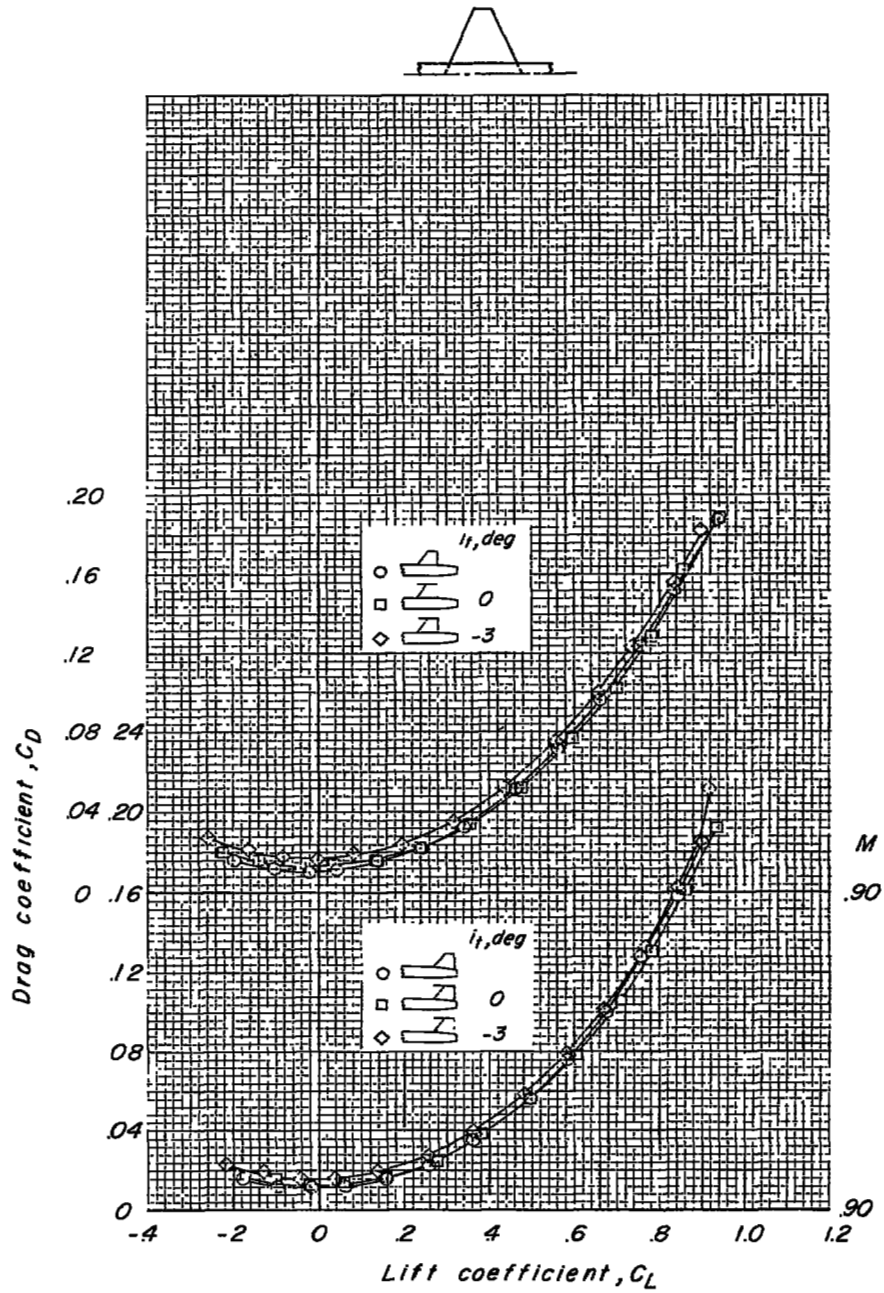
(a)  $M = 0.80$ .

Figure 24.- Variation of drag coefficient with lift coefficient for the model with a high tail and unswept wing.



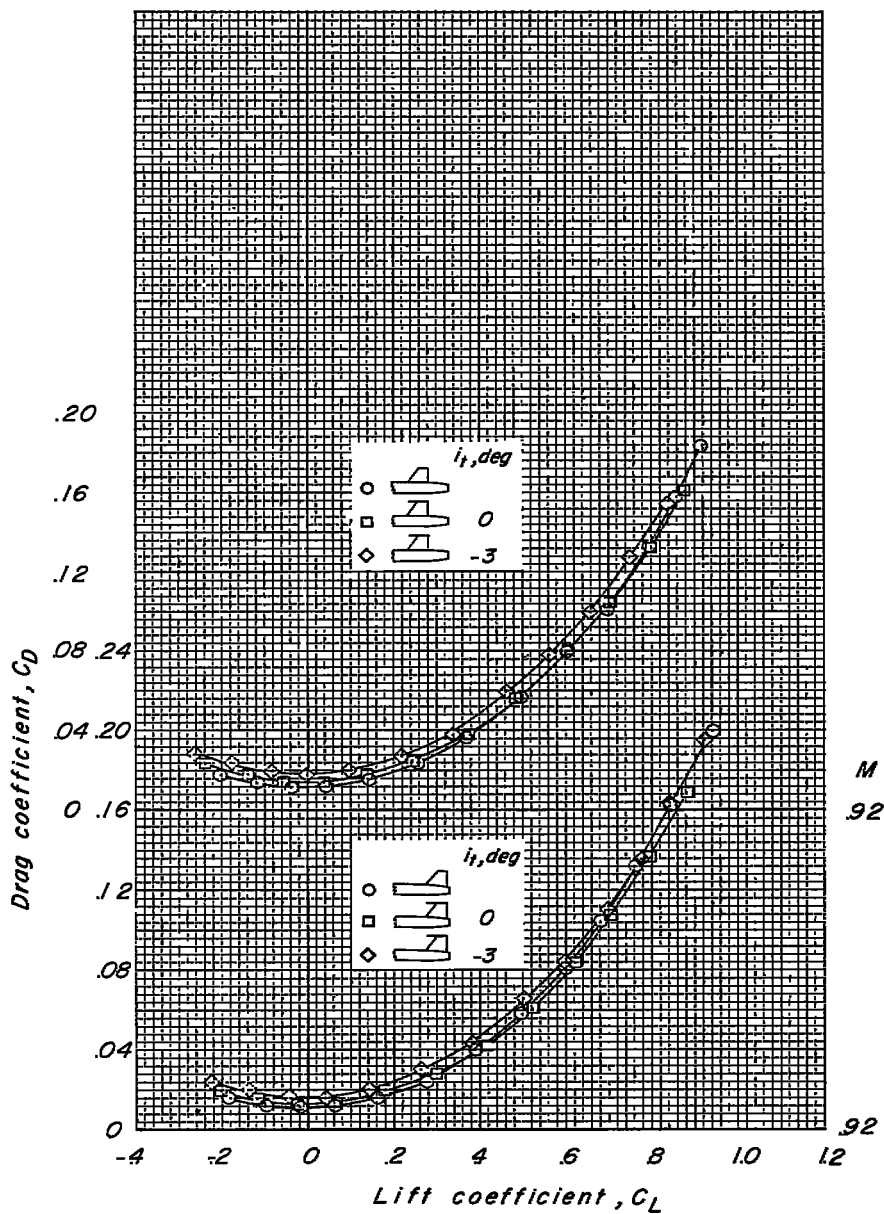
(b)  $M = 0.85$ .

Figure 24.- Continued.



(c)  $M = 0.90$ .

Figure 24.- Continued.



(d)  $M = 0.92$ .

Figure 24.- Concluded.

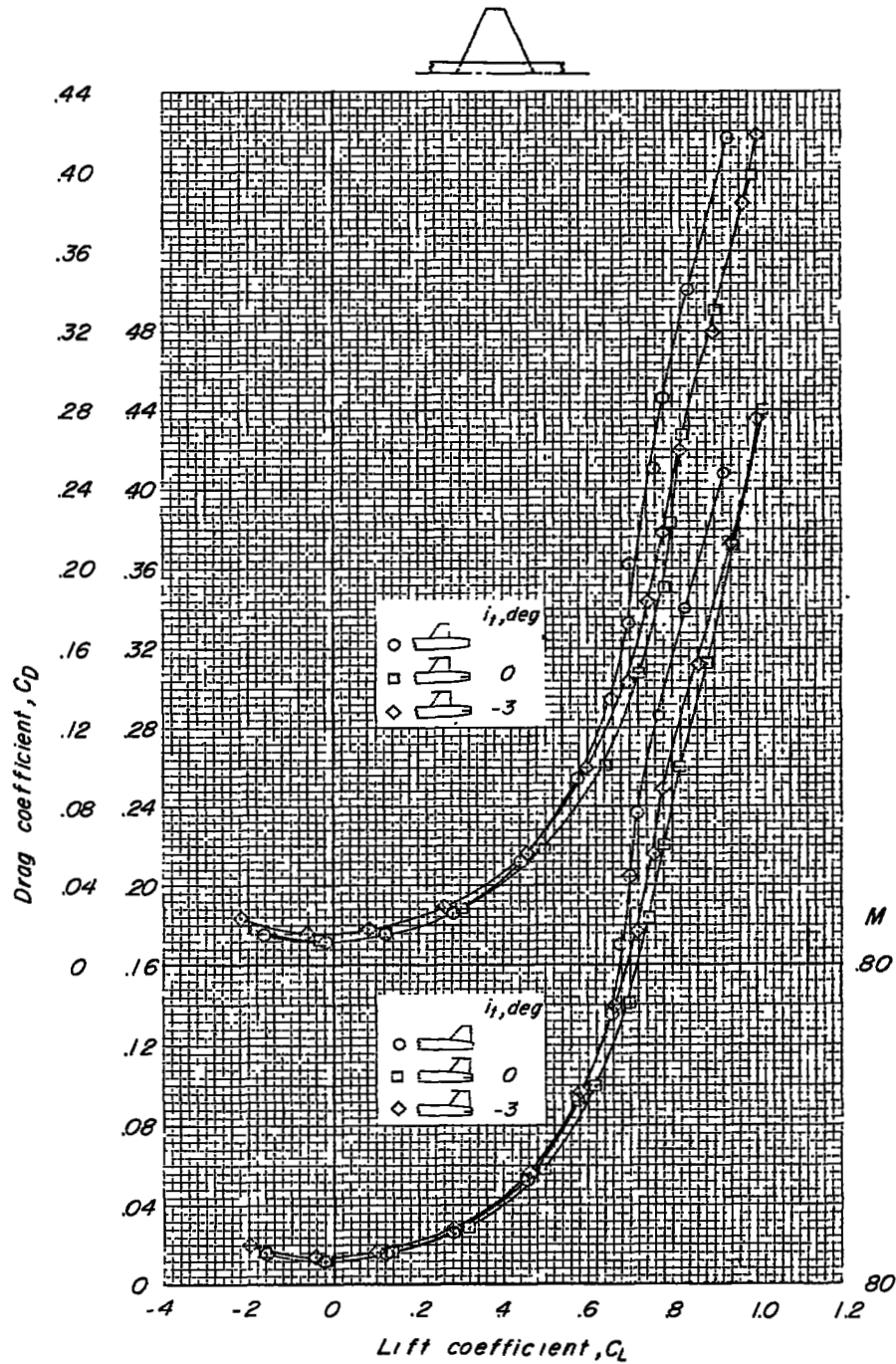
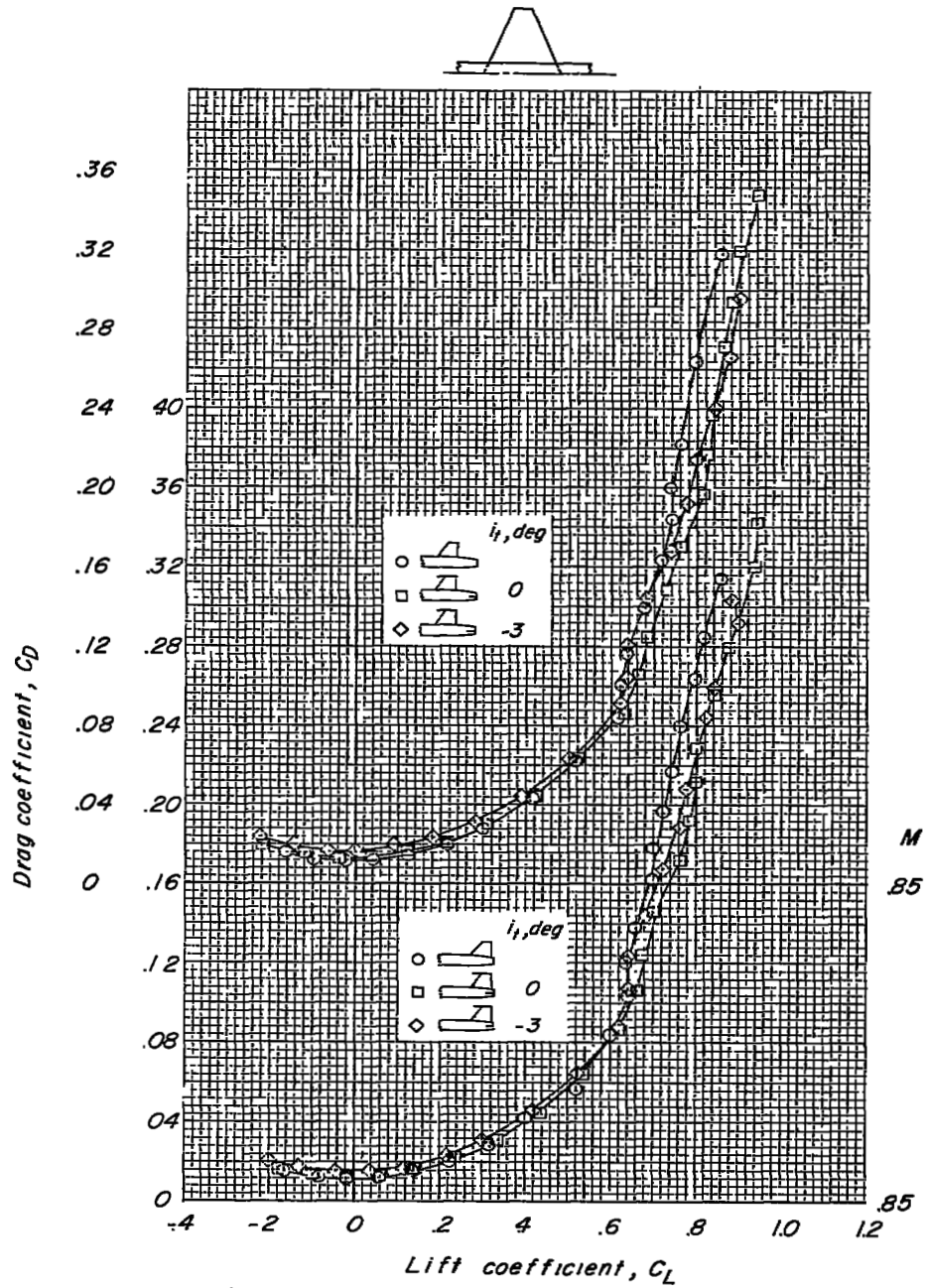
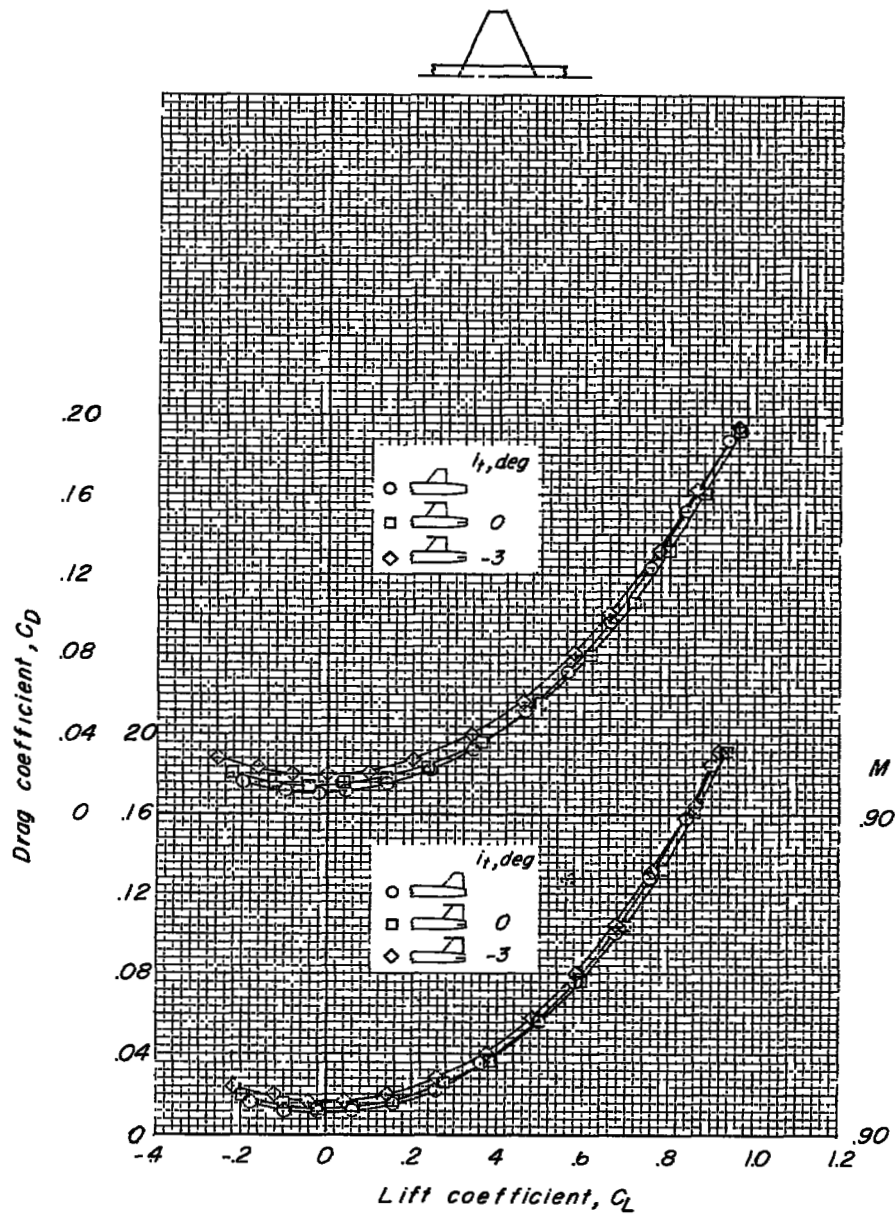
(a)  $M = 0.80$ .

Figure 25.- Variation of drag coefficient with lift coefficient for the model with a bitail and unswept wing.



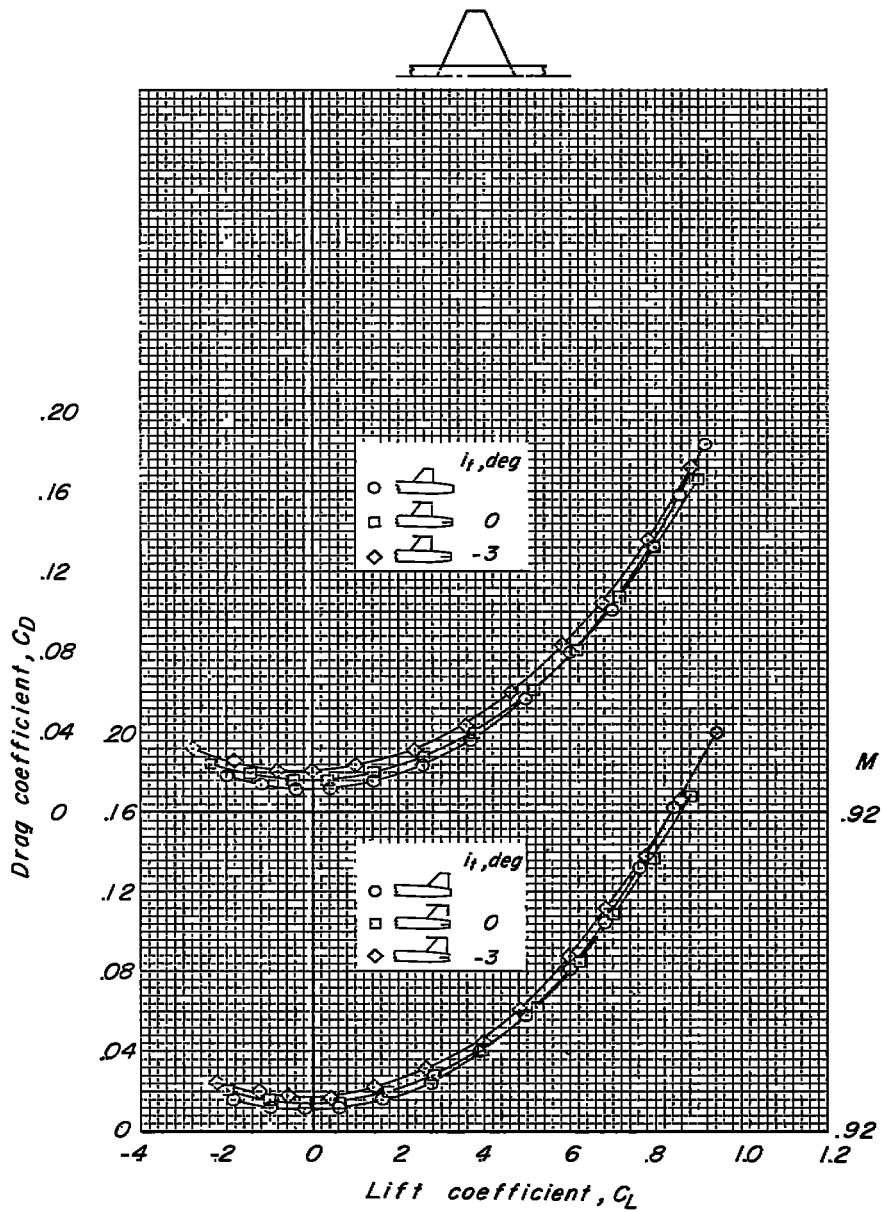
(b)  $M = 0.85$ .

Figure 25.- Continued.



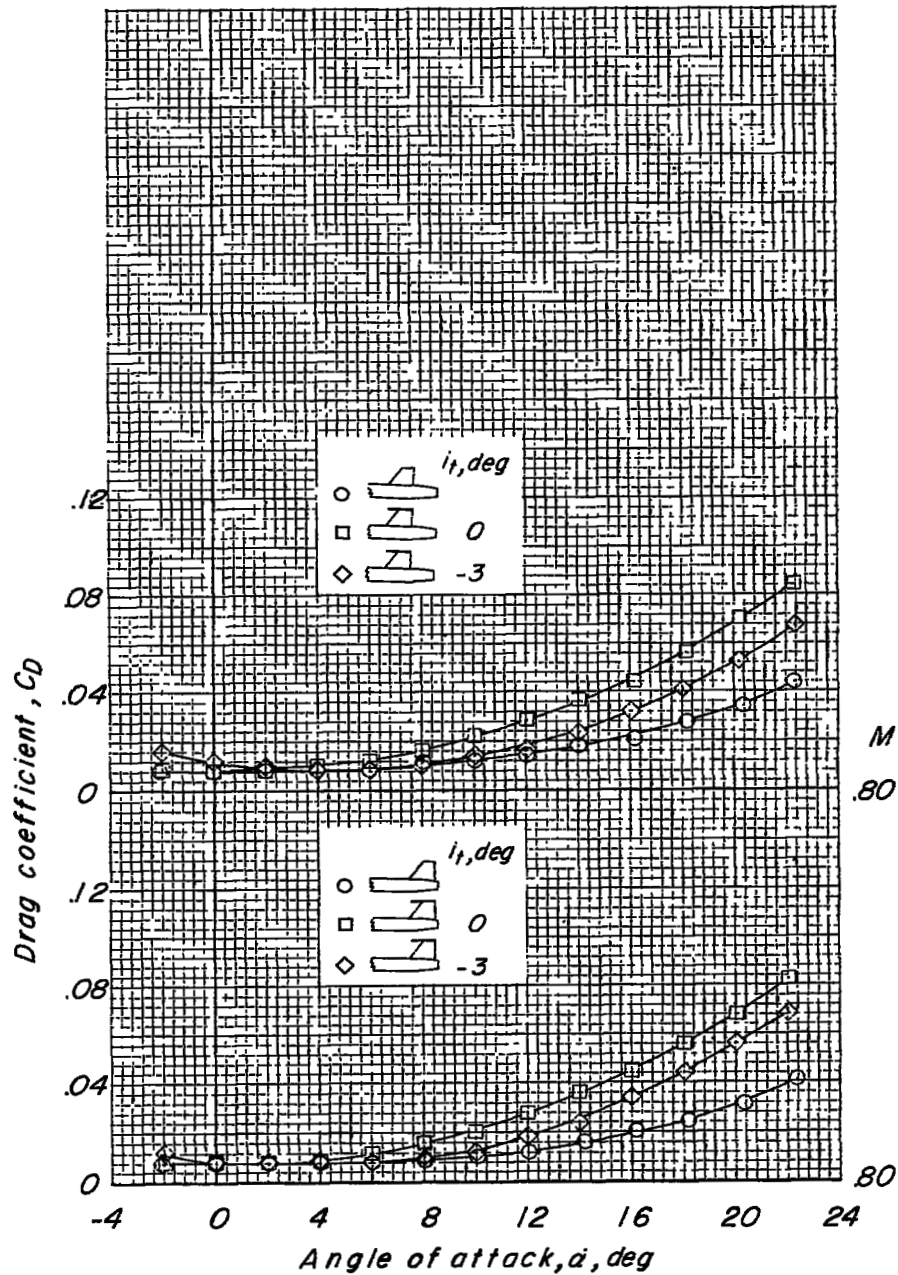
(c)  $M = 0.90$ .

Figure 25.- Continued.



(d)  $M = 0.92$ .

Figure 25.- Concluded.



(a)  $M = 0.80$ .

Figure 26.- Variation of drag coefficient with angle of attack for the model with a high tail and wing off.

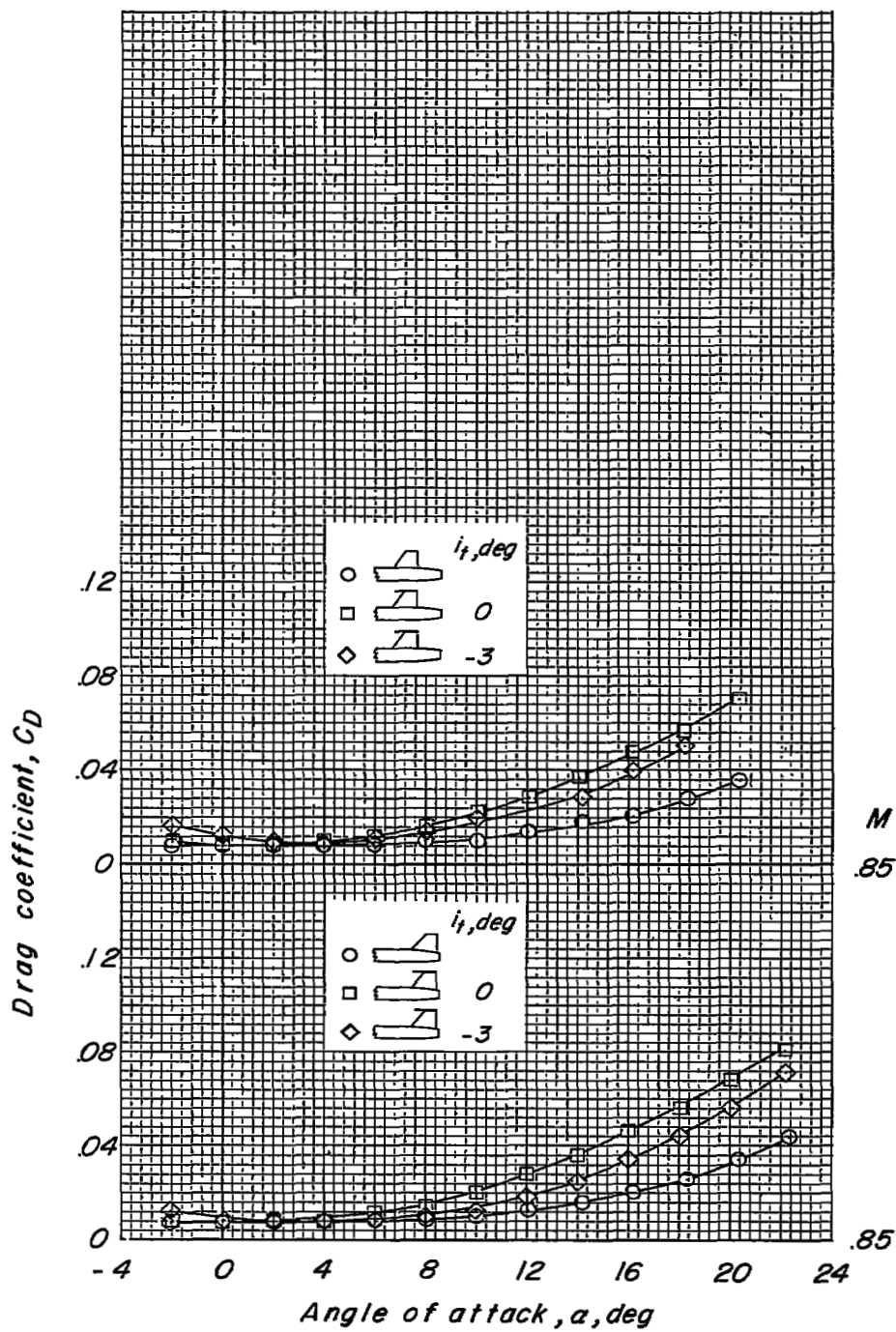
(b)  $M = 0.85$ .

Figure 26.- Continued.

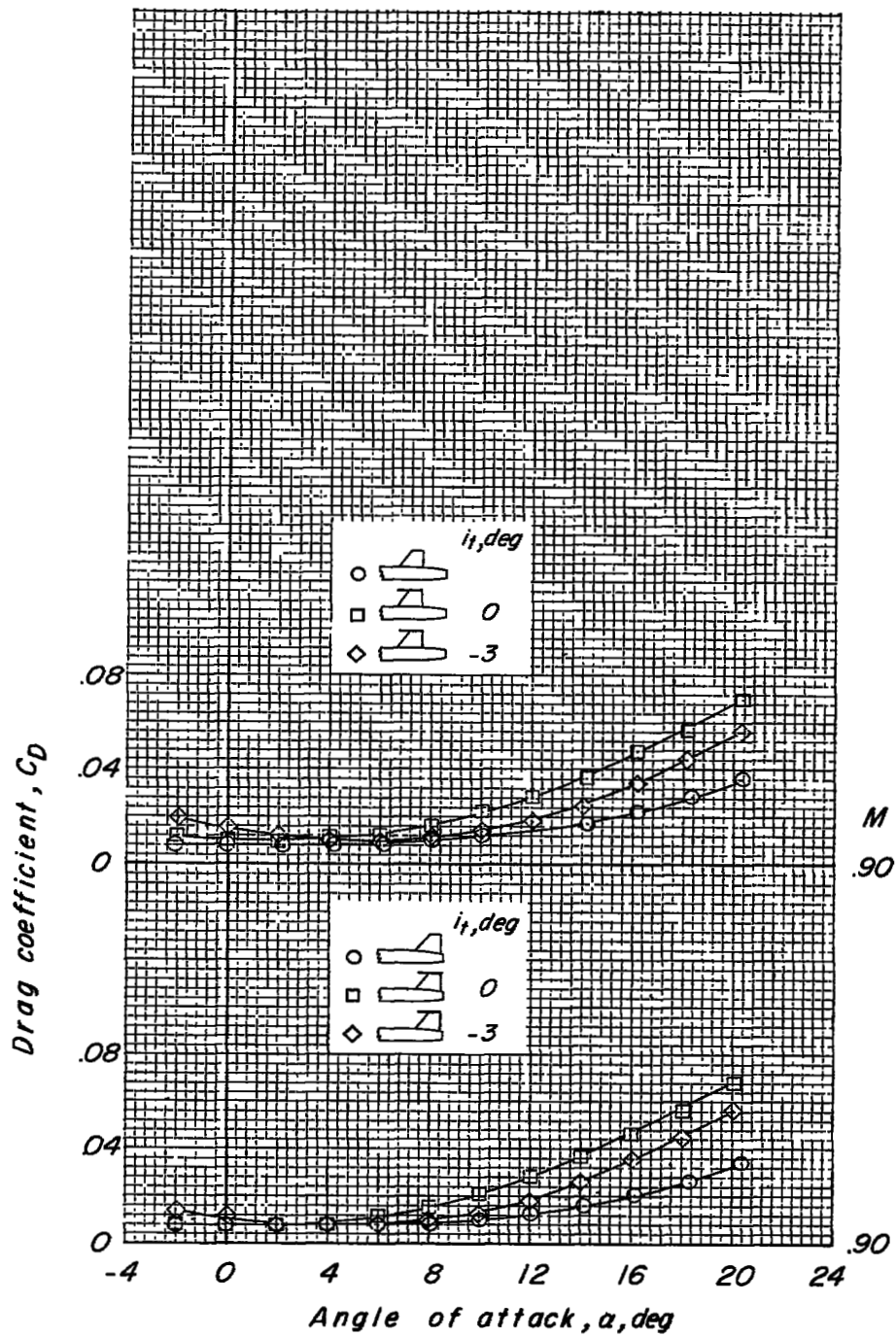
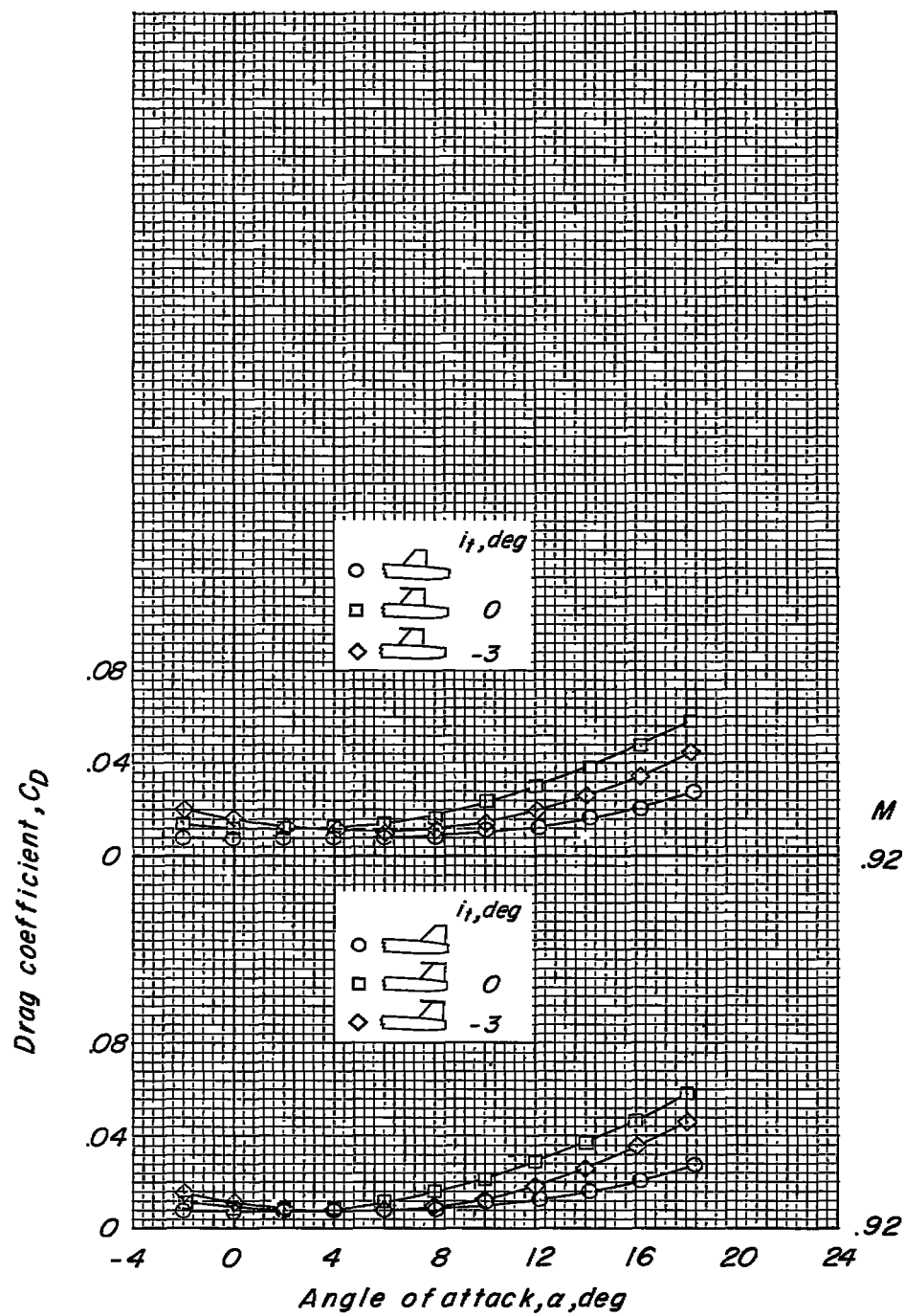
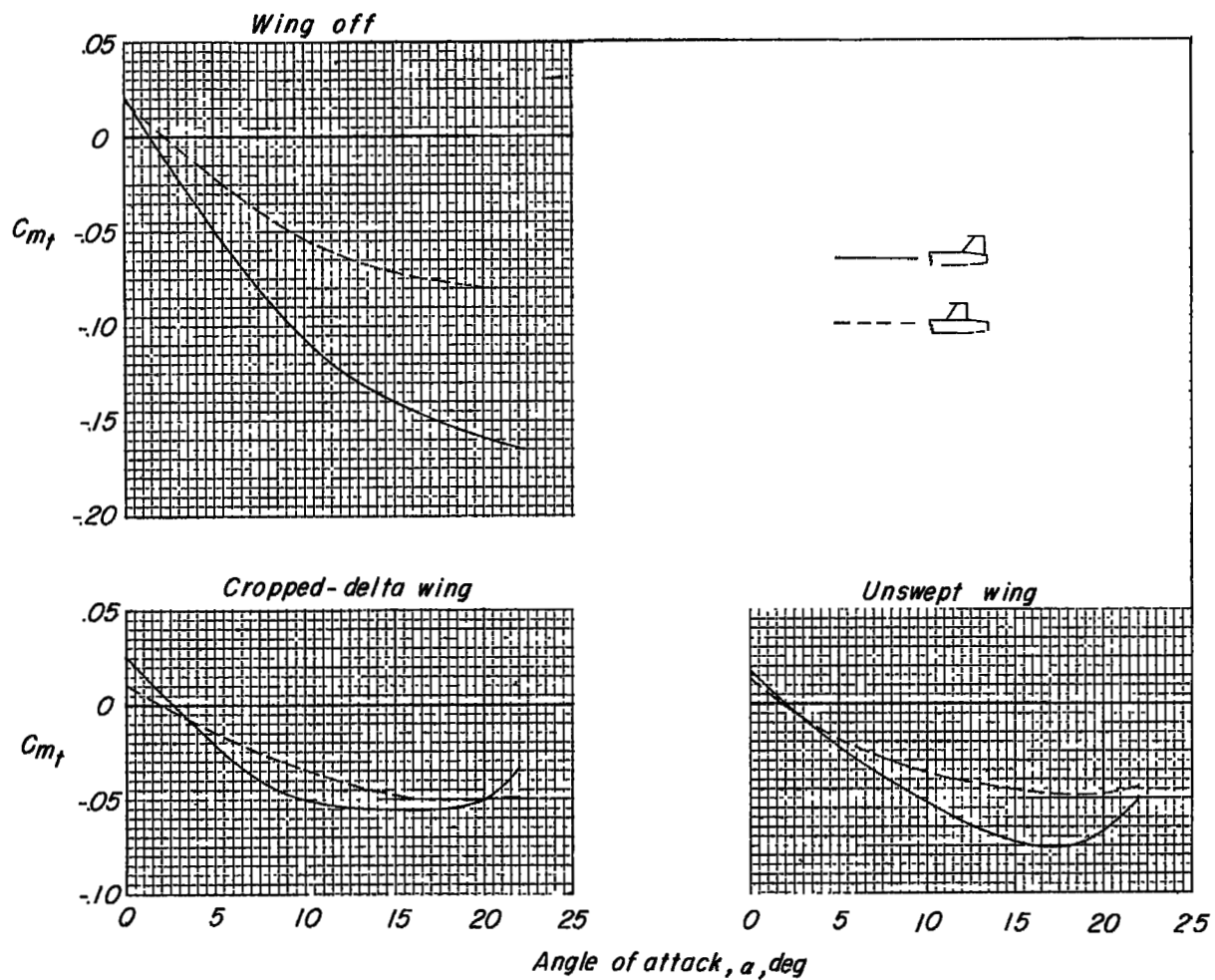
(c)  $M = 0.90$ .

Figure 26.- Continued.



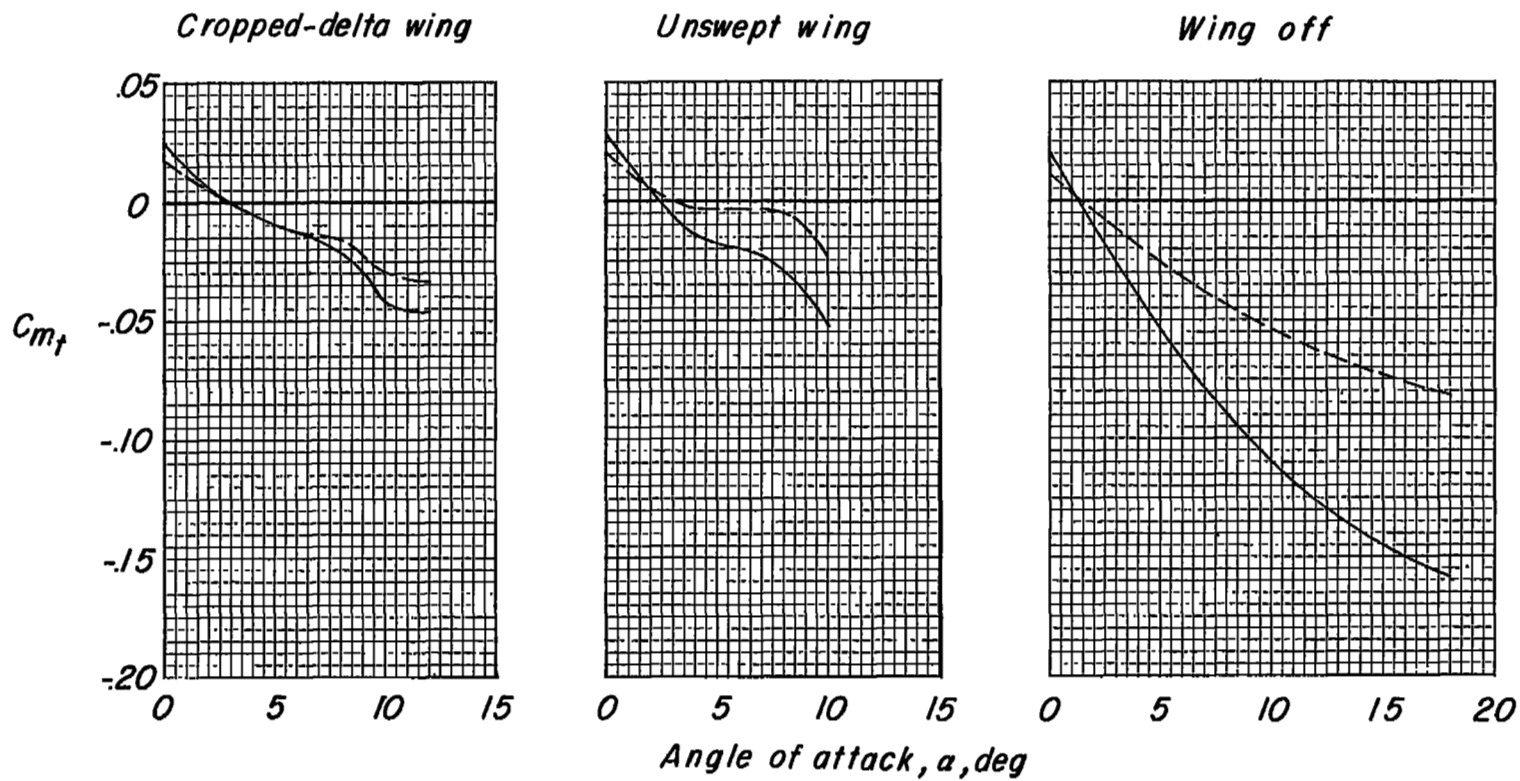
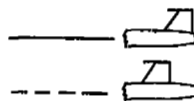
(d)  $M = 0.92$ .

Figure 26.- Concluded.



(a)  $M = 0.80$ .

Figure 27.- Effect of tail length on the tail contribution to pitching-moment coefficient.  $i_t = 0^\circ$ .



(b)  $M = 0.92$ .

Figure 27.- Concluded.

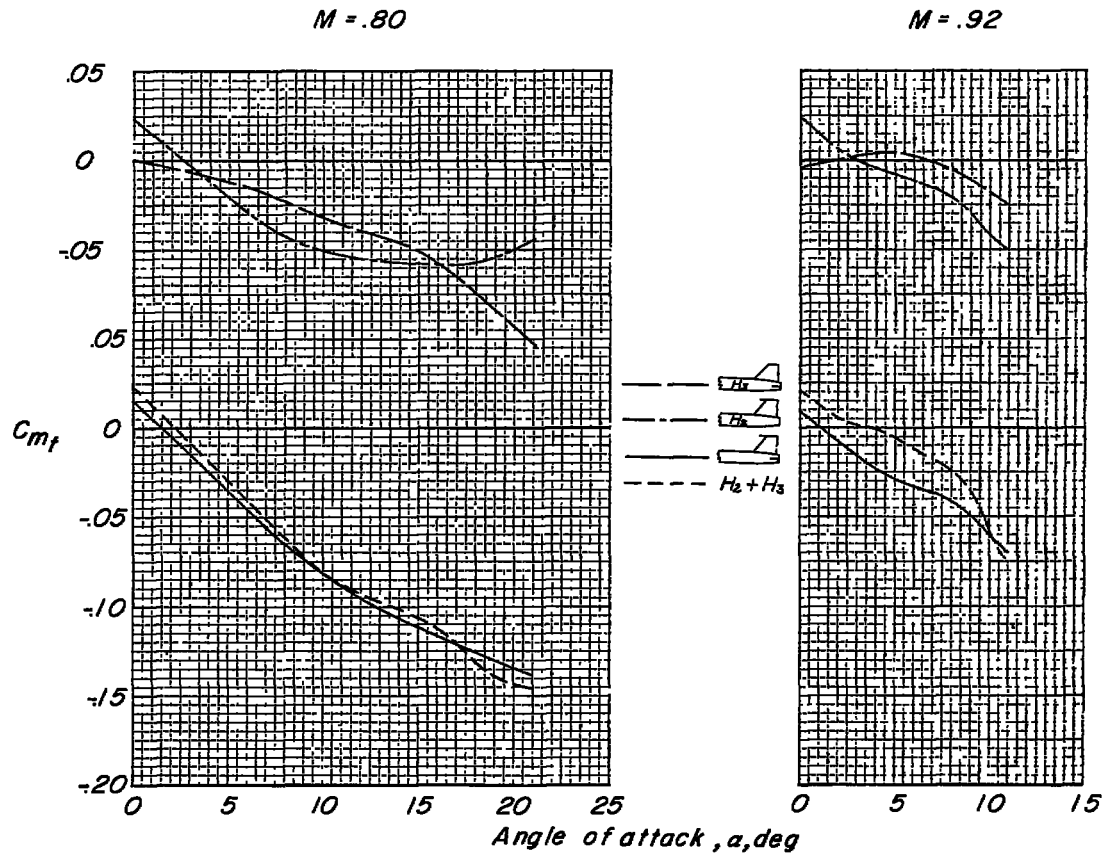
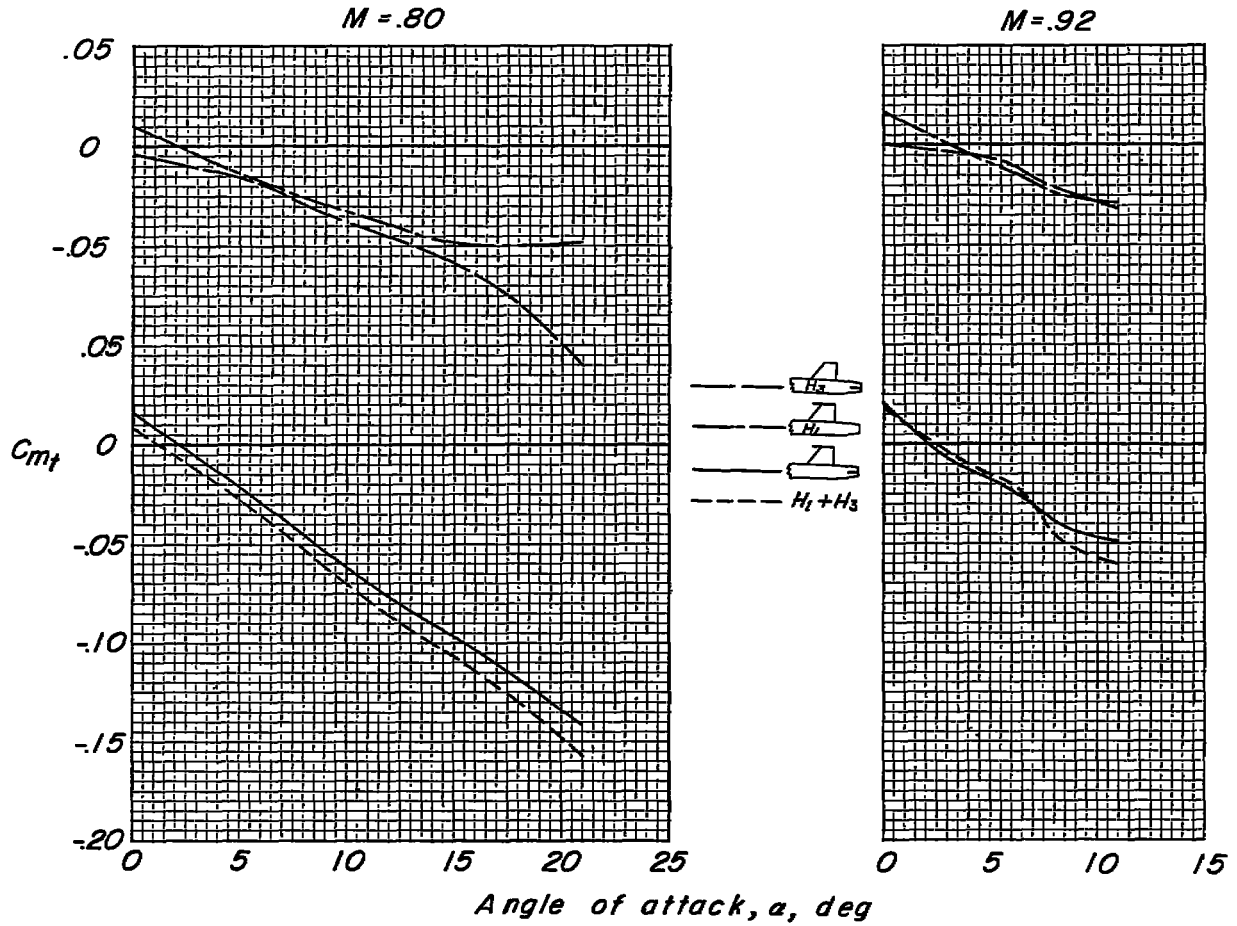
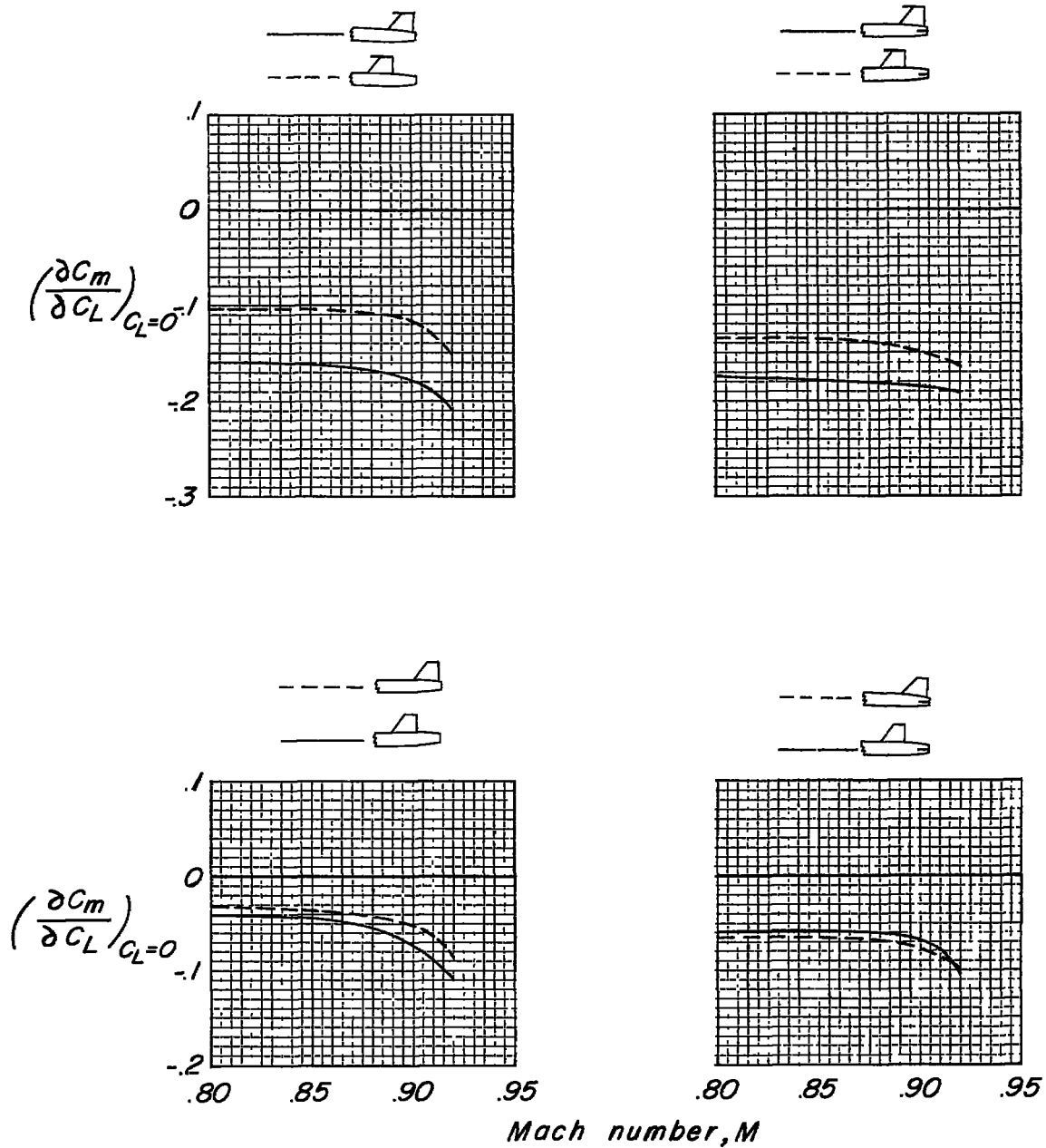


Figure 26.- Effect of various tail arrangements on the tail contribution to pitching-moment coefficient for the model with a cropped-delta wing.  $i_t = 0^\circ$ .



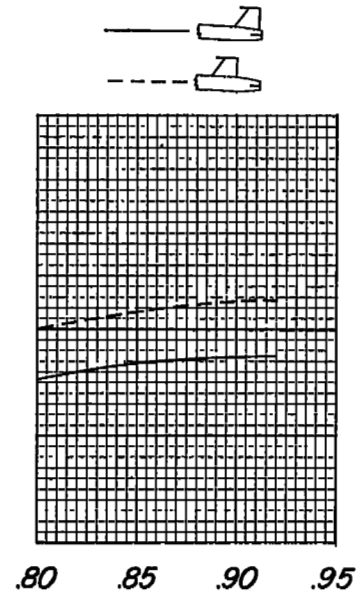
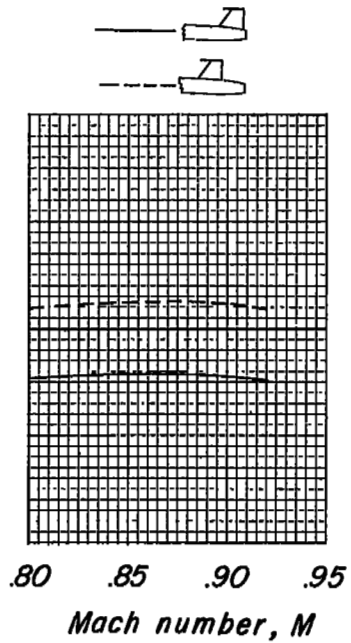
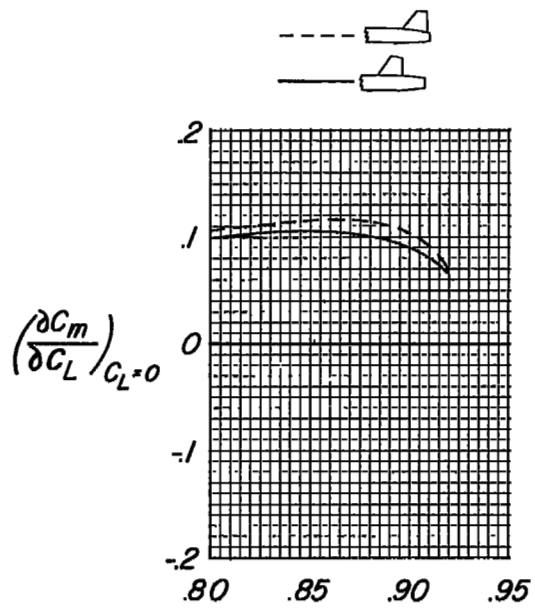
(b)  $\frac{z_t}{c} = 0.84.$

Figure 28.- Concluded.



(a) Cropped-delta wing.

Figure 29.- Effect of Mach number on the rate of change of pitching-moment coefficient with lift coefficient at zero-lift coefficient.  $i_t = 0^\circ$ .



(b) Unswept wing.

Figure 29.- Concluded.

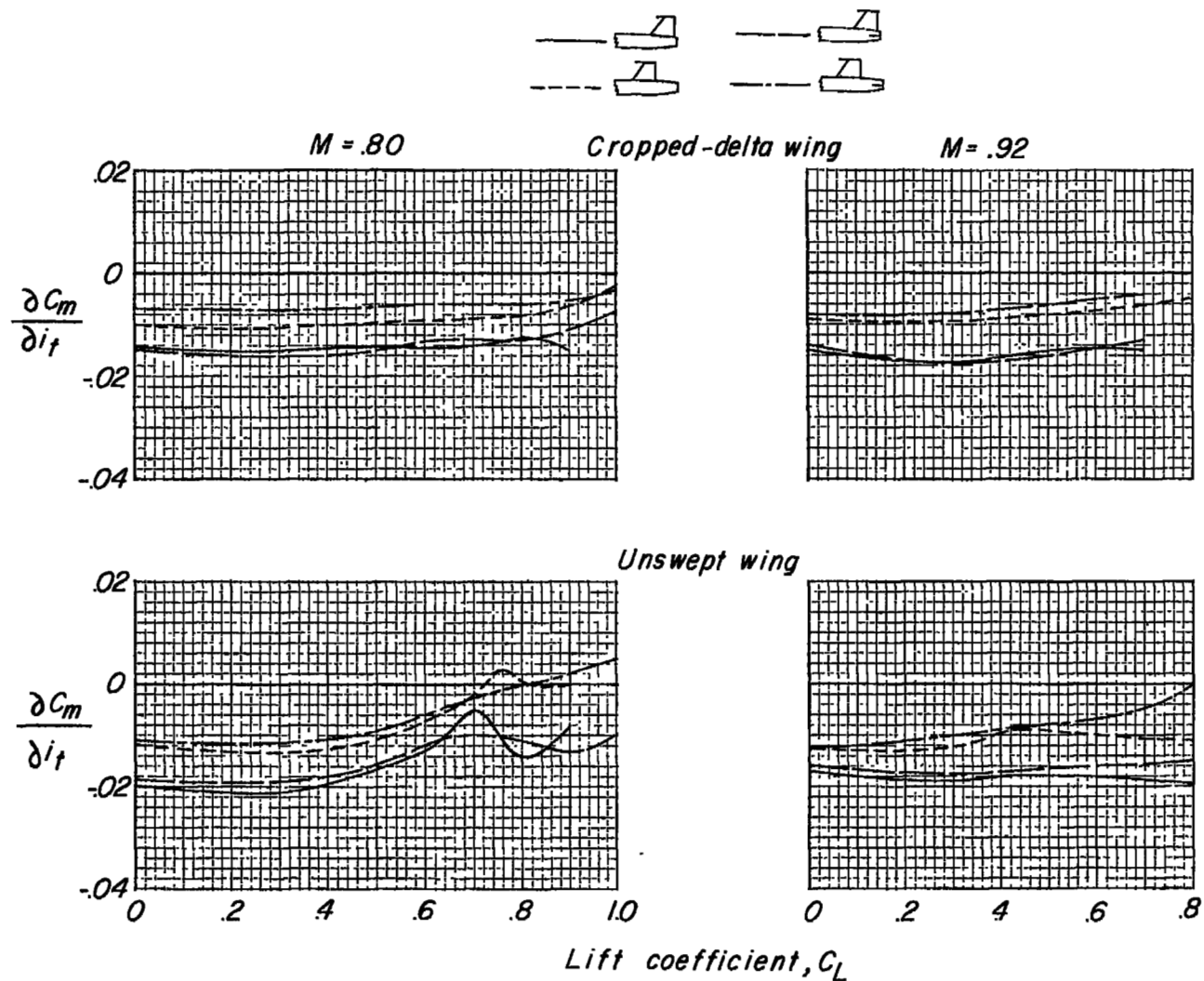
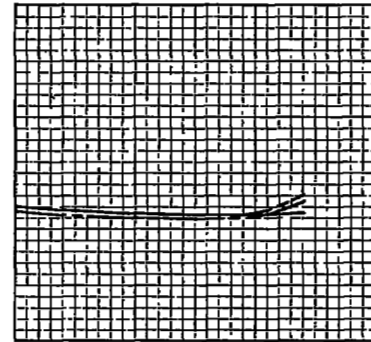
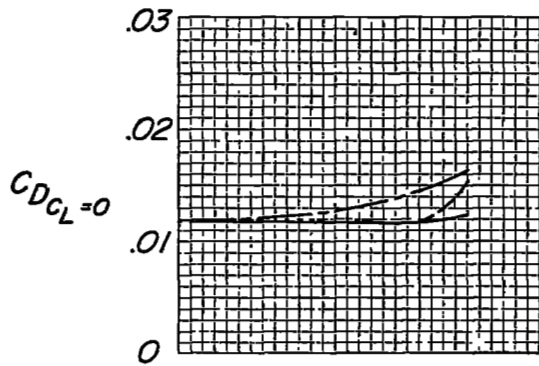


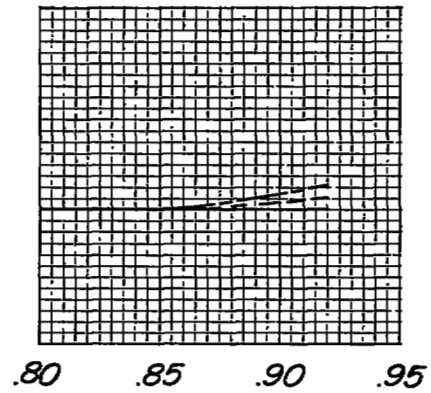
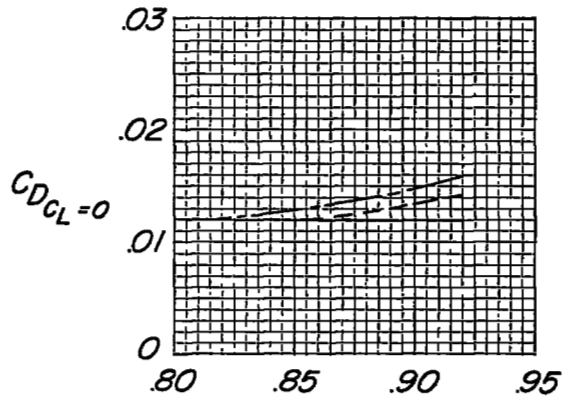
Figure 30.- Effect of tail length on the effectiveness of stabilizer in high position.



*Cropped-delta wing*



*Unswepd wing*

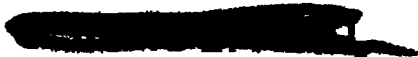


*Mach number, M*

Figure 31.- Effect of tail location on the drag at zero-lift coefficient.  
 $i_t = 0^\circ$ .



3 1176 01438 0613



1

1

1